Journal of Earth Observation and Geospatial Applications

Volume 2, Number 1 April 2026

SPECIAL ISSUE:
Best Practices and Research Work from the STEM Enhancement in Earth Science (SEES) Summer Intern Program, Supported by NASA

April 2026
Volume 2, Number 1

Journal of Earth Observation and Geospatial Applications

BEST PRACTICES

RESEARCH ARTICLES

Best Practice

Pixels and Pupils: A Comparative Analysis of Remote Sensing and Citizen Science Land Cover Data in Los Osos, CA

Shelby Taylor[1,*], Peder Nelson[2], and Russanne Low[3]

[1] 11th Grade, Morro Bay High School, Morro Bay, CA, USA
[2] College of Earth, Ocean, and Atmospheric Sciences, Oregon State University, Corvallis, OR, USA; peder.nelson@oregonstate.edu; https://orcid.org/0000-0003-3979-9051
[3] Institution for Global Environmental Strategies, Arlington, VA, USA; rusty_low@strategies.org; https://orcid.org/0000-0002-7912-4350
[*] Corresponding Author: shellbellt30@gmail.com, + 1-805-635-1106.

Academic Editor: Jeong Chang Seong
Received: 28 February 2026
Revised: 4 April 2026; 10 April 2026
Accepted: 20 April 2026
Published: 30 April 2026

Abstract: Human impact is constantly reshaping land cover dynamics. Remote sensing technology is revolutionary in its ability to provide imagery and land cover data of local and global regions. However, the accuracy of localized remote sensing data remains uncertain. This validation study uses citizen science data to assess the accuracy of remote sensing datasets at a local scale. This evaluation was performed in Los Osos, California, an environmentally sensitive region currently assessing human impact and the health of habitats and endangered species. The null hypothesis was that there would be no differences between remote sensing and citizen science data sets. Research was conducted through the two citizen science platforms: the GLOBE Observer App and Collect Earth Online. These were compared to open-source remote sensing data sets obtained through the Earth Map platform. Visual analysis of data collected at each of the 37 sample units rejected the null hypothesis because of conflicting classification patterns. Citizen science data revealed that remote sensing disagreements were often associated with the incorrect consolidation of land cover elements or confusion between similar features. While remote sensing is generally more efficient, citizen science field observations were critical to the improved understanding of the land cover of local regions. These findings demonstrate citizen science data's ability to validate remote sensing data sets and identify misclassifications. This emphasizes the need for the inclusion of field observations to improve local land cover maps.

Keywords: land cover, remote sensing, citizen science

1. Introduction

As human and environmental impacts drive changes in land cover dynamics, the demand for observational methods has become more prominent. Land cover data is significant in making informed land use decisions and understanding the root causes of impacts (Xu *et al*., 2024). A data collection method recognized for its efficiency on a global scale is remote sensing data. This is a collection method performed from a distance with instruments such as satellites (NASA, 2025a).

An example of remote sensing technology used to collect land cover data is the European Space Agency (ESA)'s Sentinel missions. The Copernicus Sentinel-2 Mission consists of partner satellites that, within a 5-day period, provide global coverage at 10 m resolution (NASA, 2025b). Google's Dynamic World (DW), ESA's World Cover (WC), and ESRI are all Sentinel-derived data sets used in this study. Despite their shared resolution, their potentially conflicting classifications stem from contrasting classification models and training. ESRI and DW were produced with deep learning models. These models were trained with a reference dataset consisting of 5 billion manually classified Sentinel-2 pixels from 24,000 individual 510 x 510 m grids. Alternatively, WC was produced with random forest classification tree algorithms. This algorithm was trained through 141,000 100 x 100 m manually classified grids (Venter *et al*., 2022; Xu *et al*., 2024). Additionally, the WC and ESRI update every year, while the DW data set is near real time and updates every 5 days. These three data sets were obtained through Earth Map Software. Earth Map is a tool that uses Google Earth Engine to provide multi-temporal environmental and climate-based analysis (Morales *et al*., 2023).

Citation: Taylor, S., Nelson, P., and Low, R. (2026). Pixels and Pupils: A Comparative Analysis of Remote Sensing and Citizen Science Land Cover Data in Los Osos, CA. Journal of Earth Observation and Geospatial Applications, 2(1), 1–10. https://doi.org/10.65372/137bv807

Along with these three data sets, the fourth was used in the study, also from Earth Map, Meta/WRI Global Canopy Height (MTC). The data for MTC focuses solely on tree cover collected at a 1 m resolution. This data set relies on a model-based training method developed by AI at Meta Research termed DiNOv2 (Meta, 2024).

Limitations to remote sensing data sets come from tradeoffs between satellite resolutions and training models. Spatial, temporal, spectral, and radiometric resolution are the four major resolutions that must be balanced. Spatial describes the smallest area a satellite can observe, otherwise known as the pixel size. The smaller the resolution, the smaller the objects a satellite can observe. Likewise, a smaller temporal resolution is optimal for increasing the frequency a satellite revisits the same place. Conversely, higher spectral and radiometric resolutions increase image detail. Spectral refers to the number of spectral bands a satellite can differentiate between, and radiometric refers to the amount of information measured in bits, in each pixel. If a satellite is multispectral, it can capture multiple wavelengths of light to produce more detailed images. A drawback to remote sensing instruments is the unattainable perfect combination of the most desirable features (NASA, 2025a).

This study aims to evaluate limitations of remote sensing data at a local scale by validating it with citizen science data. Unlike its counterpart, citizen science data is collected through field observations. Ground cover truth alleviates resolution and training model factors. This study tests the null hypothesis that there are no differences between the explored data sets. It is hypothesized that this hypothesis will be rejected and that citizen science data will identify misclassifications and increase the accuracy of localized land cover maps.

2. Study Area and Methods

2.1. Study Area

The study is conducted within the community of Los Osos, CA. The small town of the central coast of California was compelling for the study because of its unique situation and diverse land cover labels. To this day it remains a mixture of developed and undeveloped land. The area rests on a network of ancient dunes. The Mediterranean climate and resulting Baywood Fine Sands Ecosystem host an abundance of unique species. A few of the dominant natural communities include Coastal Sage Scrub, Maritime Chaparral, and Coast Live Oak Woodlands. Coastal Sage Scrub remains highly threatened and rare in California (McGraw, 2024).

Over time, measures have been taken to preserve and protect this precious community. In 1988, a building moratorium was initiated to inhibit new construction permits. This response to a residential boom in the 1970s and septic tank-related concerns lasted until October of 2024 when the moratorium was lifted (Rajagopal, 2024). Despite this, a large portion of Los Osos remains classified as an Environmentally Sensitive Area. This means federal involvement and permit approval for further development (Lynch & Shrager, 2025). The area's sensitivity stems from the recognition of four endangered species, including Morro Manzanita, Indian Knob Mountainbalm, Morro Bay Kangaroo Rat, and Morro Shoulderband Snail (McGraw, 2024). This influenced the county into taking measures to ease the permit process. In February of 2024, the Los Osos Habitat Conservation Plan (LOHCP) and Federal Incidental Take Permit (ITP) were officially approved by the U.S. Fish and Wildlife Service. Essentially, the ITP allows for legal activity that could invoke accidental harm to endangered species. The necessary inclusion of the LOHCP protects the habitats of important species by mitigating damage (U.S. Fish and Wildlife Service, n.d.). Any disturbance is met with a fine used to conserve another parcel of land of similar size. Expansion has been capped at 1 percent (approximately 50 houses). A 0.4% expansion rate was approved for the year 2026 (McGraw, 2024). Current events in the study area are relevant because the demand for land cover monitoring methods promotes further research. Research on how citizen science data validates remote sensing maps is applicable to communities seeking accurate land cover feedback.

The Area of Interest (AOI) for this case study consisted of a 3 km by 3 km grid, as shown in Figure 1 (Low, *et al*., 2021; Nelson, 2024). The grid was centered on the centroid located at (35.316155° N, 120.827508° W). The AOI was divided into 36 sample unit locations, excluding the centroid. Each unit was spaced evenly at 500 m intervals and covered an area of 100 m × 100 m. These sample units were designed to support standardized data collection and comparison. The AOI for this study was placed with consideration to the accessibility of the sample unit locations. Private property and rough terrain would inhibit the collection of field observations. After defining the AOI, it was saved as a GeoJSON file. This file ensured standardized sampling locations by storing the boundaries of the AOI and the location of each sample unit. The file was

imported into both Google Maps for directions for collecting field observations and into remote sensing data platforms.

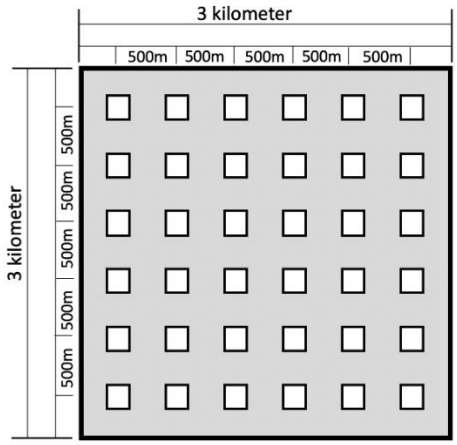

Figure 1: Adopt a Pixel, 3 km by 3 km AOI grid (Low, *et al*., 2021; Nelson, 2024). Each of the 36 squares represents an evenly spaced sample unit. Note that the centroid (sample unit 37) is not pictured.

2.2. Citizen Science Data Collection

Two major platforms were employed to collect field observations: the GLOBE Observer Land Cover App (NASA, 2025b) and Collect Earth Online (CEO) software (Saah *et al*., 2019; FAO, 2023). The GLOBE Observer App is designed for individuals interested in participating as citizen scientists. Its user capabilities include recording ground cover observations and uploading photos at desired locations.

The first step of data collection for this study was uploading the GeoJSON file to Google Maps to generate the 37 coordinate points. This added efficiency and organization to the data collection process because completed locations could be starred on Google Maps. At each location, six directional photographs were taken using the GLOBE Observer App (North, South, East, West, Up, and Down). Additionally, the software recorded the location (i.e., latitude and longitude) of the user. This information was later overlaid with the GeoJSON file using ArcGIS Online to ensure that the observations were collected in the right location. After the photos were taken, the user could choose to describe the perceived ground cover in each image. The following categories–trees, shrubs, herbaceous/grassland, barren, wetlands, open water, cultivated, and urban–are further divided into subcategories for the user to select. Each land cover type must then be followed by the percentage of the area it encompassed in the image. The point of the GLOBE Observer App observations was to capture the surrounding 100 m × 100 m area. This is the same area as the defined sample units. Once the completed photos and observations were uploaded to the GLOBE Observer Citizen Science database, photos and classifications could be accessed.

Field observations were not inherently used as a comparable data set because the photos and observations had incompatible formatting to the aerial image chips of remote sensing data sets. To standardize comparison methods, field observations were integrated into the CEO classification software. These manually classified, 100 m by 100 m image chips could then be directly compared to those derived from remote sensing data sets. Upon uploading the AOI, the CEO software provided overlap between the AOI and satellite imagery. Each of the 37 sample units became 100-point (10 × 10) plots. Each of the points was left blank until manually assigned a color to represent the land cover element beneath it. The colors represented land cover elements including Trees_CanopyCover, bush/scrub, grass, cultivated vegetation, Water>lake/ponded/container, Water>rivers/stream, Water>irrigation ditch, shadow, unknown, bare ground building, impervious surface, and wetlands. The GLOBE Observer photos and observations were continuously cross-referenced when classifying each point to improve their accuracy. Each plot was given a confidence rating on a scale of 0-100. The confidence rating conveyed the estimated accuracy of the land cover classifications. This rating increased when land cover elements were easily identified and confirmed by GLOBE Observer App images. The rating was prone to decrease when image quality or other factors left doubt on the true land cover makeup of a plot. In total, 11 of the 37 points were without GLOBE Observer images. This was due to a location's accessibility, the photo's failure to upload, and the distance data was collected from a sample unit.

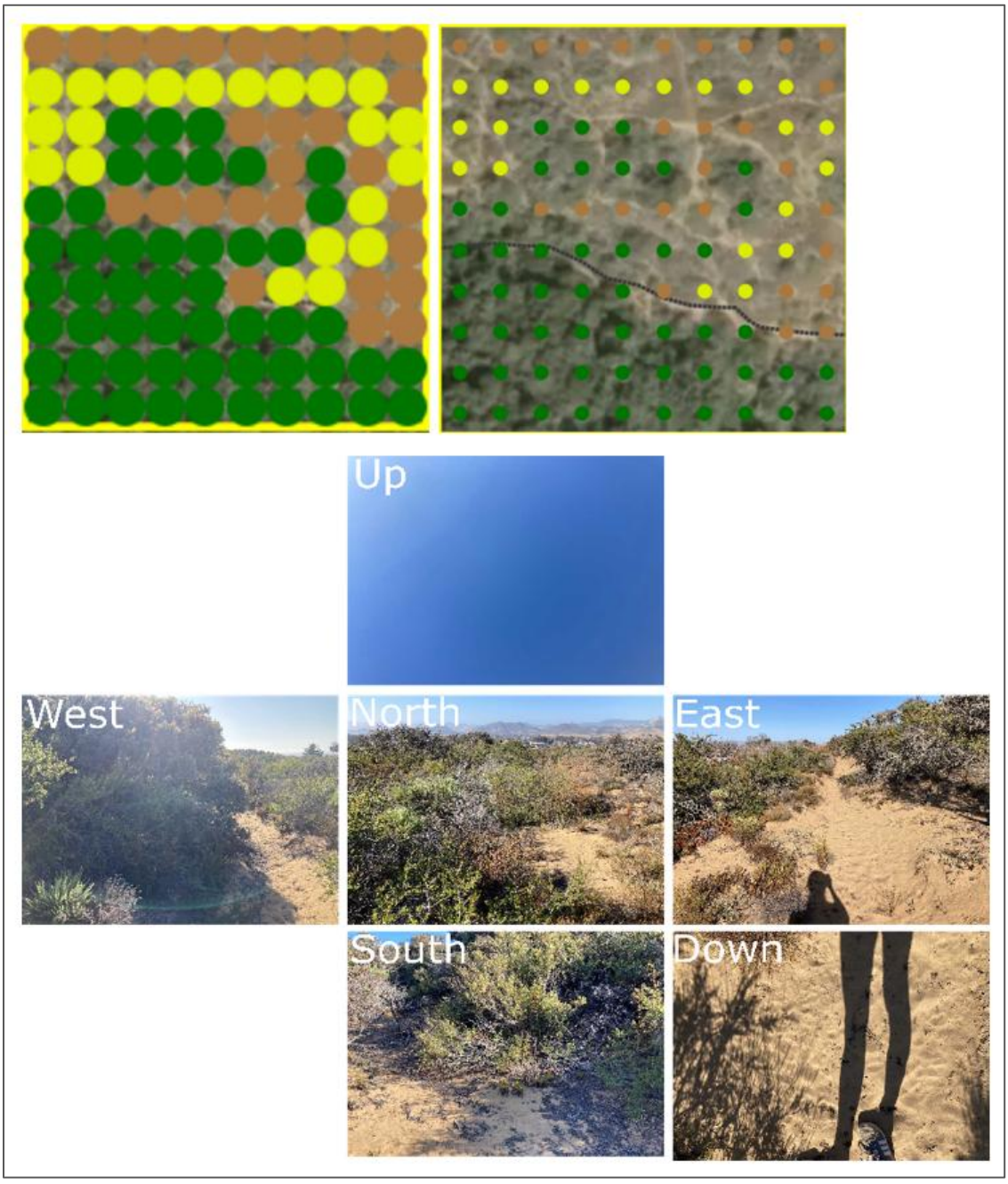

Figure 2. Top – Sample Unit 25, classified using Collect Earth Online software. Bottom – 6 directional photos from Sample Unit 25 uploaded to the GLOBE Observer App.

2.3. Remote Sensing Data Sets

The Earth Map layers provide remote sensing and land cover data. After uploading the AOI to Earth Map, a selection of data filters was overlaid with the region. To analyze Los Osos, three land cover layers were compared. They included World Cover 10 m, Dynamic World 10 m, and ESRI 10 m. They were all derived from the Sentinel-1/-2 satellites. WorldView-4's Earth Map forestry filter, 1 m Tree Canopy Meta (TCM), provided additional and detailed feedback on tree cover distribution. Visually, each filter revealed the land cover makeup of the region by color coding land elements. The land cover element options differed by data set. Within the AOI, the data sets identified differing numbers of land cover elements. In ascending order, WC had 11 land cover categories, DW 6, and ESRI 4. The difference is attributed to ESRI grouping grass

and shrubland into a singular "rangeland" category. Furthermore, WC separated water into open water and herbaceous wetland while simultaneously including barren/sparse vegetation. The TCM data set focused solely on the distribution of trees by classifying tree height on a color spectrum ranging from blue to red. Blue being 2 m canopy and red being 30 m canopy.

At each of the sample units, screenshots were taken of each data filter, as shown in Figure 3. These screenshots were then formatted into a grid. Each row represented a sample unit, and each column represented a different data set. GLOBE Observer photos and Collect Earth Online snapshots were incorporated into the grid to permit comparison of observational methods.

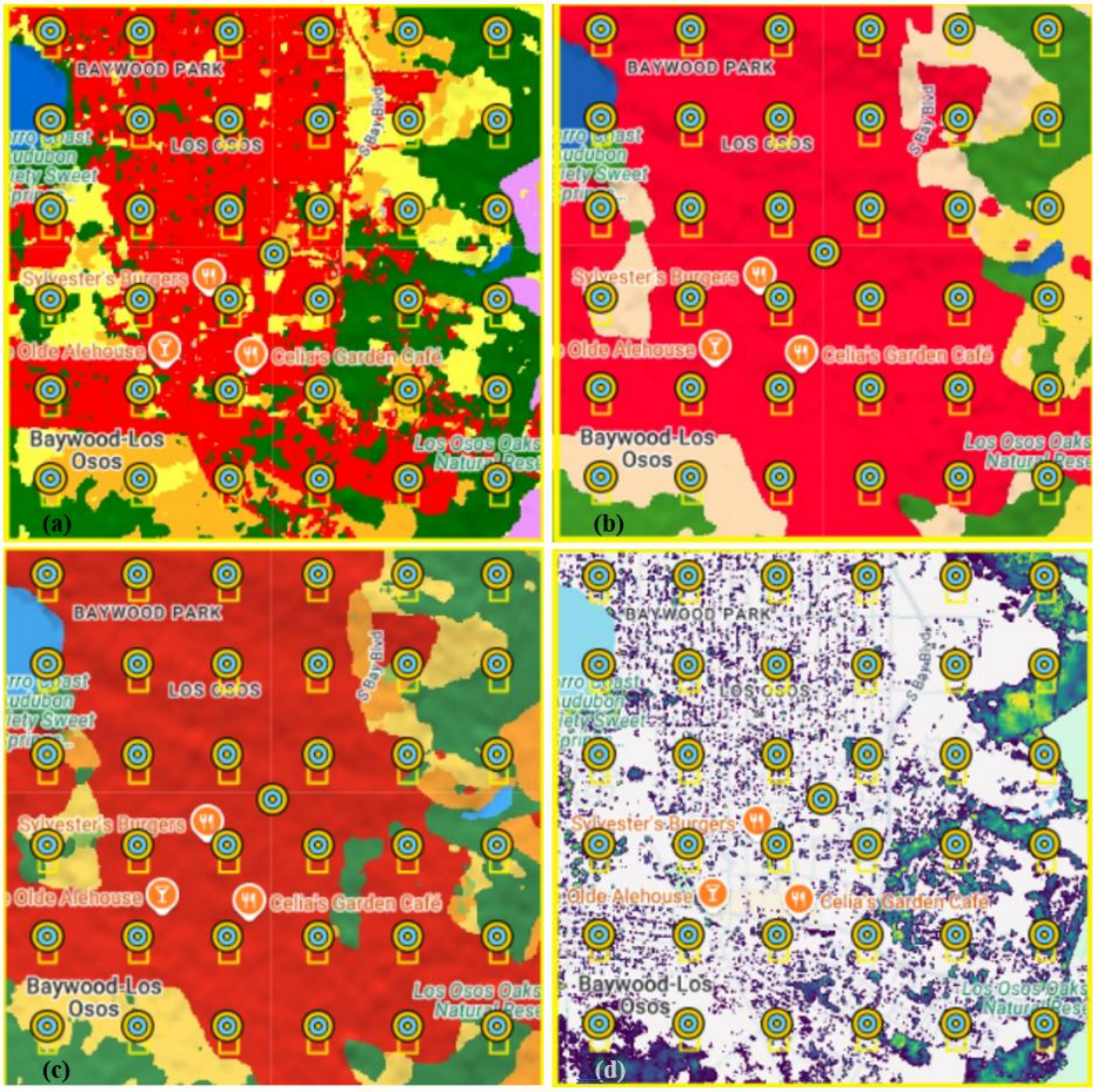

Figure 3. A comparison of Earth Map dataset layers. (a) World Cover. (b) ESRI. (c) Dynamic World. (d) Tree Canopy Meta.

2.4. Comparison Methods

The remote sensing and Citizen Science data sets were compared visually. The standard for visual comparison was a classified image chip with the same boundaries and location as the 100 m by 100 m sample units. Each image chip was color-coded to represent a land cover element specified by each data set. In total, each sample unit had 5 corresponding image chips derived from each observational method (TCM, WC, DW, ESRI, CEO). Both the image chips and GLOBE Observer photos were organized into a grid. Each row represented a sample unit and each column a different data set. Preliminary analysis followed, and each image chip was assigned a symbol depending on its agreement with the GLOBE Observer images or CEO image

chip. The three symbols included a green box with a check mark (agreement), an orange box (mixed), and a red box with an "X" (disagreement). Agreement meant that citizen science data confirmed that a sample unit map correctly identified land cover makeup. Disagreement meant that citizen science data contradicted a sample unit's classification.

Remote sensing data sets were further compared quantitatively. Quantitative data were compared within the entire 3 km by 3 km AOI. CEO data was exempt from this comparison because no numerical or statistical data for the corresponding color classified image chips was created. Additionally, citizen science data was only collected within the sample units and not for the entire AOI. Remote sensing data sets from Earth Map, however, permitted further analysis by generating land cover charts and tables. These charts and tables provided the quantity, in hectares (ha), of each land cover element observed. These were generated by using the "PROCESS" button in Earth Map with the desired data set and the selected boundaries. The initial bar chart provided information on the changing land cover make-up of a region over time. By selecting the "SHOW CHANGE MATRIX" button, a table was generated. What was confusing was that the chart and table generated for each plot provided conflicting numbers for the same location. For example, when ESRI processed the entire AOI, the initial bar chart only showed four land cover elements while the table had five. Water was excluded, as it accounted for the smallest area. For reasons not investigated, the area of the observed land cover elements also appeared to differ slightly. Extensive research was not undertaken to understand this contradiction. Despite these subtle differences, the chart data for the year 2021 was analyzed. While its accuracy is imperfect, the data it provided did reflect visual observations and were considered cautiously. This quantitative comparison was relevant because differences in the area of land cover elements observed by remote sensing data sets highlight the necessity of citizen science data validation.

3. Results

3.1. Visual Comparison

Overall, the data revealed that approximately half of the AOI was built-up areas, and the remainder consisted of similar portions of rangeland and tree cover, as well as some water and cropland. However, disagreements were common between remote-sensing data sets. This promoted the use of citizen science data to clarify what was present in the sample units. Citizen science data was able to identify misclassifications in the remotely classified sample units. Furthermore, it linked disagreement to several challenges, including similar land cover elements and varying details of the classifications.

Remote sensing's challenge with similar land cover elements was apparent between grassland, shrubs/scrub, and tree cover. This was observed in sample unit 33 (Figure 4). With the assistance of the GLOBE Observer photos, sample unit 33 could be described as a sandy trail through a dry, grassy clearing with several small groupings of trees and shrubs. This characterization was not supported by all data sets. Part of the challenge is the similarity in height and color of certain land cover elements. In some areas, short trees or tall scrub also created doubt about what was truly present and contributed to disagreement in the data sets. This was also true for grass and shrubs/scrubs. The ESRI platform categorized grass and shrubs/scrubs as rangeland. This was in part agreeable with the field observations. ESRI also however identified "built-up" land cover not supported by field observations. DW, on the other hand, classified the sample unit as part tree cover and part shrubland. While both these elements are backed by citizen science data, the grass observed in the field observations was excluded. Finally, WC classified the sample unit as tree cover and grassland. Out of the remote sensing data sets, TCM appeared more consistent with citizen science tree cover classifications. However, its focus on only the tree canopy prevents it from contributing to the understanding of grass and shrub distribution. These observations demonstrate the role citizen science data played in validating the true land cover makeup of sample units. Field observations provided the necessary knowledge to conclude land cover elements being observed, especially when land cover elements were difficult to differentiate.

Another instance where citizen science data was needed for validation was when remote sensing data sets disagreed on the number of land cover elements present. This challenge was identified as a common cause of misclassifications. It was apparent that there was disagreement between remote sensing and citizen science sample unit classifications when remotely classified maps consolidated land cover elements into significantly less categories. For example, this mostly occurred in urban areas when remote sensing data sets classified image chips as solely built-up areas, while citizen science data supported the presence of different land cover

elements. Especially for a small scale AOI, the exclusion of major land cover elements (ex. tree cover) decreased the accuracy of land cover maps.

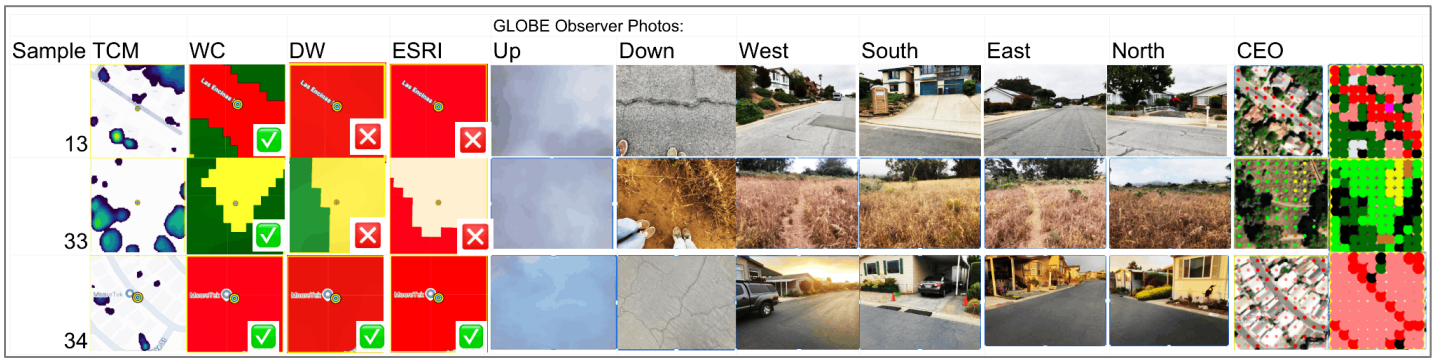

Figure 4. Portion of the grid organized by sample units and data sets. The rows represent sample units 13, 33, and 34.

The habit of consolidating land cover elements into the category "built-up area" was common in the DW and ESRI data sets. Many of these observed sample units were labeled as having "mixed" agreement because of the data sets failure to observe other land types in urbanized areas. On the contrary, the WC layer tended to differentiate each plot, when applicable, into two or more land cover elements. Among the three Sentinel-derived data sets, WC was the most agreeable with citizen science data and CEO. Additionally, WC had the most agreement with both TCM and CEO's tree cover distribution. TCM and CEO land covers were nearly identical in many instances. An example of this is sample unit 13 shown in Figure 4. Unit 13's plot is in an urban area with tree cover. DW and ESRI did not identify any trees. However, both TCM and WC did and were similar to CEO. For this location, DW and ESRI were labeled disagreeable, and WC agreeable.

Furthermore, citizen science data was used to confirm remote sensing observations. Visual inspection of the image chips revealed a common trend between the relationship between fewer observed land cover elements in the CEO classifications and increased agreement. This phenomenon was observed at sample unit 34. Consensus among the data sets concluded sample unit 34 to be an entirely built-up area, as shown in Figure 4. Along this same trend, many of the agreeable image chips had two or fewer land cover elements. While there was agreement between data sets, substantial disagreement was observed. This reveals how field observations not only identify misclassification but can be used in conjunction with remote sensing data sets to validate their accuracy.

3.2. Quantitative Comparison of Remote Sensing Data

The initial form of measuring quantitative agreement was by counting the number of agreement, mixed, and disagreement symbols for each data set. Starting with the number of agreeable image chips, ESRI had the least agreement with 4 image chips, followed by a close DW with 5 image chips. The most agreeable was WC with 12 agreeable image chips. For mixed image chips, DW had 13, and ESRI was barely ahead with 14. WC had the most with 22 mixed image chips. In terms of disagreeable image chips, DW and ESRI were tied for the most with 19. WC had only 3 disagreed on image chips.

Additional quantitative data were derived from the tables supporting visual observations. The data backed the observation that between the Sentinel datasets, WC classified the least amount of the AOI as built-up area and instead classified more as trees and rangeland. This suggests that the data set is less prone to urban consolidation. Figure 5 shows that WC classified 44.6% of the area as built-up, while DW classified 65.16% and ESRI 67.9%. Trees and rangeland areas were also disagreed on, as visualized in the table. For rangeland, DW classified the smallest area of 11.05%, ESRI 14.59%, and WC 23.04%. For tree cover, ESRI had the smallest area of 11.45%, DW had 17.58%, and WC had 28.49%. WC also identified the most cropland out of the three. These values indicate that ESRI and DW were more similar than WC. They, however, were less similar to CEO data than WC.

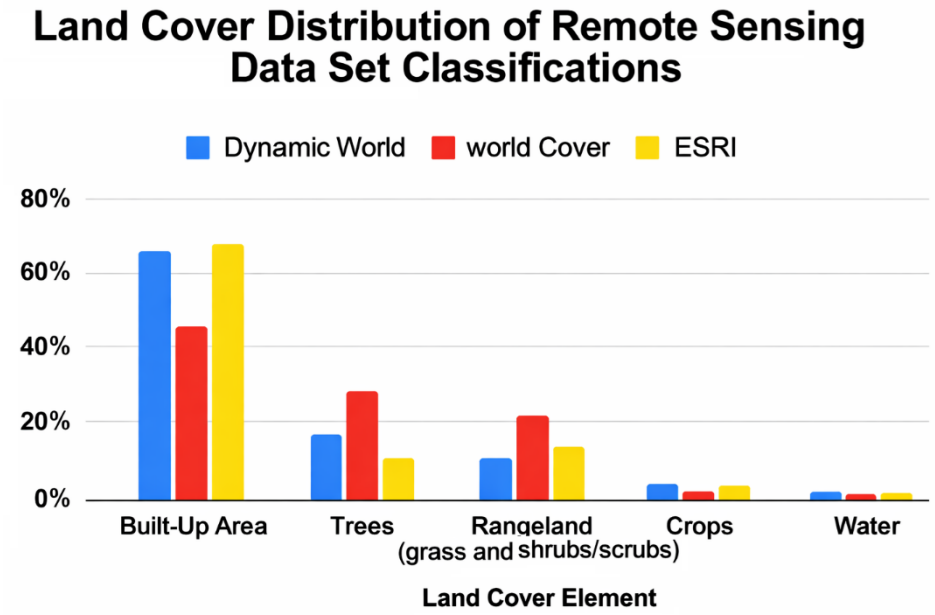

Figure 5. Quantitative comparison of the percentage each land cover element observed in the AOI by different remote sensing data sets. Data was obtained through generated tables in Earth Map.

4. Discussion

The results reveal that there were discrepancies between remote sensing and citizen science data sets. These findings demonstrate how citizen science data can be used to validate land cover maps by confirming classifications or identifying misclassifications. Furthermore, citizen science data proved more effective at separating sample units into a wider range of land-cover categories and at distinguishing between features with similar characteristics. This allowed it to pinpoint weaknesses in remotely classified maps and improve their accuracy.

Qualitative comparison permitted the observation that DW and ESRI classified more of the AOI as built-up area than WC. Additionally, WC classified more rangeland and tree canopy cover. Comparative analysis further revealed DW and ESRI to differentiate between fewer land cover types than WC, especially in urban areas. Overall, WC was most agreeable to the CEO classifications. DW and ESRI, while most similar to each other, had the most disagreement with CEO. Meanwhile, TCM focused solely on tree canopy distribution and proved to be nearly identical to the tree canopy classifications of CEO. The similarities between TCM (1 m resolution) and CEO suggest that higher resolution can improve specific feature classifications. TCM had a spatial resolution of 1 m versus Sentinel's 10 m resolution. This observation promotes the idea that different remote sensing data sets are applicable to different scenarios. Additionally, it illustrates the role of citizen science in recognizing which data sets are applicable to different scenarios because it can confirm which is most accurate. Without field observations, it could have been hypothesized that DW and ESRI more accurately classified the AOI than WC because WC was the outlier. However, citizen science data supported WC classifications more closely in this study. Nonetheless, it also identified cases where WC had incorrectly classified sample units.

In addition, citizen science data suggested there are unique applications of each remote sensing data set. For instance, DW may be advantageous for near-real-time monitoring of regions because it is updated every 5 days as opposed to once a year. However, WC was shown to be more agreeable to the citizen science data and is favorable for studies that require more detail. WC is still limited in its ability to always correctly identify important land cover features, especially those pertaining to rangeland or tree canopy. Citizen science data is assumed to be more applicable to accurate and detailed studies of small-scale regions.

Findings from this study can be applied in the context of Los Osos. The LOHCP states the necessity of continued monitoring studies to track distribution, abundance, status, and response of protected species (McGraw, 2024). This study suggests the future inclusion of field observations to accurately monitor specific land cover types. It would be useful to monitor the two endangered shrubs that the LOHCP outlines.

Meanwhile, remote sensing data could be applied to observe changes in Los Osos's urban land cover. Citizen science data would be less efficient at monitoring the area of the entire community but could check the accuracy of such classifications at sample units.

There were limitations of this study that in future studies would be interesting to pursue. The first is the lack of quantitative data provided by the citizen science data sets. Although qualitative observations were strong enough to provide a comparison with remote sensing data sets, it would be of interest to perform a quantitative comparison of the exact differences of features observed. The biggest limitation of the study was the absence of current remote sensing data. A future study using remote sensing data collected for the year 2025 would be useful for reaching greater conclusions than this study could. This study was effective at analyzing data set patterns and exploring how citizen science data could be used to add to the understanding of an AOI. Land cover is prone to constant change, and a gap as large as 5 years is less than ideal. The gap could influence the agreeability between specific image chips. While this does affect the quality of the comparison, it does not take away from the fact that there was disagreement between remote sensing and citizen science data sets because of varying levels of detail. For example, the tendency of ESRI and DW to exclude trees that have been established for well over 5 years shows that this pattern of disagreement would not be affected. Furthermore, in this study citizen science data were shown to differentiate between more land cover elements.

5. Conclusions

It was hypothesized that there would be disagreement between remote sensing and citizen science data sets. Results supported the hypothesis and promoted the use of citizen science data to validate land cover maps. When compared to remote sensing data sets, citizen science data pinpointed misclassifications present in remotely classified sample units. It also led to the observation that discrepancies were often linked to difficulties distinguishing between land cover elements. Comparison to citizen science data also supported the idea that the applications of each remote sensing data set are unique. WC exhibited the highest classification detail and was similar to citizen science classifications. This makes it suitable for in-depth analysis of a region, even those of a smaller scale. In scenarios where large areas of land are being assessed, citizen science data might seem less ideal. Nevertheless, findings illustrate citizen science data's ability to identify the accuracy of other observational methods by comparing sample unit classifications. This study encourages the future incorporation of citizen science data into localized land cover studies. As land cover continues to evolve with changing human activity and climate patterns, so does the incentive to monitor land cover in many communities. Connecting to Los Osos, the inclusion of citizen science data is highly advised to accurately track the populations of endangered shrub species. Ultimately, the study of Los Osos determined citizen science data to fill in the gaps of land cover maps with verifiable ground-cover confirmation.

Funding: This research was funded by NASA CSR SEES.

Data Availability Statement: Available at the Zenodo GLOBE community at https://doi.org/10.5281/zenodo.18795601.

Acknowledgment: The authors would like to acknowledge the support of the 2025 Earth System Explorers (ESE) Team, NASA Science Mentors, and ESE peer mentors. NASA STEM Enhancement in the Earth Sciences (SEES) Virtual High School Internship program. The NASA Earth Science Education Collaborative leads Earth Explorers through an award to the Institute for Global Environmental Strategies, Arlington, VA (NASA Award NNX6AE28A). The SEES High School Summer Intern Program is led by the Texas Space Grant Consortium at the University of Texas at Austin (NASA Award NNX16AB89A0).

Conflicts of Interest: The authors declare no conflicts of interest. The funders had no role in the design of the study; in the collection, analyses, or interpretation of data; in the writing of the manuscript; or in the decision to publish the results.

References

Food and Agriculture Organization of the United Nations. (2023). *Collect Earth Online (CEO)* [Software]. https://collect.earth (Last accessed: 25 April 2026)

Low, R. D., Nelson, P. V., Soeffing, C., Clark, A., & SEES Mosquito Mappers Research Team. (2021). Adopt a Pixel 3 km: A multiscale data set linking remotely sensed land cover imagery with field-based citizen science observation. *Frontiers in Climate, 3*, 658063. https://doi.org/10.3389/fclim.2021.658063

Lynch, J., & Shrager, C. (2025, July 3). How an endangered species review could slow Los Osos development again. *San Luis Obispo Tribune*. https://www.sanluisobispo.com/news/local/environment/article309077730.html

McGraw, J. (2024). *Los Osos Habitat Conservation Plan*. County of San Luis Obispo, Planning and Building Department. https://www.slocounty.ca.gov/departments/planning-building/forms-documents/communities-villages-forms-and-documents/los-osos-planning-documents/los-osos-habitat-conservation-plan (Last accessed: 25 April 2026)

Meta. (2024). *Using artificial intelligence to map the Earth's forests*. Meta Sustainability. https://sustainability.atmeta.com/blog/2024/04/22/using-artificial-intelligence-to-map-the-earths-forests/ (Last accessed: 25 April 2026)

Morales, C., Díaz, A. S., Dionisio, D., Guarnieri, L., Marchi, G., Maniatis, D., & Mollicone, D. (2023). Earth Map: A novel tool for fast performance of advanced land monitoring and climate assessment. *Journal of Remote Sensing, 3*, Article 0003. https://doi.org/10.34133/remotesensing.0003.

National Aeronautics and Space Administration. (2025a). *Earth observation data basics*. https://www.earthdata.nasa.gov/learn/earth-observation-data-basics (Last accessed: 25 April 2026)

National Aeronautics and Space Administration. (2025b). *Global Learning and Observations to Benefit the Environment (GLOBE) Data User Guide, 2025* (Version 3.0). https://www.globe.gov (Last accessed: 25 April 2026)

Nelson, P. (2024). *Adopt-a-Pixel Research Framework*. Global Learning and Observations to Benefit the Environment. https://storymaps.arcgis.com/stories/3c02bd1d895348e4b2ffc6ddfd5eeca2 (Last accessed: 25 April 2026)

Rajagopal, B. (2024, December 19). Los Osos receives greenlit Habitat Conservation Plan alongside historic building moratorium lift. *New Times San Luis Obispo*. https://www.newtimesslo.com/los-osos-receives-greenlit-habitat-conservation-plan-alongside-historic-building-moratorium-lift-16117075/ (Last accessed: 25 April 2026)

Saah, D., Johnson, G., Ashmall, B., Tondapu, G., Tenneson, K., Patterson, M., Poortinga, A., Markert, K., Nguyen, H. Q., Aung, K. S., Schlichting, L., Matin, M., Uddin, K., Aryal, R. R., Dilger, J., Ellenburg, W. L., Flores-Anderson, A. I., Wiell, D., Lindquist, E., Goldstein, J., Clinton, N., & Chishtie, F. (2019). Collect Earth: An online tool for systematic reference data collection in land cover and use applications. *Environmental Modelling & Software, 118*, 166–171. https://doi.org/10.1016/j.envsoft.2019.05.004

U.S. Fish and Wildlife Service. (n.d.). *Frequently asked questions regarding final Los Osos Habitat Conservation Plan, incidental take permit, and Environmental Assessment*. https://www.fws.gov/question-answer/frequently-asked-questions-regarding-final-los-osos-habitat-conservation-plan (Last accessed: 25 April 2026)

Venter, Z. S., Barton, D. N., Chakraborty, T., Simensen, T., & Singh, G. (2022). Global 10 m land use land cover datasets: A comparison of Dynamic World, World Cover and Esri land cover. *Remote Sensing, 14*(16), 4101. https://doi.org/10.3390/rs14164101

Xu, P., Tsendbazar, N. E., Herold, M., de Bruin, S., Koopmans, M., Birch, T., Carter, S., Fritz, S., Lesiv, M., Mazur, E., Pickens, A., Potapov, P., Stolle, F., Tyukavina, A., Van De Kerchove, R., & Zanaga, D. (2024). Comparative validation of recent 10 m-resolution global land cover maps. *Remote Sensing of Environment, 311*, 114316. https://doi.org/10.1016/j.rse.2024.114316

Best Practice

The Implications of Unreported Tidal Fluctuations in Satellite Imagery

McKayla Wilson-Rodriguez[1,*] and Peder Nelson[2]

[1] College of Science, Department of Integrative Biology under the School of Life Sciences, Oregon State University, Corvallis, OR, USA; wilsonrm@oregonstate.edu, https://orcid.org/0009-0000-4585-2627

[2] College of Earth, Ocean, and Atmospheric Sciences, Geography Program, Oregon State University, Corvallis, OR, USA; peder.nelson@oregonstate.edu, https://orcid.org/0000-0003-3979-9051

[*] Corresponding Author: mkwilsonrodriguez@gmail.com; +1 (631) 747-2022

Academic Editor: Jeong Chang Seong
Received: 1 March 2026
Revised: 13 April 2026
Accepted: 19 April 2026
Published: 30 April 2026

Abstract: Remote sensing data and satellite imagery can be challenging to accurately produce, especially when tidal ranges affect the variation of land cover types daily, which are not represented in any Earth Map layer. Inconsistencies among maps create confusion and daily tidal fluctuations have effects on not only the land type and change over time, but many coastal species and their behavior like the American herring gull. Three grids were established on Fire Island, NY to understand if there had been a land change over time, if there is a difference among one forestry and three land cover Earth Map layers, their accuracy to ground cover photos collected through the Global Learning and Observations to Benefit the Environment (GLOBE) app, tidal height differences, and difference in activity of American herring gulls between high and low tide. This was done by utilizing the GLOBE Program to establish grids, collect ground cover photos using the GLOBE observer app, a ground count at 10-minute intervals for American herring gull data, Landsat time-series for land change over time, and Collect Earth Online for land cover type categorization. The results showed that the layers presented inconsistencies among one another and when compared to ground cover photos. There was also a significant difference in daily tidal fluctuations between high tide and low tide, a significant difference in American herring gull activity between high tide and low tide, and the land had changed over time from the year of 1984 to present. These findings suggest the value of daily tidal representations in satellite imagery, especially land cover layers like those presented in Earth Map, as well as the implementation of ground cover photos in the production of satellite imagery to produce the most accurate and usable maps possible.

Keywords: tides, satellite imagery, ground photos, land cover, American herring gull

1. Introduction

Remote sensing is the acquisition of information from a distance and computing it into satellite imaging of various landcover types used for various purposes and research domains. It creates a map, pixel by pixel, of reflectance values by using sensors that capture electromagnetic energy emitted by the earth to make up raster grids arranged in columns and rows. Numerous sensors to capture this energy have been launched by either space-borne (orbiting around earth) or aerial imaging systems (attached to aircraft). Remote sensing is useful for solving problems and producing landcover maps which can be used within multiple disciplines (Stevens et al., 2012).

The Global Learning and Observations to Benefit the Environment (GLOBE) Program utilizes data collection and analysis from volunteers to improve the science of earth mapping (NASA, 2025). GLOBE Observer app users can collect data through photos, utilizing their personal cell phones, of various earth surface covers. These surface covers could include ocean, bare ground, developed land, etc. Participants can then upload their photos to the GLOBE open-source database utilizing the GLOBE Observer app, which is free of charge to anyone. The surface-based observations captured through photos are utilized to better our understanding of earth's various surfaces and challenge established-ideas about certain areas of the world. GLOBE can also be a tool for small to large research projects within a variety of scientific disciplines.

Earth Map (Morales et al., 2023) is a free web browser platform designed to present and analyze multi-temporal and climate datasets (Gorelick et al., 2017). It is a novel tool utilized for its climate assessment,

Citation: Wilson-Rodriguez, M. & Nelson, P. (2026). The Implications of Unreported Tidal Fluctuations in Satellite Imagery. Journal of Earth Observation and Geospatial Applications, 2(1), 11–27. https://doi.org/10.65372/ppp11k28

advanced land monitoring, and fast performance. Earth Map has multiple different categories that umbrella various data sets. Within the Landcover umbrella there are several layers, or different data sets, to represent the various land cover types of the surface of the earth. Due to the nature of having several sources provide representations, there may be discrepancies among data sets and whether they agree with one another.

Collect Earth Online (CEO) is an open-source tool that can be used to classify and categorize various land cover types (Saah et al., 2019). CEO is useful for a more zoomed in approach to interpreting areas and can be applied over time to determine changes in an area. Information categorized in CEO can be stored and utilized in data analysis and compared to other satellite imagery.

The American herring gull is a large gull species living in various habitats across North America, typically near water. Their population numbers are abundant, and they can be found along coastlines, major rivers, and large lakes. It can be identified by its white head, pale eyes, grey wings with black tips, pink legs, and a yellow beak with a red spot (Weseloh et al., 2024; National Audubon Society, n.d.). Their great population numbers and notable identification make them a useful seabird species to monitor for activity changes per tide range.

Validating remote sensing data can be challenging, especially when attempting to identify tidal ranges and land cover change over time. Satellite imagery can also be inaccurate in appropriately identifying certain land cover types which can hinder research by providing false information on the landscape (Geyman & Maloof, 2020). Daily tidal changes and ranges occur in coastal areas around the world which temporarily and/or permanently alter the landscape and affect the activity of many seabird species like the American herring gull (Daunt et al., 2002). Many user-friendly and science-based satellite imaging datasets, utilized through Earth Map, do not account for daily fluctuations in landscape due to tidal ranges. This is important because understanding how the landscape affects seabird species within it helps us understand the ecological implications of these daily and/or long-term changes. Landsat time-series in Google Earth Engine (https://earthEngine.google.com) can help scientists understand long-term changes of coastal areas, but daily changes pose an important factor in ecological activity within any given area. Interpreting everyday fluctuations ultimately provides relevant information to long-term landscape change and many ecological factors.

There have been some studied and established techniques for monitoring and measuring tidal ranges like utilizing Landsat time-series to reconstruct tidal spatial structure (Geyman & Maloof, 2020), the waterline method (Kang et al., 2023), and utilizing satellite altimeters (Pan et al., 2025). However, benchmark studies are lacking on comparing the performance of these techniques and algorithms (Vos et al., 2023), not to mention the lack of connection between these techniques and their implications on accurately assessing ecological activity; like seabird species such as the American herring gull.

Strategies for addressing these gaps could include the implementation of ground cover photos and tidal gauges. Ground cover photos utilized through the GLOBE Observer app could be merged alongside satellite data to support the production of accurate mapping images. Collecting daily information from tidal gauges to create tidal lines and tide range representations could enhance land cover maps by providing another layer for researchers to use. Additionally, providing the opportunity for scientists to communicate with map developers to discuss maps and any procedures/techniques used, could allow researchers to guide projects and contribute to satellite map layers.

Analyzing the study area with Landsat time-series imagery reveals that its landscape has undergone changes in size and/or shape over time. The analysis of four different satellite imagery datasets, presented in Earth Map, will not represent daily tidal changes nor accurately present the various land cover types shown in ground level photos 100% of the time. The agreement among Earth Map layers will not all be 100%. Utilizing the NOAA tide gauge within the study area (NOAA, n.d.), there will be a significant difference in the tidal heights between high tide and low tide. Connecting the tidal differences to seabird species, there will be a significant difference of American herring gull activity between high tide and low tide.

This study will assess whether the landscape has changed over time using the Landsat time-series database. It will also use ground cover photos to evaluate four Earth Map datasets to determine if they accurately represent the tidal changes in the area, whether they all represent the various land cover types appropriately and agreeing in the same way. In addition, the significance of the difference between high tide and low tide will be checked. Lastly, an ecological connection will be made by testing the difference between American herring gull activity from high to low tide and its significance.

There is a gap in research comparing daily tidal ranges to land cover maps/datasets provided through Earth Map and their significance to ecological research. Utilizing the GLOBE Observer app (NASA, 2025) to analyze land cover types and conduct research on a coastal seabird species, such as the American herring

gull, during different daily tidal stages has not been previously conducted nor has it been connected to the need for daily tidal range representation on land cover maps. Interpreting daily tidal changes regarding land cover and ecological factors allows ecological, geographic, and oceanography modes of research more knowledge into their designated study sites. Future research could include how to incorporate daily tidal gauge data and information from ground-cover photos into land cover maps utilized in Earth Map because it fluctuates the amount of land exposed; and it provides insight into previously mentioned scientific disciplines. Other areas of research could also aid in establishing a benchmark for tidal measurements to assess accuracy across multiple locations worldwide (Vos et al., 2023). In addition, many coastal species can be monitored to understand the importance of tides on their behavior. This may provide improved mapping data sets and a broader overview of land cover types that can support research across multiple scientific disciplines.

2. Study Area and Methods

2.1. Study Area

Fire Island (Figure 1) is a barrier island along the south end of Long Island, New York and extends to 50 km in length. While long, the island is narrow and varies in width from 200m to 1km (Pendleton et al., 2004). There are 26 miles on Fire Island that have been designated as a National Seashore to maintain its natural beauty. The western coastal region of Fire Island has a complex offshore geological framework and has been previously impacted by major storms such as the Hurricane in 1938, a nor'easter storm called the "Ash Wednesday" storm in 1962, another nor'easter in 1992 (Pendleton et al., 2004), and Hurricane Sandy in 2012. Barrier islands are crucial to ecosystems and coastal areas because their absorbance of wave energy protects the mainland from storm surge and flooding. Many factors cause barrier islands to disappear over time including erosion caused by human activities, damming and dredging projects, and climate change factors such as sea level rise and extreme weather events (NOAA, 2021).

The study area was on the western end of Fire Island, NY. The western end of the study area started at Democrat Point and spanned east to Fire Island National Seashore about 9km in length (East to West) and about 3km in width (North to South). Three grids were created by prioritizing the center point for each grid on land and assessing the number of accessible points to collect the most data.

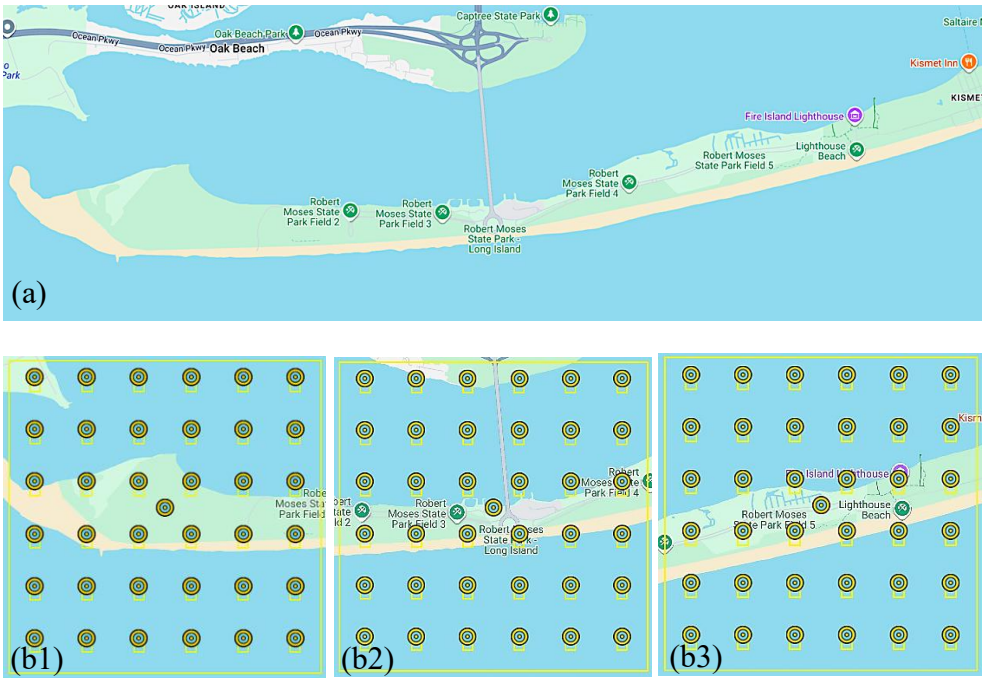

Figure 1. (a) Overview of the entire study area on Fire Island, New York without layers. (b1, b2 & b3) Grids 1, 2, and 3 from left to right of study area. (Background image courtesy of Google Earth Engine).

2.2. Data

Initial data collection came from Landsat time-series. Graphs of Normalized Burn Ratio of each primary sample unit (PSU) were collected and screenshots of each grid (3 total) within the entire sample area of each year starting from 1984 to most recent available year were also collected. Earth Map was also utilized to screenshot satellite imagery of each entire grid and each primary sample unit within the grids of four layers consisting of the land cover and forestry category in Earth Map. These layers included Global Forest Canopy Height- UMD GLAD (Tolan et al., 2024), Dynamic World (Brown et al., 2022), ESRI 2017/2024 Land Cover (Karra et al., 2021), and World Cover 10 m 2020/2021 (Zanaga et al., 2021). Tidal data was collected through NOAA Fire Island tidal gauge at Station ID: 8515186 to record peak tidal data, in feet, each time field observations were conducted (NOAA, n.d.).

Field data was collected from each accessible primary sample unit of ground photos through the GLOBE Observer app at high tide and low tide and 10-minute interval ground counts of American herring gulls, North and South, at high tide and low tide. Ground counts were categorized by either walking, walking and foraging, flying, and flying and foraging, where a bird could only be counted once among all the options.

Categorization of land cover types for each primary sample unit was collected through Collect Earth Online. This categorized 100 10-meter diameter point land cover types within each primary sample unit by selecting an identification among several choices for each. This ultimately determined land cover type percentages of each primary sample unit based on Collect Earth Online.

Visual assessment with a proportion calculation was used to produce agreements among each Earth Map layer to ground photos. This was performed by determining the primary land cover type among that Earth Map layer, such as water and no water, and using those parameters to conclude the primary land cover per PSU shown in the Earth Map layer and determining if the ground cover photos represented the same conclusion per primary sample unit. If ground cover photos could not be collected due to accessibility, then it was assumed the Earth Map layer agreed with the sample.

Further data was produced of agreements comparing each Earth Map layer to one another through a visual proportion calculation. This was done by determining how many layers, out of four, looked the same or represented the land the same way.

Conclusions on the significance of tidal differences and American herring gull activity differences per tide was done using R. A Shapiro-Wilk Normality test was done and since the data was not normally distributed for both parameters (tide heights and American herring gull activity), a Wilcoxon rank sum test with continuity correction was used for both determinations of significance. Graphic representations of these conclusions were also performed in R.

2.3. Methods

To create the sample area, three grids were produced using the GeoJSON software which was accessed through the Adopt-a-Pixel research framework (Nelson, 2024) within the GLOBE Program. Each grid produces 37 primary sample units, totaling 111 for this study, however 17 primary sample units were accessible for field data collection at high tide and low tide among the 3 grids, totaling 34 for the entire sample. At each primary sample unit, American herring gull data was collected facing North then facing South totaling 68 separate collections.

Each grid produces an individual GeoJSON file which was then uploaded to Earth Map to continue further assessments of the sample area. Earth Map was then used to record the coordinates of each primary sample unit produced by the GeoJSON file, which can be done by hovering the computer mouse over an individual primary sample unit; these coordinates were used for later field data. NOAA's Fire Island tidal gauge at Station ID: 8515186 was then used to record when high tide and low tide would occur and the peak height of the tide in feet each time field data was collected.

Using the previously recorded coordinates of the primary sample units, Google Maps provided directions to each accessible point to pursue field data collection. At each accessible point, field data collection started using the GLOBE Observer app to capture directional photos of Up, Down, North, East, South, and West. To prevent data loss, photos were also taken on our personal cell phone. Following that, we faced North 10 minutes then South 10 minutes to ground count American herring gull activity (Wetlands International, 2018). Visual parameters for counting faced in the appropriate direction spanned from east to west.

Once ground cover photo data and American herring gull activity was collected at each accessible point, Google Slides were used to organize ground cover photos from left to right with the coordinating Earth Map

layers per primary sample unit. One Google Slide was produced per grid to maintain clarity. Raw American herring gull data was organized in Microsoft Excel, and each grid was organized separately within one sheet.

Landsat time-series was used to identify the land change over time for each grid by organizing photos of each year from 1984 to present in the appropriate Google Slide for assessment. Continuing with Landsat time-series, the coordinates of each primary sample unit were inserted into the Landsat URL to collect the Normalized Burn Ratio (NBR) graph and organize it into the appropriate Google Slide. NBR is an index derived from satellite data which measures the changes in soil and vegetation; it is often used to detect burned areas or major land cover change. High, or positive NBR values mean healthy or dense vegetation and low or negative NBR values mean bare soil, water, built areas, or recently burned areas.

Collect Earth Online aided in the categorization of land cover types within each primary sample unit and produced percentages of each land cover type per PSU. Additionally, it provided the primary sample units with a numerical identification where the primary sample units for grid 1 were labeled 100-136, grid 2 was 200-236, and grid 3 was 300-336. Categorization of land cover types was done by uploading the GeoJSON grids into Collect Earth Online and going through each PSU and categorizing 100 10-meter diameter points by choosing from the categories provided. Categorization was clear for PSU's where ground photos were previously collected, and non-accessible PSUs were inferred based on the most agreed land cover type among Earth Map data sets. Once every PSU had been entirely categorized by land cover types, photos of each one were organized into the appropriate Google Slide.

Photos of each Earth Map layer grid and individual primary sample unit per Earth Map Layer were also organized into the appropriate Google Slide to make comparisons and conclusions regarding agreement compared to one another. These were organized from left to right per PSU to conduct the visual comparison with the ground cover photos taken. An agreement assessment calculation was used when determining the agreement of each Earth Map layer to ground cover photos. Figure 2 shows an example of Earth Map layers in Grid 1.

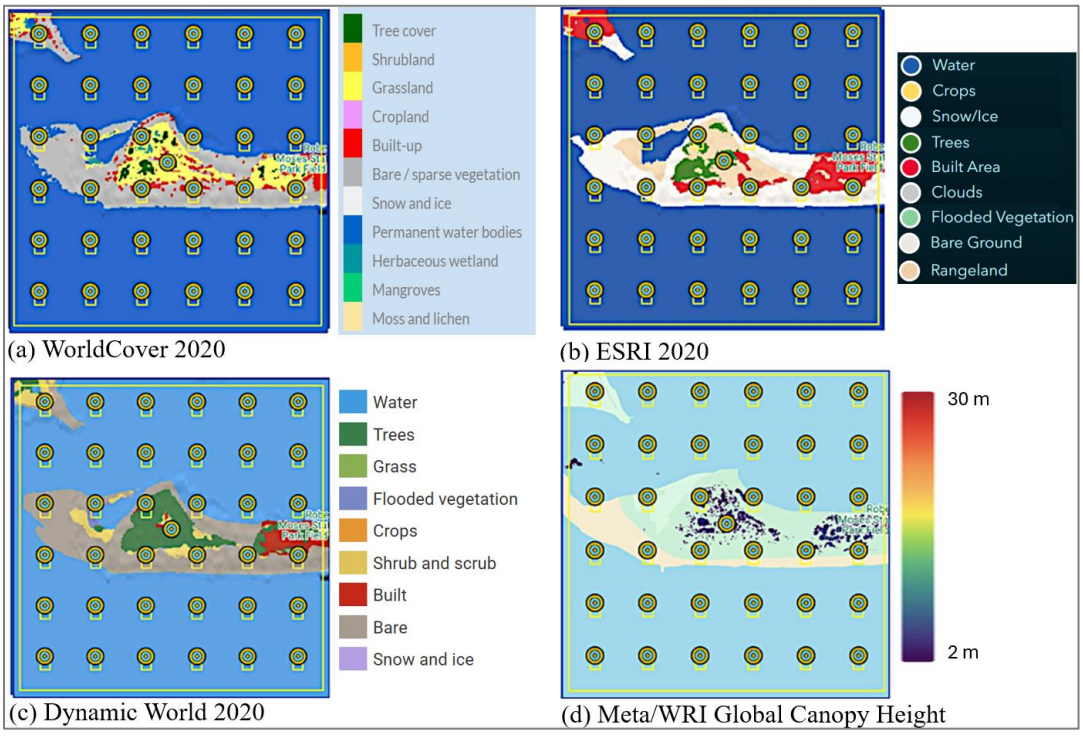

Figure 2. Land covers in Grid 1 identified by different sources with their corresponding legends.

Microsoft Excel was used to organize the raw field data of the American herring gull ground count and tidal data. All the American herring gull data was uploaded to R to conduct the two tests for high tide and low tide difference and two tests for difference in activity for American herring gulls per tide. R was also used to produce graphical representations of these results.

3. Results

When the land cover layers were compared to one another, they did not always agree, and agreement was especially inconsistent when the land became more diverse with different land cover types. Figure 3 shows an example of accuracy assessment for Grid 1, organized in a Google Slide. Assessment results are shown in the "Agree" column.

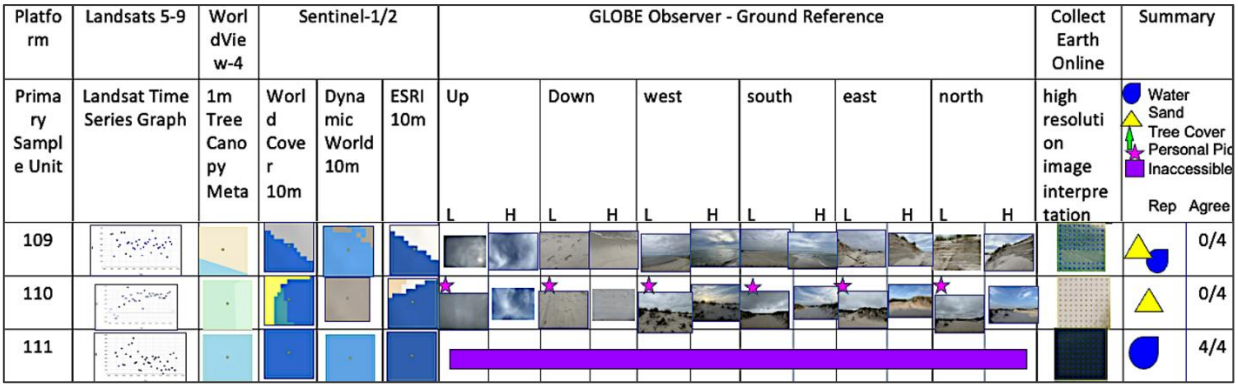

Figure 3. Example of Fire Island Grid 1 Google Slide, where the imagery data was organized and compared. "L": Low tide, "H": High tide, "Rep": Representation, "Agree": Agreement among Earth Map layers.

The table in Appendix 1 shows the land cover types labeled in Collect Earth Online and agreement percentages among the four Earth Map layers assessed. In the case of Primary Sample Unit 101, for example, visual assessment showed 100% water, Collect Earth Online also labeled 100% water, and all four Earth Map layers examined labeled 100% water, making 100% agreement percentage.

When we looked at the comparison between the maps and the ground photos of primary sample unit locations, we would expect disagreement because of the timing of daily tidal changes. Visually comparing the ground cover photos to the map layers, it was difficult to make a precise assumption about whether the Earth Map layer was more closely representing high tide or low tide. It appeared that some primary sample unit locations in Earth Map were more closely represented by high tide while others appeared more closely represented by low tide. These differences highlight the restrictions and overall inconsistencies within each Earth Map layer.

Again, it presented a trend where accuracy and agreement were especially inconsistent when the primary sample units became more diverse or showed more edge interference in land cover types. As shown in Figure 4, primary sample unit ground cover photos that were taken at low tide are organized in the L column and photos taken at high tide are shown in the H column. Results of the comparisons between the Earth Map layers and ground cover photos are shown in the row "Agreement" on each Google Slide where the imagery data was organized and compared.

The agreement assessment percentages represent a simplified way to understand if overall the Earth Map layer and ground photos represent the major land cover type. However, it does not assess individual pixels, nor does it account for exact layouts of the maps and the earth itself represented by the photos taken. Overall, the World Cover layer in Earth Map had the greatest average accuracy percentage with an average of 98% among all 111 PSUs across the three grids. However, some PSU classifications were estimated using informed classification assumptions for inaccessible locations.

The agreement assessment results across the three grids indicate that global land cover products (World Cover, Dynamic World, and ESRI) demonstrate exceptionally high user accuracy, particularly in identifying "Ocean" versus "Not Ocean" categories, with values consistently ranging between 95% and 100%. For instance, World Cover achieved a perfect 100% accuracy in Grid 1. In contrast, the 1 m Tree Canopy dataset shows a lower but consistent level of agreement, ranging from 84% to 86% across the study areas. While the 1 m Tree Canopy product avoided false positives by never mislabeling "Not Trees" as "Trees," it frequently missed actual trees; it misclassified 6 cases in Grid 1 and 5 cases in both Grids 2 and 3 as "Not Trees".

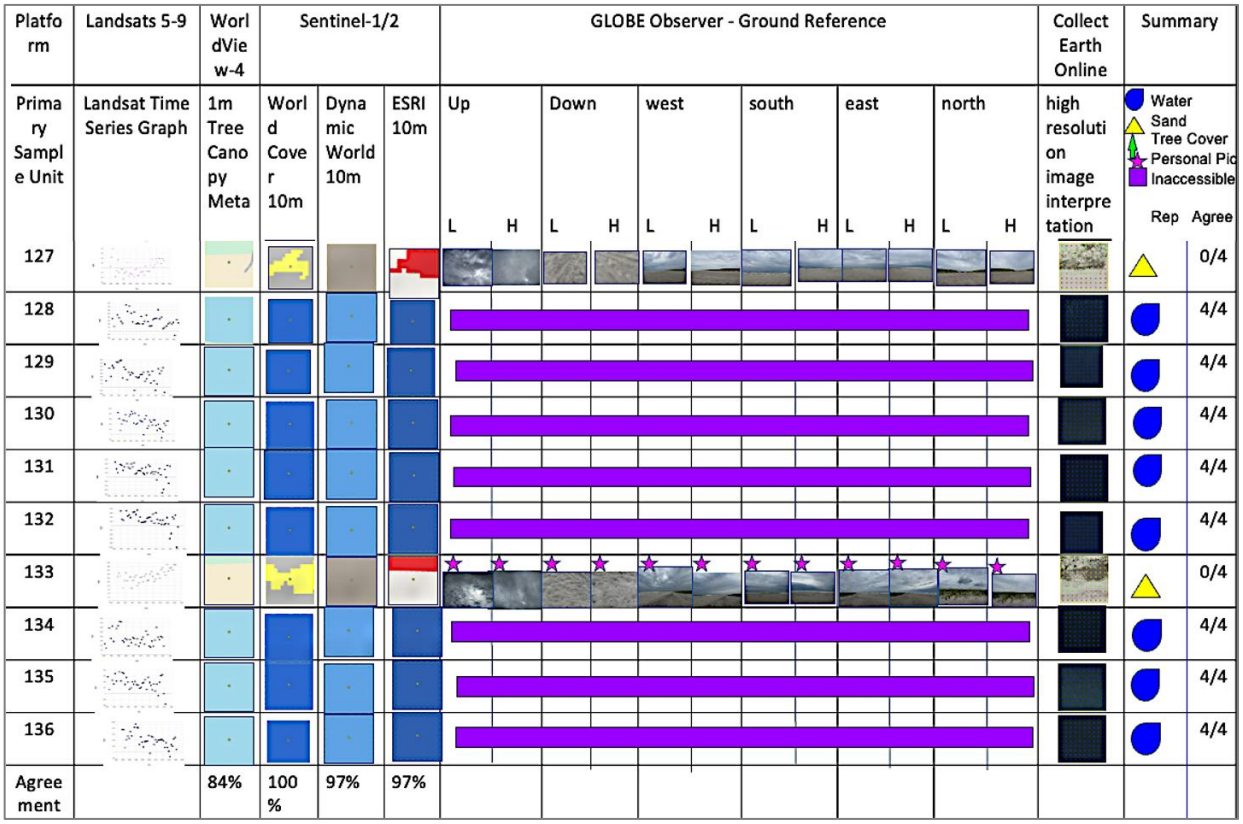

Figure 4. Example of Fire Island Grid 1 Google Slide where the imagery data was organized and compared. "L": Low tide, "H": High tide, "Rep": Representation, "Agree": Agreement among Earth Map layers, "Agreement": Comparison results between Earth Map layers and ground cover photos.

Looking at the land cover types classified through Collect Earth Online, the overall area of interest (AOI) had a high percentage of water or rivers and streams (Figure 5), with the second most percentage of bare ground which can be otherwise known as sand. Knowing that water is the dominant land cover type within the AOI infers the importance of its influence. Especially having water adjacent to bare ground primarily, since those two land cover types are often found side by side, we recognize the area is the dynamic interface of the tide, but we don't initially know the tide levels on the maps.

This additional information also allows us to recognize the possible effects of edge interference between the water and bare ground. An example of the water and sand dynamic interface can be shown by primary sample unit number 109 in the west direction, as shown in Figure 6. At low tide there is an exceptional amount of sand exposed compared to high tide where the entire area is just about covered in water.

At primary sample unit number 109, each Earth Map layer is telling a different story about what you might expect to see at this location. The 1 m Tree Canopy Meta layer tells us that there will be plenty of sand exposure when standing in this PSU. World Cover 10 m and ESRI 10 m appear to be telling a similar story however World Cover classifies the exposed land as "Barren/Sparse Vegetation" while ESRI classifies the exposed land as "Snow/Ice". Dynamic World 10 m represents a location with very little bare ground exposure

A major part of this research is to explore the dynamic interface of the water and sand. The tides allow us to understand just how different a couple of hours can look in one spot. The results showed a significant difference between high tide and low tide among the primary sample units where ground photos were taken, where $p < 0.000$. This tells us the Area of Interest is overall a landscape that is exceptionally dynamic during each day.

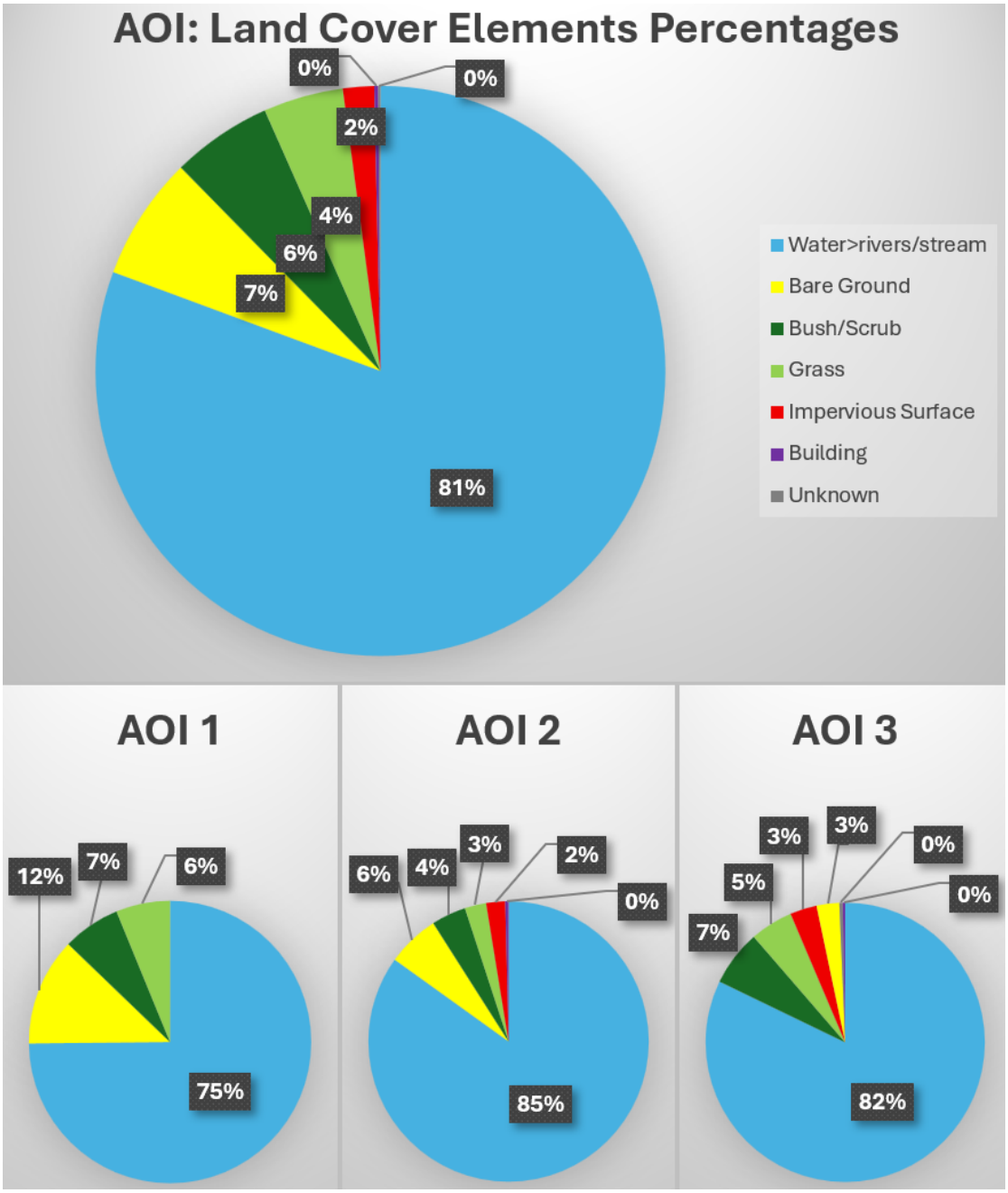

Figure 5. Pie chart of the overall Area of Interest (AOI) and pie charts of each individual AOI (grids), presenting the percentages of the land cover types categorized in Collect Earth Online.

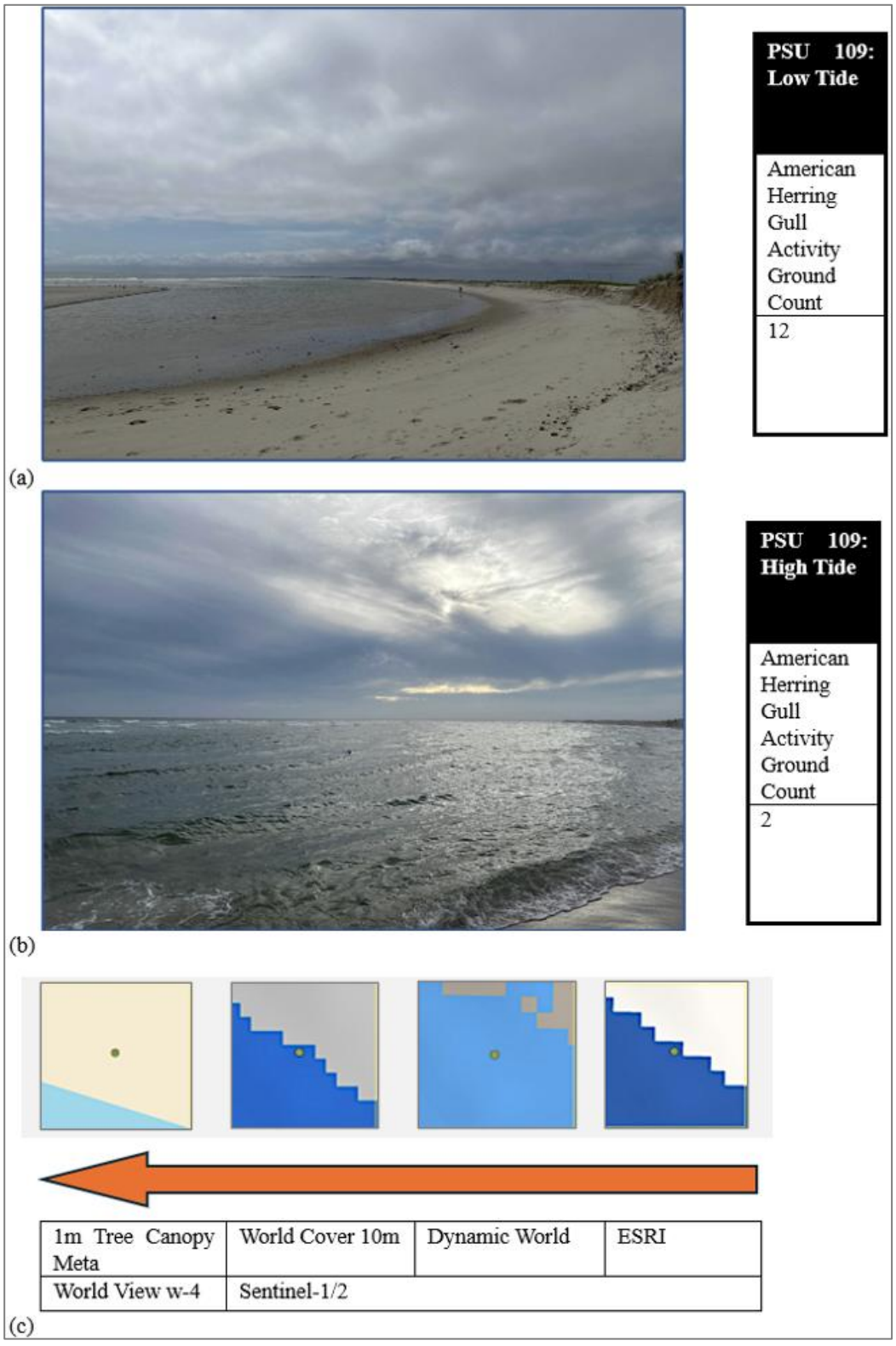

Figure 6. (a) Ground cover photo of primary sample unit number 109 in the West direction at low tide with American herring gull activity, (b) Ground cover photo of primary sample unit number 109 in the west direction at high tide with American herring gull activity, (c) Each Earth Map layer at primary sample unit 109 with its label following underneath the images. An orange arrow exemplifies the direction (west) the ground cover photos were taken.

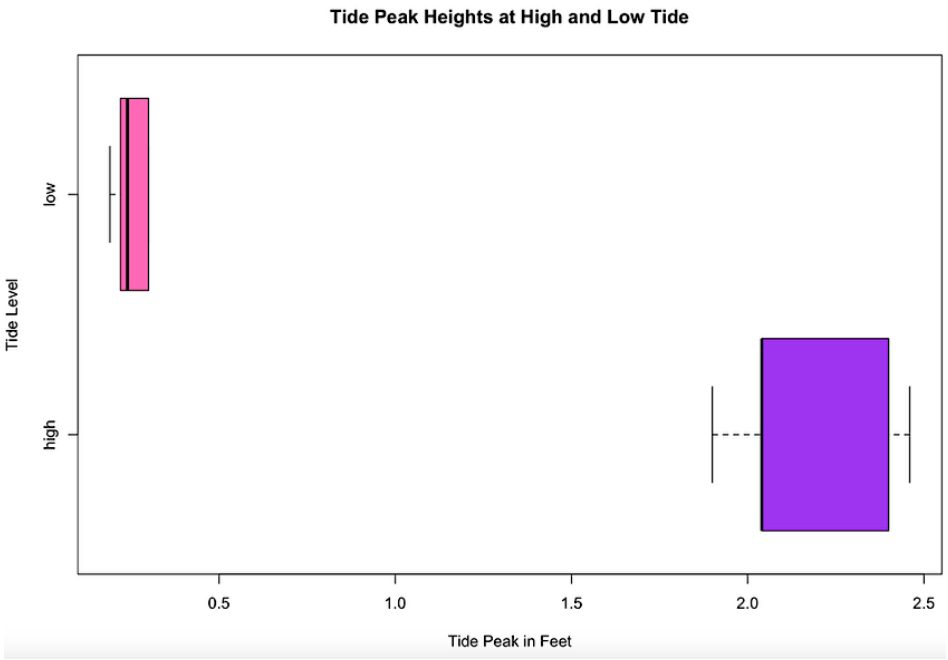

Figure 7. Box plot of the tide peak heights at high and low tide.

Understanding the difference in daily tidal fluctuations allows us to explore the dynamic interface between the water and sand, and utilizing the activity of American herring gulls helps us categorize these differences, along with the ground cover photos. Figure 7 shows the peak heights during low and high tides. The results in Figure 8 also showed a significant difference in American herring gull activity among the primary sample units where data was collected. There was more overall activity for low tide compared to high tide where $p<0.002$. These results tell us that the land is not only dynamic to itself, but it also affects wildlife behavior and the ecology of the area.

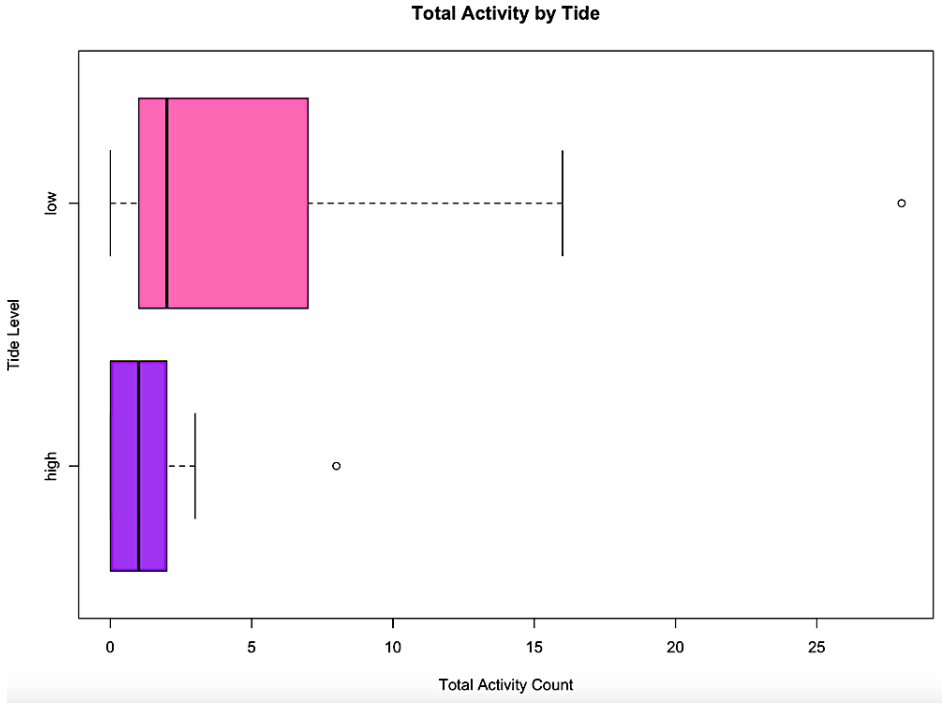

Figure 8. Box plot of total American herring gull activity at high tide and low tide.

Visual assessment, as in Figure 9, shows a land change over time according to Landsat time-series from the years 1984 to 2025. There is more sand deposition on the Northwest area of Fire Island and sand mass fluctuations throughout the West end of the island. This further emphasizes how affected Fire Island is by the daily tidal fluctuations because it ultimately provides long term changes and impacts. Not only do daily tidal fluctuations create a dynamic landscape, but they can have long term impacts on not only the land itself but on the plant and animal life as well.

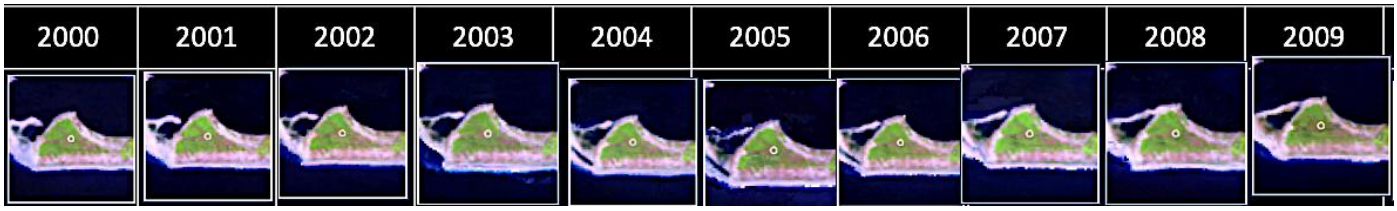

Figure 9. Example of Landsat time-series images of the Grid 1 Google Slide showing land cover change over time.

4. Discussion

The results showed that the land cover layers presented inconsistencies among one another and when compared to ground cover photos. Having 'water>rivers/stream' result in the most dominant land cover type, infers the importance of its significance, especially because water bodies influenced by tides is an ever-changing land cover type. There was also a significant difference in daily tidal fluctuations between high tide and low tide, further exemplifying its fluidity. With the inconsistencies of the satellite images, this may reduce confidence in how accurately land cover is represented. Especially if the information is not regularly updated and improved with its daily to long-term changes.

A significant difference in high tide and low tide in the study area present the result of a drastically changing landscape throughout one day. This is important to know prior to conducting field research on an area because a portion of land may or may not be exposed at certain points of the day. A dynamic landscape may affect many coastal species, and the movement of waves and tides may also influence species diversity and biomass (Brown & McLachlan, 2002). Ignoring tidal changes may overlook geological factors when mapping coastal study areas.

A significant difference in American herring gull activity between high tide and low tide suggests a relationship of American herring gulls with tidal fluctuations and how it affects their behavior. Without accounting for daily land cover changes driven by tides, ecological variation in coastal habitats can be missed.

The study area land had changed over time from the year of 1984 to present, where greater land cover, specifically bare ground, accumulated among the West and Northwest end of Fire Island due to possible longshore drift over the years of 1984-2025. Longshore drift is the transportation of sediment along the coastline and occurs from the movement of prevailing winds that cause an angled wave approach (Internet Geography, n.d.). Longshore drift affects not only the geographic layout but the location of flora and fauna as well, creating a cycle of cause and effect between living and non-living. This information may help support the making of past, present, and future inferences about species' behaviors and another key component to understanding the landscape.

These findings show differences among satellite mapping data sets and when compared with recent ground photos. Providing ground photos may support a more detailed and accurate map interpretation; in addition to providing as many photos and angles as possible. This aligns with the findings of Huang et al. (2023) because it practically implements the practice of putting together ground cover photos with satellite imaging where classification performance of land cover data sets improved as more photo views were added. Not only do the ground cover photos improve data sets for satellite imaging but our study extends from the study done by Geyman & Maloof (2020) where it is exemplified how remote sensing methods for water flux can be used to predict tides and their spatial structure. Bridging citizen science ground photos and tidal predictors may improve the accuracy and usability of data sets for satellite imaging.

There were a few limitations involved in the study. The study was limited in accessible primary sample units, creating a smaller sample size, therefore many undocumented points were deemed in agreement with

the satellite imagery when it may not have been true. While American herring gulls were researched for background and identification purposes, there is a possibility of error in identification being that many gulls are similar in size and color, not to mention the possibility of a mixed species. To eliminate false identification, an American herring gull was only tallied if it was clear and apparent; sound identification was not used. Another limitation included the inability to upload some photos to the GLOBE Observer database through the GLOBE app due to cellular connectivity restrictions and the loss of data from the GLOBE Observer database. To prevent any loss of data entirely, photos were taken on our personal cell phones at each location as precisely as possible compared to the photos we were uploading to the GLOBE app. While the photos uploaded to the GLOBE Observer database are better used for the information collection needed for satellite imaging, collecting personal photos allowed the researchers to still make ground photo comparisons to satellite imagery from Earth Map if data was lost from GLOBE Observer. There is the opportunity to improve the GLOBE observer app by saving information to be uploaded later if connectivity is low.

Future research could include implementing GLOBE observer app ground photos into satellite imagery data sets and projects to maintain accuracy. Testing to see whether satellite imagery improves with the use of ground photos can allow more insight into the importance of citizen science and its role in GIS mapping. Additional future research can test how satellite imagery might be able to implement daily tidal fluctuations and the possible collaboration among organizations with tidal gauges and those with satellite data sets. Also, the creation of a tidal baseline in satellite mapping may be useful to consider to help account for accuracy if other data sets produce maps with tidal representations. Furthermore, another research project like this one can be replicated in the same area after a few years to observe land cover changes, tidal patterns, and species activity. Providing a well-rounded map to citizens and scientists allows for a more comprehensive tool in research and the allowance for multiples disciplines to utilize it.

This project further highlighted how satellite imagery may be influenced by ecological conditions and how it may be improved using citizen science and daily tidal data. The Adopt-a-Pixel Research Framework was also useful as an ecological monitoring tool within this study. Overall, multiple environmental factors may contribute to how satellite imagery data are represented and interpreted. This supports the need for continued refinement and future research in improving satellite imagery interpretation.

5. Conclusions

The aim of this study was to determine land change over time, satellite mapping accuracy, the influence of tidal changes on land cover, and its ecological connection to the American herring gull. Understanding daily land cover changes and tidal fluctuations may provide a more complete interpretation of a study area and how the landscape has changed over time. This may help researchers better anticipate site conditions prior to fieldwork and improve interpretation when field observations are limited. It may also help strengthen the connection between GIS mapping and ecological research.

This study supports the connection between GIS-based satellite mapping systems and ecology-focused research. Land change occurred over time, and both tidal height and American herring gull data showed significance and were accompanied by inconsistencies among satellite imaging. These findings suggest that incorporating tidal markers and ground cover photos may improve the interpretation of satellite imagery for coastal research applications. This approach may provide a more useful tool for interdisciplinary research requiring accurate coastal land cover interpretation.

Funding: This research was supported by the Undergraduate Research, Scholarship, and the Arts (URSA) Engage Program and the College of Science at Oregon State University.

Data Availability Statement: DOI:10.5281/zenodo.18526975

Acknowledgment: I would like to express my sincere gratitude to Peder Nelson for his invaluable guidance, support, and mentorship throughout this project. His expertise, constructive feedback, and encouragement have been instrumental in shaping the development and success of this paper. This material is based upon work supported by the U.S. Geological Survey under Grant/Cooperative Agreement No. G23AP00683 (GY23-GY27). The views and conclusions contained in this document are those of the authors and should

not be interpreted as representing the opinions or policies of the U.S. Geological Survey. Mention of trade names or commercial products does not constitute their endorsement by the U.S. Geological Survey.

Conflicts of Interest: The authors declare no conflicts of interest. The funders had no role in the design of the study; in the collection, analyses, or interpretation of data; in the writing of the manuscript; or in the decision to publish the results.

References

Brown, A.C., & McLachlan, A. (2002, June 05). Sandy shore ecosystems and the threats facing them: some predictions for the year 2025. *Environmental Conservation*. 29(1):62-77. doi:10.1017/S037689290200005X

Brown, C.F., Brumby, S.P., Guzder-Williams, B, Birch, T, Hyde, S.B., Mazzariello, J, Czerwinski, W, Pasquarella, V.J., Haertel, R, Ilyushchenko, S, Schwehr, K, Weisse, M, Stolle, F, Hanson, C, Guinan, O, Moore, R, Tait, A.M. (2022). Dynamic World, Near real-time global 10 m land use land cover mapping. *Sci Data*. 9 (251). https://doi.org/10.1038/s41597-022-01307-4

Daunt, F, Wanless, S, Wilson, L, Peters, G, Gremillet, D, Scott, B, Sharples, J, Ross, O, Greenstreet, S, & Fraser, H. (2002). Effects of tidal currents on seabird foraging behaviour and diet in the North American Sea. *2002 ICES Annual Science Conference, Copenhagen, Denmark*. CM 2002/N:15. https://doi.org/10.17895/ices.pub.25443172

Geyman, E.C., & Maloof, A.C. (2020, January 25). Deriving Tidal Structure From Satellite Image Time Series. *Earth and Space Science*. 7, e2019EA000958. https://doi.org/10.1029/2019EA000958

Gorelick, N., Hancher, M., Dixon, M., Ilyushchenko, S., Thau, D., & Moore, R. (2017). Google Earth Engine: Planetary-scale geospatial analysis for everyone. Remote Sensing of Environment, 202, 18–27. https://doi.org/10.1016/j.rse.2017.06.031.

Huang, X, Yang, D, He, Y, Nelson, P, Low, R, McBride, S, Mitchell, J, Guarraia, M. (2023). Land cover mapping via crowdsourced multi-directional views: The more directional views, the better, *International Journal of Applied Earth Observation and Geoinformation*. 122, 103382. https://doi.org/10.1016/j.jag.2023.103382

Internet Geography. (no date). What is longshore drift? *Internet Geography*. https://www.internetgeography.net/topics/what-is-longshore-drift/. Accessed on [April 9, 2026].

Kang, Y, Lei, J, Wang, M, Guiping, L, & Xianrong, D. (2023, April 27). Topographic evolution of tidal flats based on remote sensing: an example in Jiangsu cost, Southern Yellow Sea. *Front. Mar. Sci.* 10, 1163302. DOI: 10.3389/fmars.2023.1163302

Karra, K., Kontgis, C., Statman-Weil, Z., Mazzariello, J., Mathis, M., & Brumby, S. (2021). *Global land use/land cover with Sentinel-2 and deep learning*. IGARSS 2021: IEEE International Geoscience and Remote Sensing Symposium, 4704–4707. https://doi.org/10.1109/IGARSS47720.2021.9553499

Morales C, Díaz AS, Dionisio D, Guarnieri L, Marchi G, Maniatis D, Mollicone D. Earth Map: A Novel Tool for Fast Performance of Advanced Land Monitoring and Climate Assessment. J. Remote Sens. 2023;3:Article 0003. https://doi.org/10.34133/remotesensing.0003

National Aeronautics and Space Administration (NASA). (2025). Global Learning and Observations to Benefit the Environment (GLOBE) Data User Guide, 2025, version 3.0, https://www.globe.gov.

National Audubon Society, (no date). American Herring Gull. *National Audubon Society*. https://www.audubon.org/field-guide/bird/american-herring-gull. Accessed on [April 9, 2026].

National Oceanic and Atmospheric Administration (NOAA). (2021). What is a barrier island? *National Ocean Service Website*. https://oceanservice.noaa.gov/facts/barrier-islands.html. Last access: April 9, 2026.

National Oceanic and Atmospheric Administration (NOAA). (no date). Fire Island, NY- Station ID: 8515186. *Tides & Currents*. https://tidesandcurrents.noaa.gov/stationhome.html?id=8515186. Accessed on [April 9, 2026].

Nelson, P. (2024). Adopt-a-Pixel Research Framework. Global Learning and Observations to Benefit the Environment. https://storymaps.arcgis.com/stories/3c02bd1d895348e4b2ffc6ddfd5eeca2

Pan, H, Sun, J, Gao, X, Teng, F, Xu, T, & Wei, Z. (2025, July 31). Can we accurately extract ocean tides from satellite altimeter records with substantial missing values in shallow bays? *Estuarine, Coastal and Shelf Science.* 319, 109280. https://doi.org/10.1016/j.ecss.2025.109280

Pendleton, E.A., Williams, S.J., & Thieler, E.R. (2004). Coastal Vulnerability Assessment of Fire Island National Seashore to Sea-Level Rise. *U.S. Geological Survey Open-File Report.* 03-439. https://doi.org/10.3133/ofr03439.

Saah, D., Johnson, G., Ashmall, B., Tondapu, G., Tenneson, K., Patterson, M., Poortinga, A., Markert, K., Nguyen, H. Q., Aung, K. S., Schlichting, L., Matin, M., Uddin, K., Aryal, R. R., Dilger, J., Ellenburg, W. L., Flores-Anderson, A. I., Wiell, D., Lindquist, E., Goldstein, J., Clinton, N., & Chishtie, F. (2019). Collect Earth: An online tool for systematic reference data collection in land cover and use applications. Environmental Modelling & Software, 118, 166–171. https://doi.org/10.1016/j.envsoft.2019.05.004

Stevens, J, Smith, J.M., & Bianchetti, R.A. (2012), *Mapping Our Changing World,* Editors: Alan M. MacEachren and Donna J. Peuquet, University Park, PA: Department of Geography, The Pennsylvania State University.

Tolan, J, Yang, H, Nosarzewski, B, Couairon, G, Vo, H.V., Brandt, J, Spore, J, Majumdar, S, Haziza, D, Vamaraju, J, Moutakanni, T, Bojanowski, P, Johns, T, White, B, Tiecke, T, Couprie, C. (2024, January 01). Very high resolution canopy height maps

from RGB Imagery using self-supervised vision transformer and convolutional decoder trained on aeriel lidar. *Remote Sensing of Environment*. 300, 113888. https://doi.org/10.1016/j.rse.2023.113888

Vos, K, Splinter, K.D., Palomar-Vazquez, J, Pardo-Pascual, J.E., Almonacid-Caballer, J, Cabezas-Rabadan, C, Kras, E.C., Luijendijk, A.P., Calkoen, F, Almeida, L.P., Pais, D, Klein, A.H.F., Mao, Y, Harris, D, Castelle, B, Buscombe, D, & Vitousek, S. (2023, September 29). Benchmarking satellite-derived shoreline mapping algorithms. *Communications Earth & Environment*. 4, 345 (2023). https://doi.org/10.1038/s43247-023-01001-2

Weseloh, D. V., C. E. Hebert, M. L. Mallory, A. F. Poole, J. C. Ellis, P. Pyle, and M. A. Patten (2024). American Herring Gull (Larus smithsonianus), version 1.0. In Birds of the World (B. K. Keeney and S. M. Billerman, Editors). Cornell Lab of Ornithology, Ithaca, NY, USA. https://doi.org/10.2173/bow.amhgul1.01

Wetlands International. (2018). Guidance on waterbird monitoring methodology: Field Protocol for waterbird counting. *Wetlands International*. Ede, Netherlands. https://iwc.wetlands.org/static/files/IWC-Guidance-on-waterbird-monitoring-methodology-2018-1.pdf

Zanaga, D, Van De Kerchove, R, De Keersmaecker, W, Souverijns, N, Brockmann, C, Quast, R, Wevers, J, Grosu, A, Paccini, A, Vergnaud, S, Cartus, O, Santoro, M, Fritz, S, Georgieva, I, Lesiv, M, Carter, S, Herold, M, Li, Linlin, Tsendbazar, N.E., Ramoino, F, Arino, O. (2021). ESA WorldCover 10 m 2020 v100. https://developers.google.com/earth-engine/datasets/catalog/ESA_WorldCover_v100

Appendix 1. Land cover types labeled in Collect Earth Online and agreement percentages among the four Earth Map layers assessed. An asterisk (*) is marked for the primary sample units with field data collection.

Primary Sample Unit	Land Cover Type Percentages (%)	Land Cover Labels (Collect Earth Online)	Agreement Percentage (%) Among Earth Map Layers
100	100	Bush/Scrub	0
101	100	Water>rivers/stream	100
102	100	Water>rivers/stream	100
103	100	Water>rivers/stream	100
104	8, 92	Bush/Scrub, Bare Ground	50
105	100	Water>rivers/stream	100
106	25, 29, 46	Bush/Scrub, Water>rivers/stream, Bare Ground	0
107	100	Water>rivers/stream	100
108	100	Water>rivers/stream	100
109*	21, 79	Bare Ground, Water>rivers/stream	0
110*	100	Bare Ground	0
111	100	Water>rivers/stream	100
112	100	Water>rivers/stream	100
113	100	Water>rivers/stream	100
114	100	Water>rivers/stream	100
115*	5, 45, 50	Grass, Bare Ground, Bush/Scrub	0
116	100	Bush/Scrub	50
117	100	Water>rivers/stream	100
118	100	Water>rivers/stream	100
119	100	Water>rivers/stream	100
120	100	Water>rivers/stream	100
121*	6, 37, 57	Bush/Scrub, Bare Ground, Grass	0
122	39, 61	Bare Ground, Water>rivers/stream	0
123	100	Water>rivers/stream	100
124	100	Water>rivers/stream	100
125	100	Water>rivers/stream	100
126	100	Water>rivers/stream	100
127*	43, 57	Bare Ground, Grass	0
128	100	Water>rivers/stream	100
129	100	Water>rivers/stream	100
130	100	Water>rivers/stream	100
131	100	Water>rivers/stream	100
132	100	Water>rivers/stream	100
133*	1, 29, 70	Bush/Scrub, Bare Ground, Grass	0
134	100	Water>rivers/stream	100
135	100	Water>rivers/stream	100
136	100	Water>rivers/stream	100
200*	1,6, 15, 17, 61	Bare Ground, Building, Impervious Surface, Grass, Bush/Scrub	0
201	100	Water>rivers/stream	100
202	100	Water>rivers/stream	75
203*	3,8,14, 27, 48	Bush/Scrub, Building, Grass, Bare Ground, Impervious Surface	0
204	100	Water>rivers/stream	100
205	100	Water>rivers/stream	100
206	100	Water>rivers/stream	100
207	100	Water>rivers/stream	100
208	100	Water>rivers/stream	100
209*	33, 67	Grass, Bare Ground	50

Primary Sample Unit	Land Cover Type Percentages (%)	Land Cover Labels (Collect Earth Online)	Agreement Percentage (%) Among Earth Map Layers
210	100	Water>rivers/stream	100
211	100	Water>rivers/stream	100
212	100	Water>rivers/stream	100
213	100	Water>rivers/stream	100
214	100	Water>rivers/stream	100
215*	3, 10, 87	Grass, Water>rivers/stream, Bare Ground	75
216	100	Water>rivers/stream	100
217	100	Water>rivers/stream	100
218	6, 24, 70	Bare Ground, Bush/Scrub, Water>rivers/stream	0
219	100	Water>rivers/stream	100
220	100	Water>rivers/stream	100
221*	36, 64	Bare Ground, Water>rivers/stream	75
222	2, 98	Impervious Surface, Water>rivers/stream	75
223	100	Water>rivers/stream	100
224	100	Water>rivers/stream	100
225	100	Water>rivers/stream	100
226	100	Water>rivers/stream	100
227*	100	Water>rivers/stream	100
228	100	Water>rivers/stream	100
229	100	Water>rivers/stream	100
230	100	Water>rivers/stream	100
231	100	Water>rivers/stream	100
232	100	Water>rivers/stream	100
233	100	Water>rivers/stream	100
234	16, 24, 60	Impervious Surface, Grass, Bush/Scrub	0
235	100	Water>rivers/stream	100
236	100	Water>rivers/stream	100
300	14, 28, 58	Impervious Surface, Grass, Bush/Scrub	0
301	100	Water>rivers/stream	100
302	100	Water>rivers/stream	100
303	1, 22, 36, 41	Building, Impervious Surface, Grass, Bush/Scrub	0
304	100	Water>rivers/stream	100
305	100	Water>rivers/stream	100
306	100	Water>rivers/stream	100
307	100	Water>rivers/stream	100
308	100	Water>rivers/stream	100
309*	5, 12, 25, 58	Bare Ground, Bush/Scrub, Grass, Impervious Surface	0
310	100	Water>rivers/stream	100
311	100	Water>rivers/stream	100
312	100	Water>rivers/stream	100
313	100	Water>rivers/stream	100
314	100	Water>rivers/stream	100
315*	1, 5, 37, 57	Impervious Surface, Unknown, Grass, Bare Ground	100
316	2, 18, 80	Bare Ground, Bush/Scrub, Water>rivers/stream	75
317	100	Water>rivers/stream	100
318	100	Water>rivers/stream	100
319	100	Water>rivers/stream	100
320	100	Water>rivers/stream	100

Primary Sample Unit	Land Cover Type Percentages (%)	Land Cover Labels (Collect Earth Online)	Agreement Percentage (%) Among Earth Map Layers
321*	13, 87	Bare Ground, Water>rivers/stream	100
322	1, 7, 19, 73	Grass, Bare Ground, Bush/Scrub, Water>river/stream	0
323	100	Water>rivers/stream	100
324	100	Water>rivers/stream	100
325	100	Water>rivers/stream	100
326	100	Water>rivers/stream	100
327	100	Water>rivers/stream	100
328*	2, 10, 12, 20, 56	Grass, Building, Bare Ground, Impervious Surface, Bush/Scrub	0
329	100	Water>rivers/stream	100
330	100	Water>rivers/stream	100
331	100	Water>rivers/stream	100
332	100	Water>rivers/stream	100
333	100	Water>rivers/stream	100
334*	1, 9, 36, 54	Bare Ground, Unknown, Bush/Scrub, Grass	0
335	100	Water>rivers/stream	100
336	100	Water>rivers/stream	100

Best Practice

Qualitative Analysis of Application Remote Sensing towards the Understanding of a Rural Community

Charles Quinn[1,*], Peder V. Nelson[2], and Russanne Low[3]

[1] 11th Grade, Bernards High School, Bernardsville, NJ; https://orcid.org/0009-0003-7110-7024
[2] Oregon State University, OR; peder.nelson@oregonstate.edu; https://orcid.org/0000-0003-3979-9051
[3] Next Generation Global Observatory, NY; low.russanne@gmail.com; https://orcid.org/0000-0002-7912-4350
[*] Corresponding Author: cpquinn2027@gmail.com; +1-908-432-4880

Academic Editor: Jeong Chang Seong

Received: 28 February 2026
Revised: 4 April 2026; 16 April 2026
Accepted: 20 April 2026
Published: 30 April 2026

Abstract: Remote sensing and human observation provide the resources necessary to view changes in land cover and land use (LULC) in an area of interest (AOI). Remote sensing tools have limitations and fail to accurately summarize areas individually. However, tools can be used in collaboration with human observation in order to better analyze an area and overcome their limitations. To accomplish this, numerous datasets such as the 1984–2024 Multi-Resolution Land Characteristics (MRLC), National Land Cover Database (NLCD) Viewer, various layers available in Earth Map digital software from the baseline year 2020, 1984-2025 Landsat satellite imagery, Collect Earth Online (CEO), and ground observations from the Global Learning and Observations to Benefit the Environment (GLOBE) Observer application were synthesized and analyzed. In order to collect data from the same places across all datasets, an AOI measuring 3 km by 3 km was constructed. This AOI contained 37 kernels, each measuring 10,000 m². The kernels were constructed into a 6 × 6 matrix, and the final kernel was placed in the center, totaling 37 kernels. In analyzing these datasets holistically, inconsistencies were found between remote and ground observations. Each provided important information but was sometimes inconsistent. The synthesis of remote and ground datasets, however, was able to shed light on the LULC of the study area and provide an understanding of how it has changed over time. It was found that the study area had a relatively harmonious relationship between urban/built-up elements and vegetation, but that multiple tools were needed to draw this conclusion.

Keywords: land cover, urbanization, vegetation

1. Introduction

The land we live on is instrumental in affecting how we shape our societies, earn a living, and choose where to settle. Land naturally changes over time, but human settlement changes it, too. These changes—both natural and artificial—make up the study of land cover and land use (LULC). There are numerous ways to collect and analyze LULC data. Methods include ground observations and analysis, as well as remote sensing and aerial photography. Each tool has its respective strengths and weaknesses. This study aims to understand how different tools describe Bernardsville, NJ and shed light on Bernardsville's LULC. It is hypothesized that each method of analyzing LULC (i.e., remote sensing, ground observations, aerial images) will provide the same information and conclusions about Bernardsville, NJ. In evaluating the quality and consistency of datasets, the study attempts to recognize whether differences reflect weaknesses in the tools. The paper aims to highlight the inconsistencies in the analysis of LULC in the study area. This sort of understanding could make the region viable for a quantitative analysis described in papers such as "The Sensitivity of Mapping Methods to Reference Data Quality: Training Supervised Image Classifications with Imperfect Reference Data" (Foody et al., 2016).

Citation: Quinn, C., Nelson, P.V. & Low, R. (2026). Qualitative Analysis of Application Remote Sensing Towards the Understanding of a Rural Community. Journal of Earth Observation and Geospatial Applications, 2(1), 28–38. https://doi.org/10.65372/kyjbrw63

2. Study Area and Methods

2.1. Study Area

The chosen area for this study is Bernardsville, NJ. Located in central New Jersey, Bernardsville is a community of 8,020 people (U.S. Census Bureau, 2025). The town is an example of a suburb of New York City, where some residents commute for work, but it is also a rural area with dense forest and farms populated with familial estates. Bernardsville boasts a diverse population with people from a diverse set of backgrounds, including Irish, Italian, and Guatemalan. An outdoor lifestyle makes up a significant portion of community recreation as seen in town amenities such as the town pool, pickleball courts, and turf fields. Recently, Bernardsville has increasingly experienced extreme weather. Heat anomalies are becoming more prevalent, with warmer winters and summers each year. The town was also affected by Hurricanes Irene and Sandy but sustained no extreme damage, although many trees fell. A map of Bernardsville in greater New Jersey context can be seen in Figure 1.

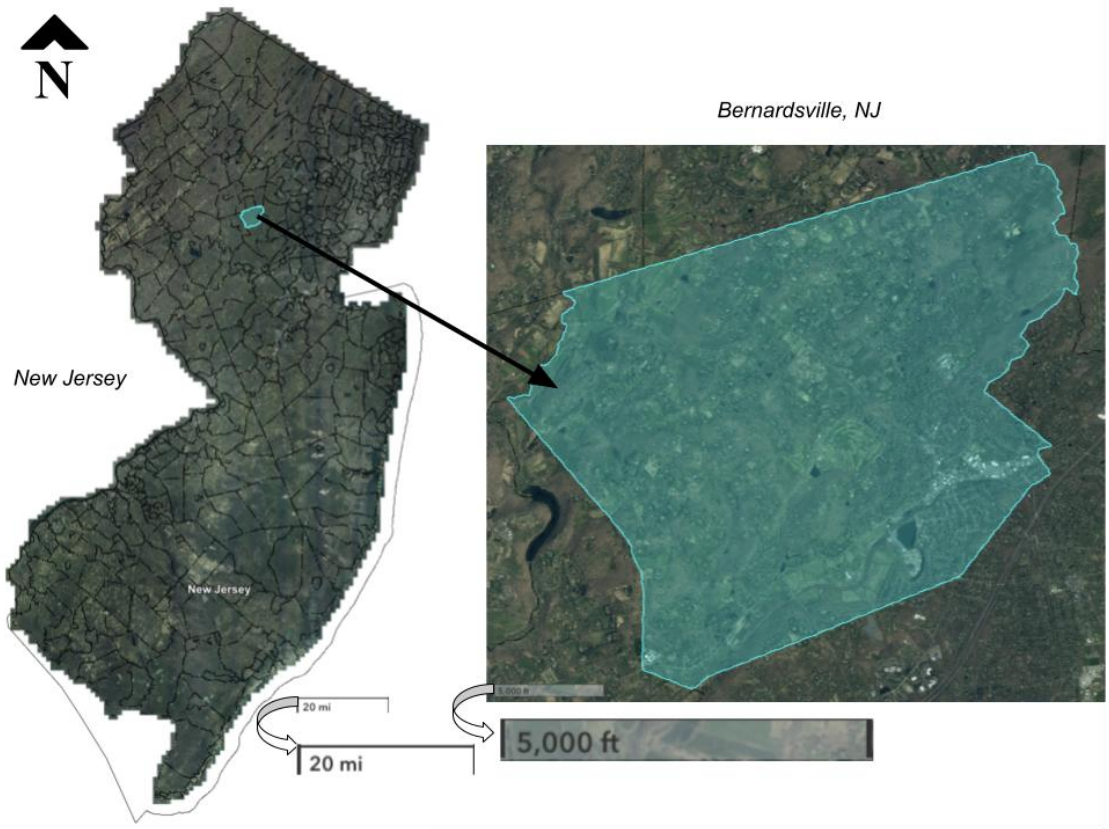

Figure 1. Map of Bernardsville, NJ, created using the NJ Highlands Resource Explorer.

2.2. Methodology and Tools

Changes in Bernardsville's land cover were documented and analyzed using multiple open-source cloud-based software tools in line with the Adopt-a-Pixel-3km (AaP3km) methodology. The AaP3km methodology is a citizen science-based approach in which a researcher selects an area of interest (AOI), divides it into evenly spaced points, and applies a variety of scientific tools to that AOI in order to analyze its LULC (Low et al., 2021). In this study, a 9 km² AOI was constructed. This AOI consisted of 36 evenly spaced points and one center coordinate, totaling 37 distinct locations. Based on the location of the centroid, some points fell outside of Bernardsville but were no more than 2,000 feet from the border. Each point was enclosed within a 10,000 m² bounding box; these 10,000 m² areas will be referred to as kernels. The kernels were numbered 0–36, where 0 was the center. Kernel one is in the bottom-left corner, and the numbering goes upwards in each column, returning to the bottom row once an entire column has been counted. The AOI grid was stored as a GeoJSON and Comma-Separated Values (CSV) file so that it could be used for different software later.

The Global Learning and Observations to Benefit the Environment (GLOBE) Observer application was used to capture ground-truth images within each 10,000 m² kernel. These images were recorded in the four cardinal directions, up, and down in each kernel. If locations were inaccessible due to private property restrictions or natural barriers, the respective ground photos do not appear in the analysis or the dataset for accuracy. These photographs were then uploaded to the GLOBE network through the GLOBE Observer application. The process of how observations are submitted on the application is outlined in Figure 2. Figure 2 demonstrates the ease with which locations can be documented and recorded. The uploading of these images allows the photos to be accessed later and ensure they were properly stored in a database.

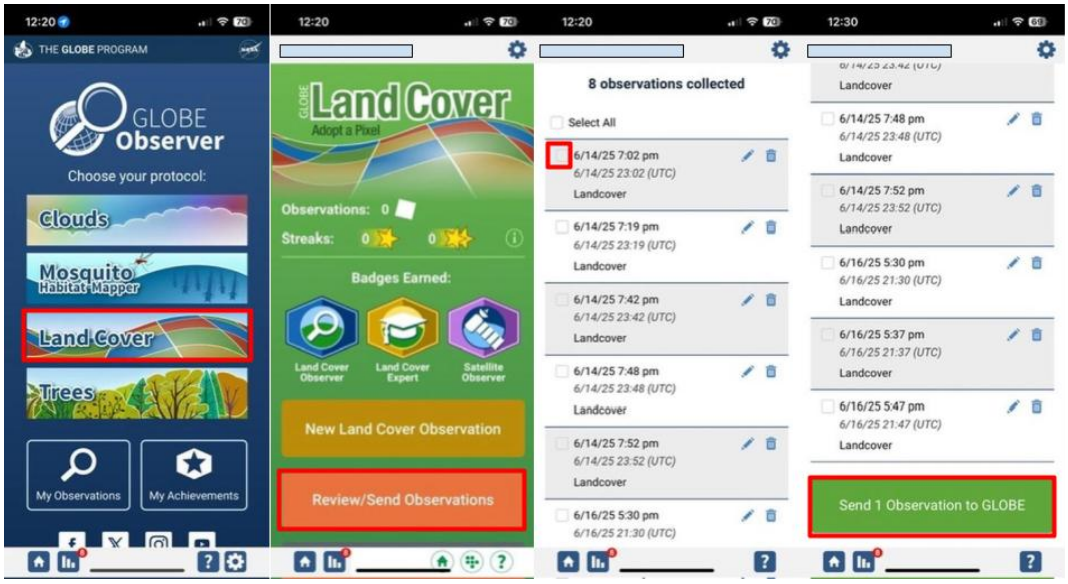

Figure 2. Example submission using the GLOBE Observer application.

The Collect Earth Online (CEO) software was then used to manually classify the land cover profile of each point using aerial photos. CEO is a service designed to bring LULC research to citizen scientists by having them classify imagery for LULC. These classifications are then applied to answer research questions or set baselines for making new satellite datasets (Saah et al., 2019). The software broke each kernel into 100 sub-points. From there, each kernel was magnified to a scale of 20 m for consistency. Then, all 3,700 generated points (37 kernels multiplied by 100 sub-points per point) were classified into one of the following categories: Trees_CanopyCover, Bush/Scrub, Grass, Cultivated Vegetation, Water > Lake/Ponded/Container, Water > Rivers/Stream, Water > Irrigation Ditch, Shadow, Unknown, Bare Ground, Building, Impervious Surface (no building), or Wetlands (Saah et al., 2019). Each filled kernel was assigned a confidence score by the user, and each kernel was assigned percentages of land cover based on the classifications of the 100 sub-points.

Earth Map's mapping software provided four different satellite datasets for the AOI and each kernel within the AOI. This information was recorded by applying the satellite dataset to a map of the AOI and then screenshotting the resulting map and bar graph generated for each kernel. Four satellite datasets were utilized: WorldView-4's Meta 1 m Tree Canopy, Sentinel 1 and 2's 10 m World Cover, Sentinel 1 and 2's 10 m Dynamic World, and Sentinel 1 and 2's 10 m ESRI. The Meta 1 m Tree Canopy package is designed to track forest ecosystems by tracking canopy height at a 1 m resolution using a mixture of temporal readings from 2009–2020 and artificial intelligence; its readings are within a mean absolute error of 2.8 m (Tolan et al., 2023). World Cover is a product designed to take readings from Sentinel 1 and 2 and classify them into one of 11 land classes at a 10 m resolution from 2020 and 2021 (Zanaga et al., 2021). Dynamic World is a satellite package that takes data from Sentinel 2 and uses deep learning to classify it; it updates with speeds as little as 2–5 days and presents the average reading of a point from the past year (Brown et al., 2022). The ESRI satellite package operates using the same satellites as World Cover and Dynamic World but runs it through an AI model trained with human classified observations into one of 9 classes of land; it has an accuracy of 75% (Karra et al., 2021). These filters were used to assess the land cover composition of an area. 2020 was used as a baseline for all four datasets in order to ensure consistency from a measuring standpoint. Figure 3 displays the resulting maps from processing the AOI with each satellite package.

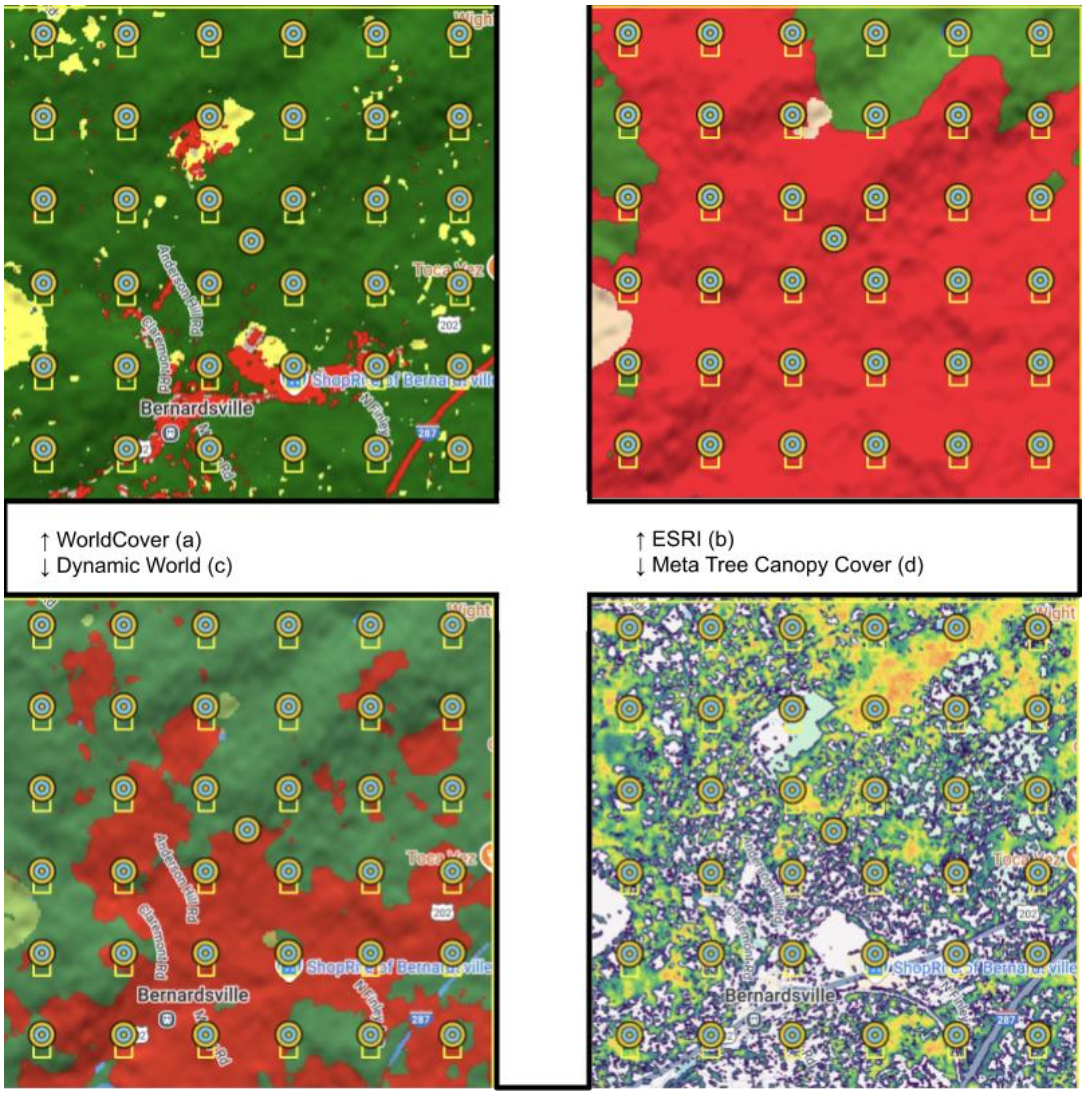

Figure 3. The AOI viewed through various satellite datasets. (a) The AOI viewed through the World Cover satellite package. Yellow refers to grassland, green to trees, red to built-up, pink to cropland, and blue to open water (Zanaga et al., 2021). (b) The AOI viewed through the ESRI satellite package. Red refers to built-up, green refers to trees, and khaki refers to rangeland (Karra et al., 2021). (c) The AOI viewed through the Dynamic World satellite package. Red refers to built-up, dark green refers to trees, light green refers to grass, and blue refers to water (Brown et al., 2022). (d) The AOI viewed through the Meta Tree Canopy Cover satellite package. Cool colors refer to trees and warmer colors refer to taller trees. All heights are on the interval 2 m to 30 m (Tolan et al., 2023).

The next remote sensing platform used was the Landsat time-series (LTS) through Google Earth Engine software. Data from the LTS were used to measure and analyze land cover change in the AOIs during the period of 1984 to 2025. To gather the LTS data for each kernel, the longitude and latitude were uploaded to Google Earth Engine, which generated an LTS map and Normalized Burn Index (NBR) graph of the region in each year from 1984 to 2025 (Gorelick et al., 2017). NBR measures vegetation health and can be used to determine whether vegetation is natural or controlled. High, scattered values indicate healthy, natural vegetation; low values indicate a lack of vegetation; and consistent values indicate maintained vegetation. A kernel's graph with high values and scattering is exhibited in Figure 4. Points on the graph reflect annual NBR readings. The higher values are green while lower values are purple/brown. These graphs were generated for all 37 kernels. In addition to generation of NBR vs. time graphs for each kernel, Earth Engine generated an overlaid NBR map of the AOI for each year. These maps can be seen in Figure 7. Note the yearly consistency.

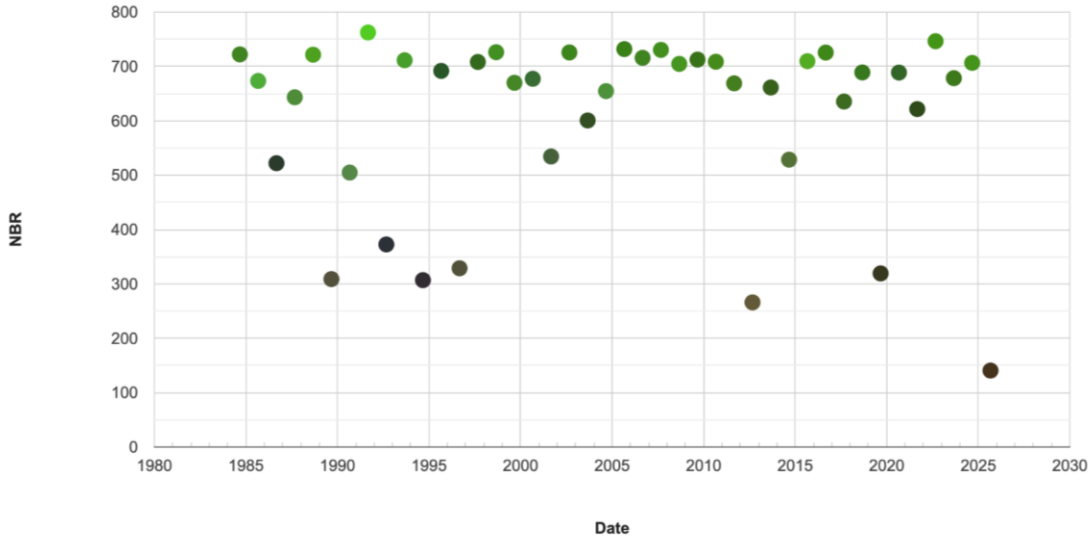

Figure 4. An example of a NBR graph generated from Google Earth Engine.

Changes in land cover were also measured using the Multi-Resolution Land Characteristics (MRLC) National Land Cover Database (NLCD) package (USGS, 2024). MRLC provides NLCD data from 1984–2024. The bounding box for the AOI was input to MRLC using the centroid's latitude and longitude coordinates. However, it is possible that the entire AOI was not covered by MRLC since it rounded to five decimal places for longitude and latitude, whereas the rest of the services offered more accuracy, location-wise, allowing for complete coverage of the AOI. The Annual NLCD package was downloaded, offering sub-packages that presented comprehensive overviews of each AOI through different lenses, such as land cover use trends, impervious surface expansion, tree canopy development, spectral changes, and more. The sub-packages of Fractional Impervious Surfaces (FIS) and Tree Canopy Cover (TCC) were selected to analyze the change in urbanization and the change in vegetation size (USGS, 2024). These sub-packages were selected since the four satellite packages displayed high concentrations of vegetation and impervious surfaces as seen in Figure 4. Each sub-package presented data in the form of a heatmap GIF that displayed its changing concentrations in the region, where one frame represented one year. The download also provided the statistical data in XML files for their respective GIFs. Lastly, each individual frame was provided as a TIFF image. All data was then assembled into a grid in order to organize data and optimize ease of viewing and analysis.

2.3. Data

Bernardsville was classified differently by each satellite package dataset. These differences can be visualized in Figure 3, but also through the statistical data Earth Map provides along with each map. World Cover classified Bernardsville as nearly all forest/greenery (includes both trees and grass), 89.2% forest/greenery by ha, while ESRI classified it as nearly all impervious surfaces and buildings: 3.0% forest/greenery by ha (Karra et al., 2021; Zanaga et al., 2021). Dynamic World provided a reading of 57.4% by ha for Trees and 41.2% by ha for Built-Up land cover. Meta 1 m Tree Canopy demonstrated an abundance of trees with a mean height of 9.53 m, but the AOI map demonstrates there are regions with a much higher tree density than others (Tolan et al., 2023). Collect Earth Online demonstrated a mix of both but indicates that tree canopy primarily describes the majority of the kernels (Saah et al., 2019). MRLC's NLCD packages demonstrate another trend that shows the land cover has had an increase in impervious surface and decrease in canopy cover over time, but both changes were relatively minute. These changes can be visualized in Figure 5. These small changes were marked by rises and drops in the mid-2010s, but they have relatively leveled out within the past 5 years. Bernardsville's land cover currently rests at around 61.5% tree cover. The drop in canopy cover (~5%) was likely the result of expansion projects and hurricanes in 2011 and 2012, as similar large drops are not present in more recent years.

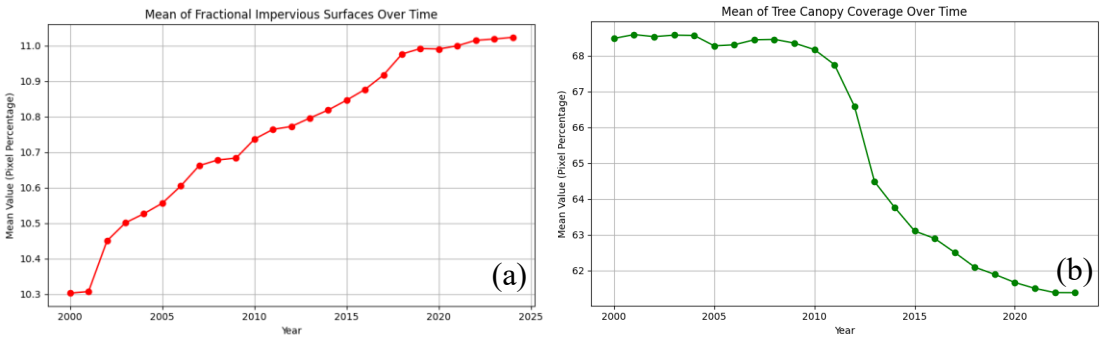

Figure 5. (a) Impervious surfaces vs. Time. (b) Tree canopy cover vs. Time. Graphs from the MRLC NLCD data, courtesy of Vineeth Erram.

3. Results

With the data collected, it became possible to compare and contrast them. To do so, the pictures were arranged for visual analysis. This allowed simultaneous viewing and comparison of the datasets. Selected rows from this grid display results for their respective kernels. Each row of the grid features a kernel's LTS graph, map and bar graph for all four satellite packages, its GLOBE Observer ground-based imaging, and its CEO classifications. These selected rows can be seen in Figure 6.

Comparisons were first made between the four satellite packages. As seen in Figures 4 and 6, the Meta 1 m Tree Canopy dataset demonstrates that there is an abundance of trees in the area. This is indicated by the near complete coverage of the map in Figure 3 and tree presence in every selected kernel's map. Bernardsville thus has an abundance of tree cover. This is further confirmed by the GLOBE Observer imagery, in which trees are present in each selected kernel. These trees could cause classification issues for the other datasets, however. Dynamic World and World Cover's maps show near-total "Tree" classification in the areas where tree canopy is highest; this can be visualized using Figure 3. This could be the result of the trees' height and density, blocking features such as roads and houses underneath the canopy from being captured. Hence, these homes and roads have the potential to go unnoticed by satellites and aerial services such as CEO. Thus, there is a demonstrated need for ground observations underneath the canopy to comprehensively analyze the land cover. This explains the differences in the land cover exhibited in the GLOBE Observer photographs of each kernel and its respective imagery. There is also similar disagreement between CEO observations and GLOBE Observer photographs. This disagreement between CEO and GLOBE Observer is marked by a camera flashing emoji as seen in Figure 6. The tree canopy in Bernardsville thus creates limitations when trying to analyze land cover using remote sensing or aerial analysis. It demonstrates the need to have ground truth imagery to compare the disagreements to. Without having a baseline truth to compare to, the analysis of LULC becomes more difficult.

Figure 6. Selected points from the grid containing data from various tools.

In analyzing where the four sets differed from one another and comparing them to CEO and GLOBE Observer, the data revealed other patterns. One of these patterns was that ESRI tended to make major generalizations by over-classifying built-up areas. There are instances where ESRI marked land as built up when CEO and GLOBE Observer observations showed opposite results. Figure 6 demonstrates this pattern in kernel 34, where it was documented by CEO and GLOBE Observer to be forested and grassland, but ESRI classified it as "Built-Up." Hence, it may be that ESRI serves better as an indicator for land use; this is because kernel 34 is a residential property. The majority of Bernardsville's vegetation and canopy are used for urban activities such as athletics or other outdoor events. This could demonstrate that ESRI tried to account for the fact that it was not reaching the ground due to canopy cover and compensated through its AI model to classify it as "Built-Up."

World Cover seems to overgeneralize opposite to ESRI, classifying a large portion of the AOI as "Tree." As seen with kernel 25 in Figure 6, there is a parking lot that is not captured by World Cover. Rather it classifies the area as forested, but GLOBE Observer images disprove this providing the knowledge there is development underneath. This is likely the result of the abundance of canopy within the region.

Dynamic World does not have the same degree of inconsistency as ESRI or World Cover. Dynamic World overgeneralizes both "Tree" in certain areas and "Built-Up" in others. Dynamic World's overgeneralization of "Built-Up" can be seen through kernel 0 in figure 26, where the lawns, bushes, and trees go undetected. Dynamic World overgeneralizes to "Tree" as seen through kernel 25 of figure 6, where the parking lot on the ground is not read by the satellite.

Analyzed holistically, the satellites' errors in land cover distinction could mean that a spatial resolution of 10m (as used in all 3 satellite packages) may not be small enough to classify Bernardsville, especially given its high tree density. It demonstrates the need for ground observations when possible because that provides comparable truth reading. None of the three LULC satellite packages picked up Bernardsville extremely well, rather, they all made generalizations that tended to be inaccurate when compared to the ground truth observations.

The LTS data demonstrates that Bernardsville's LULC has remained relatively the same over the past 40 years. There is an abundance of green (reflected by the canopy) in every frame as seen in Figure 7. The green does not deteriorate over time. It does fluctuate over some years, such as 1992, 1996, or 2003, but it returns to the same vibrant green reflectance every time after dipping. These anomaly years have been hypothesized to be years in which trees did not gain their leaves until later in the season, thus giving them less time to reflect green back to the satellites, accounting for the changes. There are no repeated years in which there is a notable lack of green. There is also little deviation in the green and brown colors reflected in the LTS except for 1986, where there is lots of purple/blue as seen in Figure 7. Given that these colors indicate pavement and buildings in addition to an understanding of Bernardsville's history, it can be inferred that the change was either the construction or expansion of Bernardsville's local shopping plaza. This plaza is still standing today and happened to be one of the kernels. This kernel can be seen in Figure 6 as kernel 20. It was one of the few kernels where the satellite packages showed more agreement than not, as the satellite packages classified it as built up. CEO and GLOBE Observer corroborate this conclusion about kernel 20, too, making it one of the few kernels where every dataset showed significant agreement. The satellite datasets, however, did miss some shrubbery in the kernel, but this is likely due to their spectral resolution rather than generalization.

The MRLC NLCD, TTC, and FIS data tell the same story: there is very little change. The NLCD image chip looks essentially the same across all 40 years with some ebb and flow. The overall shape and composition of land cover remains generally the same. As seen in Figure 5, Bernardsville has only gained ~1% impervious surface and lost ~6% of tree canopy across 20 years. Part of the loss in canopy could be attributed to damage from hurricanes as well, especially given that the largest drops occur in 2011 and 2012—the same years as Hurricanes Irene and Sandy respectively. Even though the magnitude of the canopy's change was larger than that of the impervious surfaces, it still makes up >60% of all land cover within the area, and impervious surfaces make up ~11%, showing little land cover change in context of the entire area. Figure 7's display of the NLCD data shows the same story, with expansion of the red (built up regions) and little change in the other green (trees) regions.

Our analysis leads us to reject the hypothesis that every dataset would show the same trends and thus the same conclusions about the LULC in an AOI.

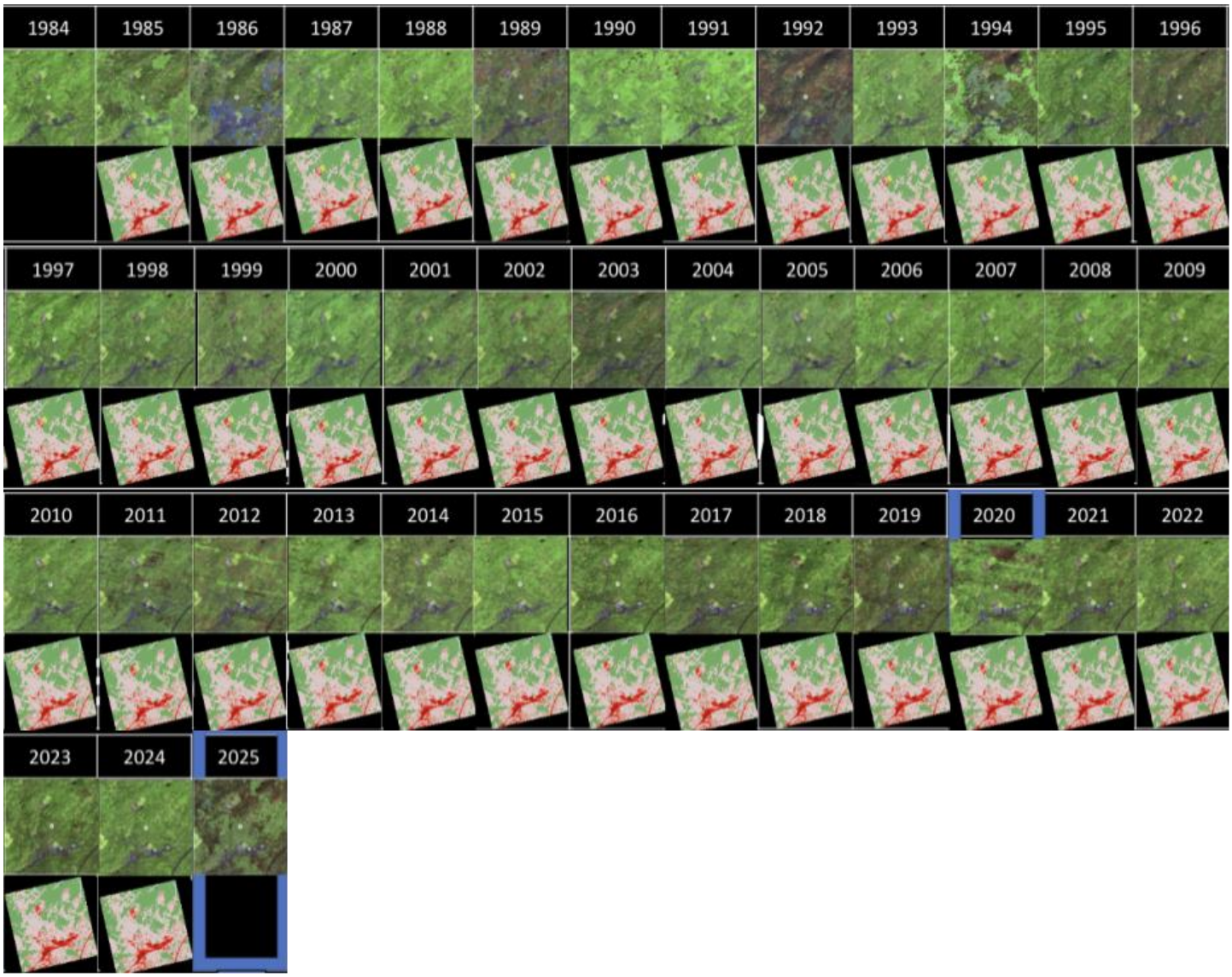

Figure 7. LTS and NLCD data. Landsat is on top, NLCD is on the bottom. LTS data shows NBR maps where green tones represent higher NBR values and brown/blue colors represent lower NBR values (Gorelick et al., 2017). In the NLCD data, green represents deciduous forest, khaki represents grassland, and red represents developed land, the darker the red, the more concentrated the development (USGS, 2024).

4. Discussion

Analysis of Bernardsville requires multiple tools to be synthesized in order to provide a strong understanding of LULC in the area. This study confirms the ability to apply the AaP3km method as outlined in the paper "Adopt a Pixel 3 km: A Multiscale Data Set Linking Remotely Sensed Land Cover Imagery with Field Based Citizen Science Observation" due to its effectiveness at gathering substantial data capable of being analyzed for LULC through citizen science (Low et al., 2021). Through the synthesis of different tools, the data revealed the abundant presence and relative balance between urban and plant elements. The findings in Bernardsville, NJ are significant because they can provide insight on potential impacts of upcoming projects, like the future construction of affordable housing. This study may also be used to help further research of the patterns of LULC across the U.S. Finally, the study demonstrates the imperfection of datasets and provides avenues for further research of these discrepancies.

The AaP3km Framework enabled LULC study to be brought to a suburb without any tools except a smartphone and laptop. It further demonstrates the power of citizen science as this research was not

performed by a professional. The AaP3km method thus brings possibility both in furthering the study of LULC and fostering the growth of citizen science to bring research and data to the public (Low et al., 2021). Its techniques enable both the sharing and analysis of LULC data by citizen scientists. This study also confirms that the AaP3km's need for satellite imagery to be compared with ground-truth images and observations; Bernardsville, NJ would not have had meaningful results without these comparisons (Low et al., 2021). The satellite data packages each told different stories and provided conclusions that would have lacked strength without comparison to ground-truth images had they only been compared to one another. While the potential of this methodology is demonstrated, its practicality is not as easy to apply to every AOI.

There was difficulty in gathering data for the AaP3km framework. For example, we encountered challenges collecting GLOBE Observer photos and data for kernels; but the cloud-based resources did not pose similar difficulty. Some kernels were placed in inaccessible areas such as private property or areas that would have been unsafe to access (e.g., railroad tracks, creeks). Data were collected as close as possible when observations were inaccessible, but these were not included in analysis of land cover for purposes of accuracy since they were not the 10,000 m² bounding box. Hence, GLOBE Observer imagery only reflects about half of the 37 kernels. The lack of accuracy in these points has the potential to make comparison to satellite imagery extremely difficult, something that is critical to ensuring significant results through the AaP3km methodology. This inaccessibility speaks to the composition of land ownership of Bernardsville. Most of it is composed of neighborhoods with large lots. Many homes have large, fenced-in backyards that are inaccessible to the public. Kernels that fell inside these properties were inaccessible from anywhere except the street, if at all. This meant that these areas could have provided more insight into the AOI but were unable to. It also meant that almost every photo in the downward direction is on pavement, which may not fully speak to the land cover of the point–especially if the majority of the point would have had dirt on the ground. Therefore, areas with a lack of public land may struggle to have enough ground-truth points to compare with satellite imagery for the AaP3km methodology.

As shown in the results, changes in LULC in Bernardsville, NJ can most likely be attributed to large construction projects that are relatively infrequent. Looking at Figure 7, the last time there was a major change in LULC was in 1986. This change was most likely the result of construction on the local shopping plaza, where the LULC change occurred. The town is currently planning to build affordable housing in a major construction project. The affordable housing serves to make Bernardsville a more cost-effective place to live, drawing in more workers, and improving downtown commerce. While this may seem like a threat to the harmony between impervious surfaces and vegetation, the project is taking place in areas that have already been built up. To do this, the town is taking down current buildings and replacing them with new ones. This, therefore, will not have a major impact on the percentages of current tree canopy and impervious surface presence in the area. This may lead to some short-term ecosystem damage, but as seen in Figure 7, these changes often resolve themselves within one or two years. The goal of this expansion project may not have been to preserve ecosystems, but it inadvertently does. This demonstrates that Bernardsville's balance between forest and urban elements is stable and has the potential to last well into the future. Bernardsville thus demonstrates how remote sensing packages can be applied in fields beyond science such as urban planning. Remote sensing tools like the MRLC NLCD Viewer and LTS can allow urban planners to observe the effects of past construction on the LULC of a region in order to predict the impact their construction will have.

The results and data discussed could be applied to Earth Science and further research. As a suburb, Bernardsville, NJ is able to sustain harmony between vegetation and urban elements. This could differ greatly from cities such as New York or Detroit, rural areas in the West, or suburbs that have only been incorporated within the last 25 years. Scientists could utilize the remote sensing patterns seen in Bernardsville and compare them to the aforementioned areas to determine how different types of communities influence LULC. Could Bernardsville's balance be unique to the mid-Atlantic U.S? Could cities in the U.S. have similar patterns despite being more urban? These are potential research questions that could continue research into areas like Bernardsville, NJ. Further research could also aim to quantify the imperfections of data. This could be done through the processes outlined in "The Sensitivity of Mapping Methods to Reference Data Quality: Training Supervised Image Classifications with Imperfect Reference Data" (Foody et al., 2016). This is possible given that this study has proved imperfections and inconsistencies within datasets when analyzing Bernardsville.

5. Conclusions

The study aimed to discover whether tools for analyzing LULC in a rural area agreed, and what conclusions could be drawn using those results. We found that satellite land cover datasets are insufficient by themselves and that they need other ground-truth or aerial observations to corroborate data to provide meaningful results. Furthermore, certain datasets tended to overanalyze and make extreme generalizations such as ESRI, World Cover, and Dynamic World. This outlined the need for truth comparison through Collect Earth Online and GLOBE Observer. In order to observe change in land cover across time, more data was collected through LTS and NLCD MRLC datasets. Once all these different datasets had been collected, they were viewed holistically and used to come to the conclusion that Bernardsville represents a harmony between urban and forest elements, having significant relatively unchanging concentrations of both. Bernardsville was also found to have a large canopy cover. The canopy could be the underlying cause for the differing results across satellite packages. Bernardsville has also undergone very little change in the past half century, gaining little impervious surfaces and losing little canopy cover. Bernardsville demonstrates the strength of the AaP3km methodology in citizen science and LULC research but also shows the difficulty of applying that framework to areas that do not have lots of public land (Low et al., 2021). The study can also be applied towards furthering LULC research to find greater national trends or to demonstrate the power of remote sensing to inform urban planning projects. The AOI is also a good candidate for potential further research into analyzing the LULC quantitatively through processes outlined in papers like "The Sensitivity of Mapping Methods to Reference Data Quality: Training Supervised Image Classifications with Imperfect Reference Data" (Foody et al., 2016).

Funding: This research was funded by NASA CSR SEES

Data Availability Statement: Data are available at https://doi.org/10.5281/zenodo.18795870 and https://doi.org/10.5281/zenodo.18795820

Acknowledgment: The authors thank the NASA CSR SEES program, The 2026 Earth System Explorers Team, Mr. Peder Nelson, Dr. Rusty Lowe, Dr. Cassie Soeffing, Dr. Brianna Lind, Mr. Andrew Clark, and Mr. Vineeth Erram

Conflicts of Interest: The authors declare no conflicts of interest. The funders had no role in the design of the study; in the collection, analyses, or interpretation of data; in the writing of the manuscript; or in the decision to publish the results.

References

Brown, C.F., Brumby, S.P., Guzder-Williams, B, Birch, T, Hyde, S.B., Mazzariello, J, Czerwinski, W, Pasquarella, V.J., Haertel, R, Ilyushchenko, S, Schwehr, K, Weisse, M, Stolle, F, Hanson, C, Guinan, O, Moore, R, Tait, A.M. (2022). Dynamic World, Near real-time global 10 m land use land cover mapping. *Scientific Data*. *9* (251). https://doi.org/10.1038/s41597-022-01307-4

Foody, G., Pal, M., Rocchini, D., Garzon-Lopez, C., & Bastin, L. (2016). The Sensitivity of Mapping Methods to Reference Data Quality: Training Supervised Image Classifications with Imperfect Reference Data. *ISPRS International Journal of Geo-Information*, *5*(11), 199. https://doi.org/10.3390/ijgi5110199

Gorelick, N., Hancher, M., Dixon, M., Ilyushchenko, S., Thau, D., & Moore, R. (2017). Google Earth Engine: Planetary-scale geospatial analysis for everyone. *Remote Sensing of Environment*, 202, 18–27.

Karra, K., Kontgis, C., Statman-Weil, Z., Mazzariello, J. C., Mathis, M., & Brumby, S. P. (2021, July). Global land use/land cover with Sentinel 2 and deep learning. In *2021 IEEE International Geoscience and Remote Sensing Symposium IGARSS* (pp. 4704-4707). IEEE.

Low, R. D., Nelson, P. V., Soeffing, C., Clark, A., & SEES 2020 Mosquito Mappers Research Team. (2021). Adopt a Pixel 3 km: A Multiscale Data Set Linking Remotely Sensed Land Cover Imagery With Field Based Citizen Science Observation. Frontiers in Climate, 3. https://doi.org/10.3389/fclim.2021.658063

Tolan, J., Yang, H., Nosarzewski, B., Couairon, G., Vo, H. V., Brandt, J., Spore, J., Majumdar, S., Haziza, D., Vamaraju, J., Moutakanni, T., Bojanowski, P., Johns, T., White, B., Tiecke, T., & Couprie, C. (2023). Sub-meter resolution canopy height maps using self-supervised learning and a vision transformer trained on aerial and GEDI lidar. *arXiv*. https://doi.org/10.48550/arXiv.2304.07213

United States Census Bureau. (2025). *QuickFacts: Bernardsville borough*, *New Jersey*. https://www.census.gov/quickfacts/fact/table/bernardsvilleboroughnewjersey/PST045224

U.S. Geological Survey. (2024). *Annual NLCD Collection 1 Science Products (Version 1.1)*. https://doi.org/10.5066/P94UXNTS

Saah, D., Johnson, G., Ashmall, B., Tondapu, G., Tenneson, K., Patterson, M., Poortinga, A., Markert, K., Nguyen, H. Q., Aung, K. S., Schlichting, L., Matin, M., Uddin, K., Aryal, R. R., Dilger, J., Ellenburg, W. L., Flores-Anderson, A. I., Wiell, D., Lindquist, E., ... Chishtie, F. (2019). Collect Earth: An online tool for systematic reference data collection in land cover and use applications. *Environmental Modelling & Software, 118*, 166–171. https://doi.org/10.1016/j.envsoft.2019.05.004

Zanaga, D., Van De Kerchove, R., De Keersmaecker, W., Souverijns, N., Brockmann, C., Quast, R., Wevers, J., Grosu, A., Paccini, A., Vergnaud, S., Cartus, O., Santoro, M., Fritz, S., Georgieva, I., Lesiv, M., Carter, S., Herold, M., Li, L., Tsendbazar, N. E., Ramoino, F., & Arino, O. (2021). *ESA WorldCover 10 m 2020 v100*. https://doi.org/10.5281/zenodo.5571936

Best Practice

Analyzing Urban Land Cover and Demographic Shifts through Remote Sensing Technologies

Swarup Nugehalli[1,*], Peder Nelson[2], and Russanne Low[3]

[1] 11th Grade, Lawrence D. Bell High School; https://orcid.org/0009-0007-0157-4646.
[2] Oregon State University; peder.nelson@oregonstate.edu; https://orcid.org/0000-0003-3979-9051.
[3] Institute for Global Environmental Strategies; low.russanne@gmail.com; https://orcid.org/0000-0002-7912-4350
[*] Corresponding Author: swarupnugehalli@gmail.com; (+1) 817-368-1434

Academic Editor: Jeong Chang Seong
Received: 28 February 2026
Revised: 13 April 2026
Accepted: 20 April 2026
Published: 30 April 2026

Abstract: This study investigates patterns of urban land cover change in Euless, Texas, using an integrated framework of satellite remote sensing and field-based observation. A 900-hectare area of interest was divided into a 37-point sampling grid, where ground photographs were collected using the GLOBE Observer application to validate and interpret satellite-derived classifications. Multiple remote sensing datasets, including Landsat Time Series Explorer (normalized burn ratio, NBR), ESRI Land Cover (2017/2024), WorldCover 10 m, Dynamic World (2016/2024), Meta/WRI Global Canopy Height, and MRLC NLCD Fractional Impervious Surfaces, were analyzed to quantify changes in built-up area, vegetation cover, canopy height, and surface imperviousness over time. Results indicate a clear increase in built-up land and impervious surfaces across much of the study area, accompanied by an overall reduction in tree canopy; however, localized anomalies in the southwestern portion of the area of interest, especially at sampling points 25 and 26 of the area of interest, demonstrated sustained canopy density and improved vegetation health, with exemplified NBR values increasing over the years. These findings highlight the spatial heterogeneity of urban growth and demonstrate that remote sensing, when validated with field observations, can effectively identify both broad development trends and localized ecological stability within a suburban landscape.

Keywords: Landsat, Euless, remote sensing, urbanization, land cover

1. Introduction

The transition from rural to urban environments has been a consistent global trend since the Industrial Revolution. Urbanization and population growth have dramatically reshaped landscapes around the world as a result of this demographic and geographic trend. As cities expand, natural ecosystems are either displaced or completely replaced by residential, commercial, and industrial zones, altering both environmental and social dynamics within the community and local area. The need for tracking, recording, and observing such effects on society followed a similarly dramatic rise as well. This necessity was met with the aid and support of remote sensing technologies, which have allowed changes on Earth's surface to be observed from space over time.

Remote sensing data collection methods can appear slightly ambiguous at first glance; however, most of it is rooted in simplicity when broken down to its fundamental components. Satellite imagery is a fundamental component of remote sensing, providing the primary data source for analyzing Earth's surface characteristics. The process involves a satellite or some sort of remote-sensing-based aircraft detecting changes in the physical characteristics of the land by recording the radiation which is emitted from the land (Kshetri, 2023). This is then interpreted through a scientific database, which produces comprehensive results and findings about the land cover in a certain area. These satellites or typically drone-based aircraft geo-reference, or map, the level of individual objects or even entire landscapes. At smaller geographic scales, higher amounts of land density and varying landscape features are allowed to be interpreted in similar ways (Singh, 2000). There are many ways remote sensing can be useful and utilized in a way that makes the most appropriate sense. For instance, some satellites or drones may record tree height or, in a slightly different way, the number of trees in a given area. These technologies could map the crown density of trees in a given plot of land or the density

Citation: Nugehalli, S., Nelson, P. & Low, R. (2026). Analyzing Urban Land Cover and Demographic Shifts Through Remote Sensing Technologies. Journal of Earth Observation and Geospatial Applications, 2(1), 39–50. https://doi.org/10.65372/zesm3j31

of the tree count in that same plot. The remote sensing data that can be extracted from such satellite imagery is instrumental in grasping a quantitative sense of how the land has changed with certain aspects and to what degree. Not only is remote sensing useful for the residential and commercial aspects of society, but it is also revered in chemical, biological, and military contexts. The satellites that work on the latter contexts tend to provide scientists with the same quality of data for remote areas in less developed countries as they do for urbanized areas in highly developed countries, such as New York City, NY, U.S.A. (Kshetri, 2023). The data that is provided through these satellites is not biased or favored in one area over another due to the holistic, uniform coverage that the technology offers. This style of obtaining data in a broader sense allows for the complex tasks to be broken down into smaller, simpler tasks that can be managed efficiently; for example, the census data of any larger population, such as the United States, tends to face issues with misrepresentation by overcounting or undercounting their demographics. The surveying methods that are being utilized to fix this issue involve the utilization of remote sensing satellites with greater accuracy and precision, especially since many remote sensing satellites orbit the earth at the same time every day and take pictures detailing how the land has changed. Overall, the general use of remote sensing allows for a great deal of development to occur properly, given the context of the land and how it has changed over a period of time.

Remote sensing data collection methods come in different forms as they aim to achieve slightly different goals. There are 2 main types of techniques in which remote sensing is utilized: active and passive sensing (Jia et al., 2021). Passive remote sensing, which tends to be the more traditionalized method for remote sensing in vegetation contexts, is analogous to a camera whose source of optical EM energy is the sun. When using passive remote sensing technology, natural energy such as solar energy sites is transmitted through, absorbed, emitted from, or reflected off an object or surface nearby, which is sensed by the satellite (Weishampel et al., 1996). The information that it reads from the reflections is then sent back in a visual way, which shows how the land has changed from previous pictures or media. This process is done by satellites such as the Landsat and NASA's Terra and Aqua remote sensing orbital technologies. There are, however, drawbacks with this method as only a fraction or small portion of the energy that is reflected from the surfaces encompasses the received signal. The magnitude of what is captured is highly dependent on the natural elements from the surrounding environment, which can consequently deem this traditional method of remote sensing inefficient, or at the very least, unreliable at times.

The other method of gathering data regarding land cover change involves active remote sensing. Active remote sensing functions similarly to a camera with a flash, since both the energy source and the sensor are located on the same medium. Since these active systems rely on their own source of illumination, they don't require nor are they reliant on sunlight or any solar angle to obtain important data regarding the land cover. Among these non-traditional active systems, radio detection and ranging is the most widely used, especially in forms such as synthetic aperture radar (SAR), which is commonly applied to forest canopy analysis (Waring et al., 1995). By functioning similarly to optical sensors, radar systems respond to the wavelength and spatial resolution of the instrument, but differ in what they exactly detect. Optical data is influenced primarily by pigment and moisture content, whereas radar signals, with wavelengths measured in centimeters, tend to respond to the structural and foundational characteristics of vegetation. Shorter radar wavelengths primarily interact with smaller canopy elements like leaves and twigs, while longer wavelengths penetrate deeper, which causes larger components such as branches or trunks to be more sensitive to the detection technology (Jia et al., 2021). Examples of active remote sensing satellites include Radarsat, NASA's ICESat-2, NASA's GPM core observatory, and Envisat. In this study, "demographic shift" is used in a descriptive sense to refer to observable changes in neighborhood composition and residential continuity reported in census-level summaries, rather than a directly modeled variable.

2. Study Area and Methods

2.1. Study Area

The area of interest (AOI) utilized for the studied area is Euless, Texas, which resides within the larger Hurst-Euless-Bedford mid-cities settlement, commonly referred to as HEB. This area is located in the larger Tarrant County in the north-central portion of the state and forms part of the broader Dallas-Fort Worth Metroplex. Euless lies just west of the Dallas/Fort Worth International Airport, and covers about 16.3 mi^2 (42.1 km^2). The city was officially incorporated in 1953, and over the decades, it has evolved from a smaller farming community into a suburban municipality with a diverse population and housing landscape, especially

in the past fifteen years. Topographically, Euless is characterized by relatively flat terrain typical of the North Texas region, with gentle slopes, urban infrastructure, residential areas, commercial zones, and smaller remnants of older agricultural or semi-rural land uses in some areas as well. Its proximity to major transportation infrastructure, such as major highways (State Highways 183, 360, 820) and the DFW airport, has exacerbated its acceleration in suburbanization, making it a zone of both commuter residence and local economic activity. The built environment includes single-family homes, multi-family dwellings, retail zones, and many warehousing centers linked back to the airport, as mentioned earlier. In a demographic sense, Euless is notable for its diversity and recent immigrant community growth, with the significant influx of Nepalese and Tongan minority groups. As of 2023, 19.3% of residents were born outside the United States, and the median property value was $294,500, which highlights a middle-income suburban profile (Data USA, 2023). The city is about 47.8% White, 17.3% Black or African American, 13.4% Asian, 1.67% Native Hawaiian or Pacific Islander (US Census Bureau, 2024). In particular, however, the Tongan and broader Polynesian community has an immensely strong presence in and around Euless. The area is attractive due to its proximity to the airport and the employment opportunities that have arisen in recent years (Niche, n.d.). In addition to the established Tongan community, the Nepalese population exhibits a similar growth pattern within Euless. The city presents itself as a transitional suburban zone from pressures by urban development, transportation corridors, and housing sprawl, in contrast to the existing vegetation and open spaces from earlier decades. Euless combines a well-defined geographic footprint with active demographic and built-environment change. Its evolving community composition adds a social aspect to land-cover change that is often overlooked in conventional physical analyses. Consequently, Euless serves as a case study linking remote-sensing land cover data with demographic and community change, providing insight into the environmental and urban dynamics as well as the socio-spatial context of suburban transformation.

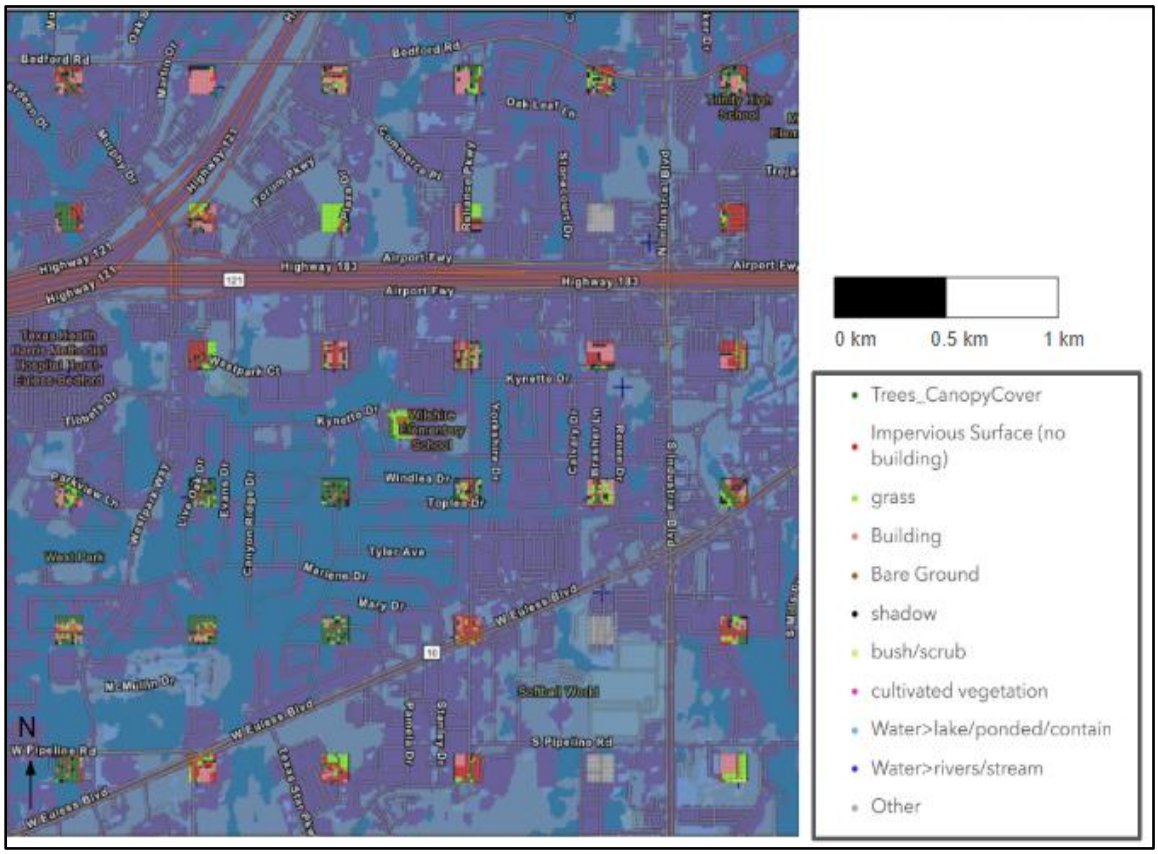

Figure 1. The area of interest surrounding the cities of the Hurst–Euless–Bedford region with land cover classifications derived from Collect Earth Online. Each color represents a classification (e.g., red = impervious surfaces, dark green = forest/trees). The grid represents a 3 km × 3 km (900 ha) study area. The map is oriented with north at the bottom left, and a scale bar is included to provide spatial reference.

2.2. Data

Euless proved to be agreeable in the context of land cover change and data within the ESRI 2017/2024, Collect Earth Online classifications, and Meta/WRI Global Canopy Height datasets. In this context, "agreeable" refers to datasets whose spatial resolution, temporal coverage, and classification schemes align well with the 3 km × 3 km (900 ha) AOI and the 37-point sampling grid, allowing for consistent comparison across models. Datasets that are not fully agreeable typically introduce inconsistencies due to mismatched spatial resolution, differing land cover definitions, or temporal gaps that may obscure short-term changes, particularly in heterogeneous suburban environments such as Euless where built and vegetated land are interwoven at fine scales. As a result, datasets with moderate-to-high spatial resolution and clearly defined classification structures were prioritized to improve comparability and reduce classification uncertainty across platforms.

The spatial and temporal resolutions of the datasets used in this study vary and directly influence their interpretability. The WorldCover dataset provides land cover classifications at a spatial resolution of approximately 10 m for 2020–2021, while the Dynamic World dataset also operates at approximately 10 m resolution with near-daily temporal updates spanning 2016–2024. The ESRI Land Cover dataset provides annual global classifications at approximately 10 m resolution for 2017 and 2024. In contrast, Landsat-based datasets, including the Landsat Time Series Explorer, operate at a coarser 30 m spatial resolution but offer a long-term temporal record from 1985 to 2025, making them well suited for identifying multi-decadal trends rather than fine-scale spatial variation. Similarly, the Meta/WRI Global Canopy Height dataset provides canopy height estimates at approximately 30 m resolution for circa 2020. These differences in resolution are important because higher-resolution datasets capture localized heterogeneity in suburban landscapes, while coarser-resolution datasets provide greater temporal continuity but may generalize smaller land cover features.

The ESRI dataset, when applied to the GeoJSON file of the AOI consisting of 37 different points (equally spaced from one another in a grid-like pattern), highlighted a growth of "Built Area" within the 900 ha area. The built area in 2017 was categorized as 881.3 ha, while "Trees" were categorized as 1.3 ha out of the entire area. The trend of increased urbanization and commercial development in commercial sectors presented itself as the Built Area grew to 892.1 ha in 2024, while Trees followed an expected inverse relationship, decreasing in coverage to about 0.4 ha. The Meta/WRI Global Canopy Height dataset shows that the average height of the tree canopy within the 900 ha sample area in 2020 is 5.47 meters, with a maximum canopy height of 23 meters and a minimum of 1 meter, likely representing shrubs or very young trees. Variability in canopy height is commonly influenced by multiple interacting ecological and anthropogenic factors, including forest age structure, urban management practices, and development-driven vegetation removal or pruning (Waring et al., 1995). As a result, canopy height differences can reasonably be interpreted as a combined signal of both natural growth conditions and human land-use intensity. These datasets were complementary to the data that the Dynamic World dataset produced when applied to the AOI. The Dynamic World 2016/2024 dataset showed that from 2016 to 2024, there was a significant change in Built Area, as it increased substantially from 813.67 ha in 2016 to 850.57 ha in 2024. This suggests a notable expansion of built-up areas in the analyzed region during those nine years, indicating continued urban development and sprawl.

The Landsat Time Series Explorer graphs for vegetated points utilized the normalized burn ratio (NBR), calculated using near-infrared (NIR) and shortwave infrared (SWIR) reflectance values derived from Landsat imagery, providing a spectral index for analysis. NBR is commonly used to assess vegetation health, biomass, and disturbance over time, making it appropriate for this study because it provides a long-term, consistent measure of vegetation condition that can be compared across decades of urban development. The graphs showed a logarithmic proportionality with NBR over 40 years from 1985 to 2025. For instance, the NBR was at 0.378 on July 31, 1989, whereas it was found to be 0.474 on July 31, 2006, indicating an increase in vegetation health that gradually stabilizes over time. The findings from the Landsat Time Series Explorer differ slightly from the other datasets, as they do not indicate a strong net decline in vegetation but instead show reduced growth rates or stabilization rather than consistent loss.

$$NBR = \frac{(NIR - SWIR)}{(NIR + SWIR)} \quad (1)$$

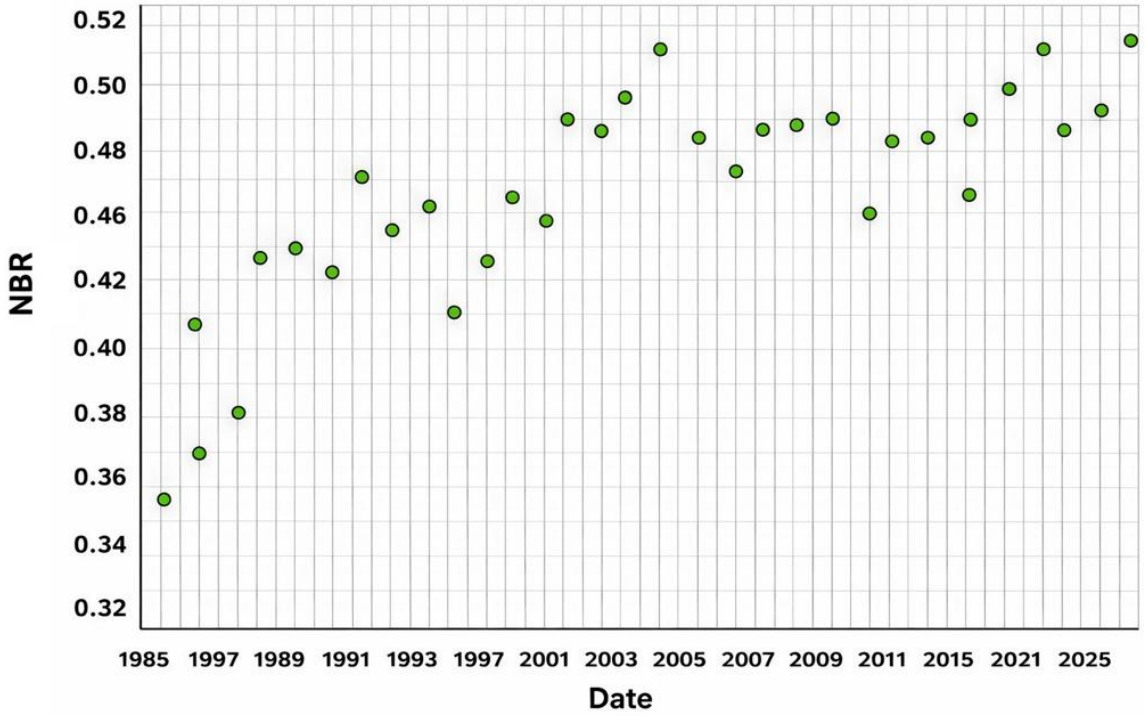

Figure 2. Landsat Time Series Explorer graph showing NBR trend of growth shown on point 26 of 37 in the AOI of Euless, TX. Point 26 is chosen to be an example as it falls under the area where there is comparable vegetation and tree growth. Courtesy of Google Earth Engine.

2.3. Methods

Many software and applications were utilized to obtain a thorough analysis of the AOI of Euless, Texas. One of these applications includes Global Learning and Observations to Benefit the Environment (GLOBE) Observer, a NASA-backed software that aids in the categorization of satellite data through field data, such as pictures. GLOBE Observer was the first field-based software to be used to gather the foundational fieldwork necessary for further analysis through other media (Kohl, 2019). The first step to examine such data was to take ground observations through the app.

Using the NESEC (NASA Earth System Explorers Community) geospatial sampling framework developed during the NASA SEES (STEM Enhancement in Earth Science) internship, an Area of Interest (AOI) was initially established consisting of 37 individual sampling units spanning approximately 900 ha. The centroid of the AOI was chosen accordingly, and a grid with 36 equidistant points was generated. The area of interest was inclusive of a 100 m^2 square-like grid, where point 0 was marked as the centroid of the square. Point 1 was marked as the most northwestern point, or in the top-most left miniature square. Points 2 through 6 followed a left-to-right pattern, with Point 7 returning to the left-most square in the row below. This pattern continued until Point 36, being the bottom-most right box. Once the grid was generated via Nesec, it was saved as both a CSV and a GeoJSON file, where all the information regarding the locations of each point was stored.

The GeoJSON file was uploaded to Google Maps to obtain traveling directions to the exact coordinates as generated by the SEES software. A few of the points were unable to be reached as they were closed off for various reasons, such as private vehicle lots or construction. In that case, the photos would not be included in the field observations as they would be highly inaccurate and undermine the integrity of the land cover analysis. Many of the points were placed in locations of private property or in front of residential areas, which made it harder to get permission for fieldwork observations; however, all of the points that were not blocked off, such as the aforementioned lots or construction areas, were able to be recorded and observed.

At the locations of each point, GLOBE Observer was used to take 6 photos in all cardinal directions, as well as photos marking an up and down direction for increased accuracy of the surrounding environment. Additional photos for distinction were able to be taken if deemed fit. Once the minimum of 222 photos were

taken, they were uploaded to the NASA SEES 2025 server and approved for inspection. The pictures of each of the 37 different locations were able to be seen through the GLOBE Observer app after they were approved.

The AOI grid structure and spatial layout are presented in Figure 1, which illustrates the 3 km × 3 km study area and the distribution of the 37 sampling points used for analysis. At this stage, the necessary groundwork was complete, so many other applications, such as EarthMap, Collect Earth Online, and Landsat Time Series Explorer, were used to gather data about the land cover change over many years and the land cover itself at the time of observation.

Once the GeoJSON file was uploaded to EarthMap, a plethora of datasets were uncovered and were able to be layered to discern notable features regarding the land cover of not only each individual 100 m^2 box, which included each individual point as its center, but also the entire 900 ha area of interest as well. The datasets that were most useful and were included in observational examination included Land Cover - Dynamic World, ESRI 2017/2024, Meta/WRI Global Canopy Height, and WorldCover 10m 2020/2021 (ESA).

The Dynamic World dataset helped classify and uncover the Built Area, Trees, Grass, Shrub & Scrub, Bare Ground, Crops, and Water of the selected areas from the years 2016 and 2024, specifically. This was indicative of how the land had been utilized over a period of 8 years and provided a more precise characterization of what other factors were at play for the change to occur in such a specific manner. The ESRI layer showed how the combination of vegetation and the built environment relates to each other in the context of land cover. ESRI 2017/2024 showed a similar spread of classifiable characteristics such as Water, Trees, Flooded Vegetation, Crops, Built area, Bare Ground, Snow/Ice, Rangeland, and Clouds. The ESRI feature showed, in a similar fashion to the Dynamic World dataset, that the Trees and Built Area followed an inverse relationship with each other. The ESRI was able to include information regarding the reduction in both the rangeland and bare ground of the 900 ha area, which confirmed the classifications of the other datasets as well as the ground photos that were taken.

The Meta/WRI Global Canopy Height layer honed in on a specific type of land cover change in the area, which was highly useful in discovering potential causes for why the area is the way it is, not only in an environmental sense, but also in a demographic and social context. This layer showed the differing heights of tree canopy in the AOI grid on a scale from 2.00 meters to 30.00 meters, as well as how sparsely or densely populated some pockets of the AOI were with tree vegetation. This dataset helped highlight forest loss or gain over time and the social effects of that, such as whether or not deforestation or restoration efforts were made.

The WorldCover 10m 2020/2021 dataset included a more diverse crop-based spread of sub-categories to help increase the accuracy of what type of vegetation was present in the land, as opposed to classifying all vegetation as one section. The dataset included various factors such as Trees, Shrubland, Grassland, Cropland, Built-Up (urban development), Barren/Sparse Vegetation, Snow and Ice, Open Water, Herbaceous Wetland, Mangroves, and Moss and Lichen. In the Euless-based AOI, there were not many areas that could be classified under most of the subsections of vegetation, as the area is severely urban with pockets of trees, grassland, and cropland, mainly.

Collect Earth Online, or CEO, was used for investigation on the land cover which could not be classified through the other methods or datasets due to other factors such as vegetation or man-made structures blocking the observable land. CEO was used to manually record, declassify, and categorize the land of each of the 37 points to a far greater precision. Once the CSV file of the computer-generated grid was connected to the CEO server for the NASA SEES Earth System Explorer 2025 group, each location that was observed in the field showed up virtually on the CEO server with the help of aerial photographs.

Each picture, representing one point out of the 37 total points in the entire grid, was broken down into 100 equidistant points with different categories such as Tree Canopy Cover, Bush/Scrub, Cultivated Vegetation, Water (lakes and ponds), Water (rivers and streams), Water (irrigation), Shadows, Unknown, Bare Ground, Wet Land, and Impervious Surface. The goal of CEO was to compare the GLOBE Observer photos that were taken at the site with the aerial photos included in CEO's database for the specific point. An important part of the tedious process to note is that if the ground had a shadow due to tree canopy, it should be categorized as the land cover that was observed in the field, versus selecting shadow and moving on to the next point out of the 100.

This aimed to reduce the amount of unknown information regarding the environment. Since there were 100 smaller points to manually categorize, there were, consequently, 3,700 different points to categorize, which required lots of time to get through. Once each photo was complete with the manual categorizations,

a confidence score from 0-100 was required for the observation, along with any notes that were helpful in the process of uncovering the conspicuous nature of the elements.

The Landsat time-series Explorer (LTSE) was used for quantitative reasoning and analysis, as it showed the growth of the healthy vegetation in a specific area once the coordinates of the latitude and longitude were inputted into Google Earth Engine. The NBR is a spectral index calculated from Landsat bands that's usually used to detect burn severity, vegetational health, and changes in biomass. The LTSE provides graphs of the NBR against the years from 1985 until 2025. A plateauing or stabilization in the NBR over time indicates that the area reached a stable vegetation cover due to likely urban landscaping or mature tree growth, whereas a constant increase in NBR would indicate a positive growth in healthy vegetation in the area, while the opposite holds true for a constant decrease over time. High values of NBR indicate high levels of healthy vegetation, whereas low values highlight low levels of healthy vegetation. Pictures of the given area were provided for each year as well to visually showcase the observable change that the land went through. The graphs of the NBR over time were provided and generated via Google Earth Engine Apps for every single point out of the 37 total grid markings.

The Multi-Resolution Land Characteristics (MRLC) National Land Cover Database (NLCD) was utilized to obtain individual data for each pixel in every image chip. The MRLC gave the data provided by the NLCD for each year for each chip from 1984 to 2024, allowing for extensive, thorough data to be analyzed. However, a limitation with this program was that it lacked precision, as there was a limit to how many decimal places could be inputted in each coordinate box. The miniature square box that encapsulated the specific point contained gradients of data on a scale from 0 to 100% for various datasets, such as tree canopy and impervious surfacing, among many more. This was done by downloading the NLCD for the datasets and combining them with the MRLC software. This analysis allowed for a thorough understanding of urban development as it visually tracked the change in different datasets for the many pixels of each individual image chip.

Due to the improving rates of urbanization in Euless, the dataset that seemed most appropriate to track was the FIS, or Fractional Impervious Surfaces. This sub-category allowed for the presentation of data in the aforementioned gradient style, which helped show how deeply affected a certain sub-region of the 100 m^2 box was by increased urbanization over the span of 40 years. The data derived from the FIS dataset is especially valuable because it provides a direct quantitative representation of how much of the land's surface has transitioned from natural or semi-permeable states (like grass or soil) to impervious ones, such as roads, buildings, and parking lots.

This information can then be correlated with environmental and socio-economic trends in the Euless area, such as population growth, infrastructure expansion, and rising housing density. A consistent increase in impervious surfaces indicates a higher degree of development and reduced capacity for water infiltration, which can have notable environmental consequences. These include increased surface runoff, higher flood risk, and elevated local temperatures due to the urban heat island effect. Over time, this expansion of impervious cover also leads to the fragmentation of natural habitats, limiting biodiversity and reducing the presence of tree canopy cover that plays an essential role in maintaining air quality and providing shade in urban areas. Ultimately, the use of the MRLC NLCD datasets, especially through the FIS sub-category, provided a dynamic visualization of Euless' transformation over four decades. It enabled a precise and accessible method of tracking patterns of growth, surface alteration, and the resulting environmental effects, which formed a foundational component of the study's analysis.

At the end of the study, ArcGIS was used to connect to the NASA SEES Earth System Explorers server, where a storyboard showing how the land cover change impacted different aspects of the area of interest was meant to be created. In the form of a website, the storyboard, or Community Chronicles, blended together both the foundational components on what made the AOI, or Euless in this case, what it was, as well as the present and future on how the land has and will change for either the better or worse and what impacts and repercussions that would have on social aspects of the community. To move beyond qualitative comparison between ground observations and satellite-derived classifications, a structured validation approach was applied using the GLOBE Observer field photographs as reference data.

Each sampled point was assigned a dominant land cover class based on field interpretation, which was then compared against the corresponding classification outputs from ESRI Land Cover, Dynamic World, and WorldCover datasets. Agreement between ground-based and satellite-based classifications was evaluated in a pairwise manner at each point across the 37 point grid, allowing for a basic accuracy assessment of classification consistency. While a full confusion matrix and derived statistical measures such as Cohen's Kappa coefficient would provide a more formal assessment of classification accuracy, the scope of this study and the heterogeneous nature of suburban land cover limited the feasibility of strict pixel-level

correspondence across datasets with differing spatial resolutions. As a result, the validation approach in this study is best interpreted as an agreement-based assessment rather than a fully statistical accuracy evaluation, where consistency across multiple independent datasets is used as a proxy indicator of classification reliability.

3. Results

Through the employment of a spread of datasets, programs, and applications, the land cover change in the environment was able to be displayed in both quantitative and qualitative senses, which provided a rich understanding of what occurred to the area of interest, or in this case, Euless, over time. Remote sensing via satellite data helped back the dataset data, which paired well with the field observations with GLOBE Observer. Even though some image chips may not have aligned with the graphical data provided by the satellite information, both types of field work help come together to create a narrative on the types of change that the area of interest has undergone.

When going through the different datasets, there were many agreements on how they interacted with the GLOBE Observer photos that were taken. For instance, the WorldCover 10m dataset showed that the Built-Up (which corresponds to the Built Area of other datasets) for the 900-hectare grid had increased from 2020 to 2021 by almost 50 hectares; however, the tree life had declined by almost 4 hectares, showing a definitive urban development trend. On the actual AOI grid of Euless, the points marked as points 25 and 26 were surrounded by significant vegetation and tree canopy cover. Those points were both residential houses located in what is considered a “green” community in the Hurst-Euless-Bedford region. The Meta/WRI Tree Canopy dataset showed a layer of trees that were highly populous in those areas, which confirmed the satellite data of the other two generalized datasets. Not only were the trees in the region highly prevalent in context to the other points on the 37-point grid, but the trees were also taller, as they were noted to be around 13-14 meters in height. This draws a stark contrast to the majority of the other trees in the region, which average around 5.7 meters in height. While there were a few discrepancies within some smaller subsections of the 100m sampling points when layering 2 or more datasets, such as the Meta/WRI Global Canopy Height and the WorldCover 10m 2020-2021, they followed a highly similar pattern and trend of tree canopy, as there were more trees in some areas than others. If at all, the only inaccuracy with the layers seemed to be the categorization of bare ground, as in points 25 and 26; there seemed to be a discrepancy with how the Global Canopy Height dataset showed that there were trees in the bare ground regions marked by the WorldCover 10m dataset. This seemed to be a pattern as it appeared more than once in the sampling squares. This could very well be explained using the Collect Earth Online software, which allowed for manual categorization of land cover. In the CEO, many areas in the AOI had shadowed areas due to the tree canopy areas, especially around points 25 and 26. Consequently, this allowed for the satellite pictures to not pick up on important surfaces such as bare ground or impervious surfaces like roads, sidewalks, pools, and more. This would help explain those differences in the individual layers in EarthMap since the datasets in the application are derived from the source material of aerial photographs via satellites.

The ESRI dataset seemed to show a significant amount of built-up areas compared to the other datasets, such as the WorldCover 10m 2020/2021. It showed barely any trees, at least visually, so there was a harder time differentiating between what the quantitative data was showing about the trees when there was no color difference showing that there were, in fact, trees present across the entire AOI grid. The bar graphs that were generated in EarthMap showed a majority of built area in 2017 as well as 2024; however, even with the difference in substantial urban development, the trend of fewer trees and vegetation seemed to be present, affirming the notion that Euless has undergone increased levels of urbanization in the past decade, at the very least.

The Landsat Time Series Explorer graphs seemed to be highly reflective of the type of change that was seen by the GLOBE Observer photos that were taken at the beginning of the study. In the past 1 year, there has been increased renovation done on nearby parks and schools, which has yet to be reflected on the graphs, however. The greenery that blanketed nearly all the image chips that were generated in the Landsat Time Series Explorer seemed to have stayed constant through the years. Only when a drastic geographic change, such as the renovations that occurred, did the image chips reflect that. Aside from that, the image chips drew a deep parallel to the actual city on how it was when the photos were taken.

Although, even though there seemed to be little to no change in the landscape, especially in the context of the natural environment, there obviously seemed to be some fluctuation in the NBR as those values were

not the same every year, nor did they show a continued constant relationship. In many of the chips, such as point 26, the generated graph showed a slightly linear increase in the NBR over the years from 1985 to 2001, but then changed to a logarithmic plateau from 2001 to 2024. On July 31, 2025, the data point for the NBR drastically increased to 0.509 from 0.476 in 2024, indicating a sudden, significant increase in healthy vegetation in the area. This change would be less surprising considering the context in which point 26 is located in Euless. This could indicate that the areas where there are substantial amounts of tree canopy and forestry amid residential homes have been undergoing a potential urban greening or reforestation initiatives to increase the healthy vegetation and tree canopy despite the trends of urbanization that are noted by all the other datasets, even if they don't show the other aspects of the city as well as their complementary datasets do.

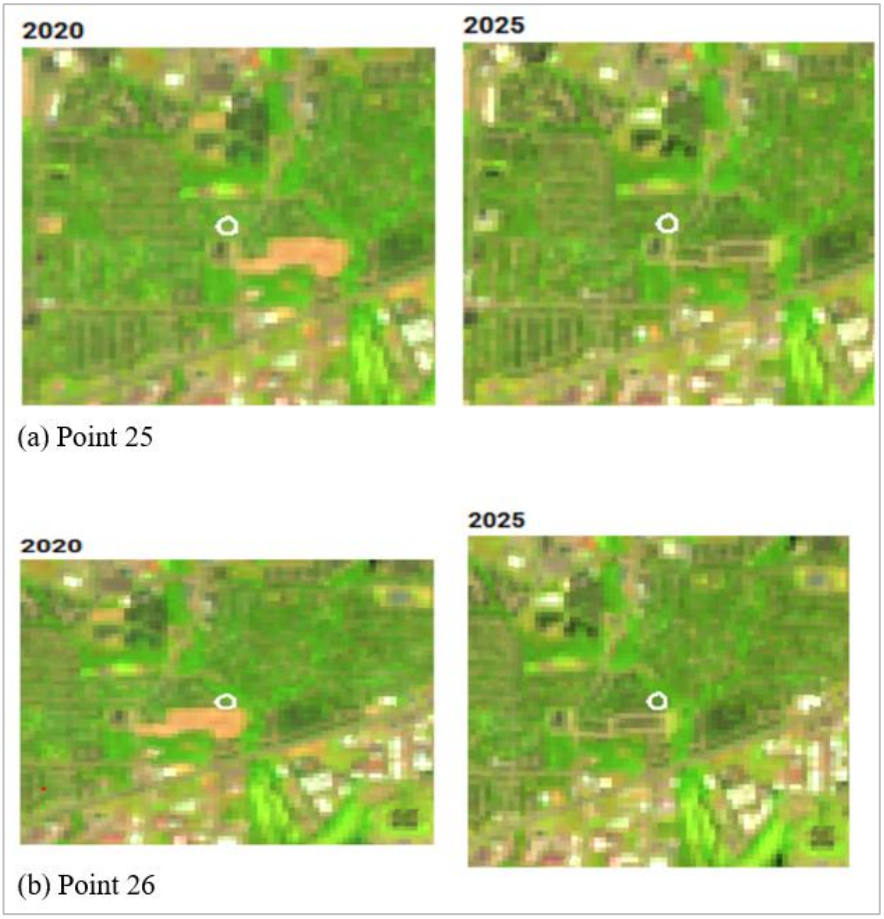

Figure 3. Landsat Time Series Explorer visualization showing temporal vegetation dynamics at points 25 and 26 within the AOI. The imagery compares vegetation and canopy conditions across multiple time intervals over a five-year period, highlighting localized stability and variability in vegetation health within residential zones.

This finding complements the ESRI 2017/2024 recording on point 26 specifically, as it showed that the built area in 2017 and 2024 stayed the same. Initially, this may appear counterintuitive, as it would be expected that there should have been an increase in built area considering the pronounced trend of urbanization in Euless. However, it should be noted that the entire southwestern area that includes points 25 and 26 is in residential areas and communities with high levels of tree canopy compared to other areas. This means that there would be no land to urbanize as there is already a planned built settlement there. The only explanation for why that would change would be renovations or a city-wide planning demolition of the community, which would be exceedingly rare.

The number of trees recorded by all of the EarthMap datasets uniformly decreased in all regions. Since all of the datasets that were used in the EarthMap application did not include the present year of 2025, they were unable to show that some areas have begun to increase their healthy vegetation. This could only have been recorded by the Landsat Time Series Explorer program, as it updates more frequently than the EarthMap

layers, which it did. Many of the surrounding areas of Euless faced commercialization, where smaller homes or businesses were demolished in favor of larger commercial chains, especially in the fast food industry. This ground observation was highly reflected in every single one of the datasets in EarthMap, as well as the Landsat Time Series Explorer. The utilization of Collect Earth Online with the comparison of the actual GLOBE Observer photographs helped showcase that some residential areas which had more tree canopy had different types of surfacing which was not picked up by some of the datasets; however, in most of the 37 individual smaller 100m sampling squares, the built environment was captured in a detailed manner which could have only been labeled as impervious surfacing in Collect Earth Online with a high confidence rating since it confirmed the findings and visual observations of the GLOBE Observer photos. The study confirms that Euless, Texas, has undergone significant urbanization, characterized by the expansion of built environments. To a high degree, the satellite-backed datasets of EarthMap and Landsat Time Series Explorer seemed to agree with the ground photographs uploaded and analyzed with GLOBE Observer.

4. Discussion

Euless has experienced significant demographic and environmental change over the past decade, reflecting how human settlement patterns interact with land cover over time. While much of the city has seen increased urban development and built-up infrastructure, certain residential areas diverge from this broader trend, particularly in the southwestern portion of the AOI around points 25 and 26. As Euless has become one of the most demographically diverse cities in the Dallas–Fort Worth region, Tongan and Nepalese communities are present in parts of the city, although this study does not directly quantify demographic influence on land cover change. Instead, the observed spatial differences are more reliably interpreted through physical land-use structure, residential continuity, and redevelopment intensity. These neighborhoods exhibit the highest tree canopy coverage and tallest vegetation recorded in the study. WorldCover and Meta/WRI datasets indicate a citywide increase in built-up land between 2020 and 2021, accompanied by an estimated loss of approximately four ha of tree cover; however, points 25 and 26 function as clear anomalies. Tree canopy in these zones remained dense, with average heights of 13–14 meters compared to a citywide average of roughly 5.7 meters, and satellite imagery and GLOBE Observer field photos characterize them as older, established residential neighborhoods with limited redevelopment pressure. Landsat Time Series Explorer data further supports this pattern, as point 26 showed an increase in vegetation health, with NBR values rising from 0.476 in 2024 to 0.509 in 2025.

Together, these findings suggest that long-term residential stability and lower redevelopment turnover may contribute to vegetation persistence within specific neighborhoods. Rather than following a single trajectory of vegetation loss, Euless demonstrates localized variation where social, residential, and land-use factors intersect, producing areas of relative ecological stability amid broader urban expansion. Satellite datasets quantify overall land cover change, while field-based observations provide contextual information on local land-use structure and neighborhood characteristics that help interpret spatial variation within the AOI, or an urbanizing landscape.

Despite these insights, the study could be strengthened by extending both its temporal and spatial scope. Several datasets capture only short-term land cover change, which limits the ability to separate long-term residential stability from temporary fluctuations in vegetation or development. Incorporating longer Landsat or Sentinel time series and higher-resolution canopy data would improve trend reliability, while additional field observations and housing or zoning data could help more directly connect community continuity to redevelopment pressure. These improvements would allow for a clearer understanding of how social structure and land cover interact over time, particularly in neighborhoods that diverge from broader urban patterns.

Despite these findings, several limitations must be acknowledged. One major limitation is the mixed-resolution nature of the datasets used. While high-resolution datasets such as Dynamic World and WorldCover (10 m) capture fine-scale spatial variation, coarser datasets such as Landsat-based products and Meta/WRI canopy height (30 m) generalize land cover features over larger areas. This mismatch can introduce scaling inconsistencies, particularly in suburban environments like Euless where land cover changes occur at very small spatial scales (individual housing lots, narrow tree buffers, and fragmented green space). As a result, some localized vegetation or impervious surface changes may be underrepresented or generalized in coarser datasets.

Additionally, the physical landscape of North Texas presents inherent interpretive complexities. Euless contains a highly fragmented suburban structure with a mix of residential zoning, commercial redevelopment

zones, and remaining vegetated pockets. Seasonal variation, drought conditions, and landscaping practices common in Texas suburbs may also affect vegetation indices such as NBR, complicating the distinction between long-term ecological change and short-term environmental variability. Model-based limitations are also present as land cover classification algorithms (such as ESRI and Dynamic World) rely on probabilistic classification, which can introduce uncertainty in transitional zones where built and vegetated classes overlap. Similarly, canopy height models derived from remote sensing may misclassify shadowed regions or underestimate vegetation height in dense residential areas due to occlusion effects.

Despite these limitations, the multi-dataset approach strengthens the reliability of the findings. By integrating high-resolution classification models, long-term Landsat time-series, canopy height estimates, and ground-based validation from GLOBE Observer and Collect Earth Online, the study reduces reliance on any single data source. This cross-validation approach allows for stronger identification of consistent urbanization trends while also revealing localized anomalies that may not appear in individual datasets alone. The combination of multiple spatial resolutions and data types therefore provides both a broad temporal perspective and a fine-scale spatial interpretation of land cover dynamics in Euless.

5. Conclusions

The combined use of remote sensing technologies and field observations provides a comprehensive understanding of how Euless, Texas, has changed over time, both in terms of its physical landscape and its demographic composition, by allowing for the analysis of spatial and temporal patterns in urban development, vegetation health, and tree canopy structure with a level of precision that would not be achievable through ground observations alone. By leveraging multiple datasets, including the WorldCover 10meter dataset, Meta/WRI Tree Canopy and Canopy Height datasets, ESRI layers, Landsat Time Series Explorer graphs, Collect Earth Online classifications, and GLOBE Observer photographs, this study was able to identify and quantify land cover changes across the city while accounting for potential inaccuracies in satellite-derived data, such as misclassified vegetation or shadowed areas in regions with dense tree cover. Overall, the results indicate a clear trend of urban expansion across much of Euless, with built-up areas increasing significantly between 2020 and 2021 and an associated loss of nearly four hectares of tree cover, reflecting broader processes of redevelopment, commercialization, and urban sprawl that are consistent with global patterns of vegetation reduction in growing metropolitan areas, while also highlighting potential implications for local climate, stormwater management, and the maintenance of ecosystem services that are often disrupted by the replacement of natural landscapes with impervious surfaces.

Despite these overall trends, land cover change within Euless is highly heterogeneous, with specific neighborhoods in the southwestern portion of the area of interest, particularly points 25 and 26, demonstrating a markedly different trajectory that is more plausibly associated with differences in neighborhood development history, housing stability, and redevelopment pressure rather than direct demographic or cultural links. These neighborhoods retained dense and healthy tree canopy with vegetation heights of 13 to 14 meters, far exceeding the citywide average of approximately 5.7 meters, while Landsat Time Series Explorer data indicate modest improvements in vegetation health over time, as evidenced by rising NBR values. The preservation of canopy in these areas appears to be associated with long-term residential continuity, larger lot sizes, reduced redevelopment pressure, and the maintenance of established green spaces, indicating that cultural practices and social cohesion may play a critical role in sustaining ecological stability within urban neighborhoods, while also suggesting that demographic settlement patterns can intersect with environmental processes to produce localized resilience even in the context of citywide urbanization.

Ultimately, by comparing neighborhoods experiencing intensive redevelopment with those exhibiting environmental stability, this study highlights the importance of integrating social context into analyses of urban land cover change, demonstrating that the effects of urban growth are not uniform across a single city and that human settlement patterns can significantly influence ecological outcomes, particularly in terms of tree canopy preservation and vegetation health, which are critical for maintaining ecosystem services and quality of life in densely populated areas. The combination of high-resolution satellite data, time-series analysis, and field-based verification provides both quantitative and qualitative insight into these complex interactions, emphasizing the need for urban planning and environmental management strategies that account for the ways in which human communities curate natural landscapes, while also illustrating the broader applicability of remote sensing as a tool for understanding the intertwined dynamics of social structure and cultural practices within urban ecosystems.

Funding: This research was funded by NASA CSR SEES.

Data Availability Statement: Data are available at Zenodo: 10.5281/zenodo.18795944, 10.5281/zenodo.18795671

Acknowledgment: The author would like to acknowledge the support of the 2025 Earth System Explorers (ESE) team, NASA science mentors, and ESE peer mentors. This research was conducted as part of the NASA STEM Enhancement in the Earth Sciences (SEES) high school internship program. The NASA Earth Science Education Collaborative leads Earth Explorers through an award to the Institute for Global Environmental Strategies, Arlington, VA (NASA Award NNX6AE28A). The SEES high school summer intern program is led by the Texas Space Grant Consortium at the University of Texas at Austin (NASA Award NNX16AB89A0).

Conflicts of Interest: The authors declare no conflicts of interest. The funders had no role in the design of the study; in the collection, analyses, or interpretation of data; in the writing of the manuscript; or in the decision to publish the results.

References

Data USA (2023). *Euless, TX.* https://datausa.io/profile/geo/euless-tx.

Jia, J., Sun, H., Jiang, C., Karila, K., Karjalainen, M., Ahokas, E., Khoramshahi, E., Hu, P., Chen, C., Xue, T., Wang, T., Chen, Y., & Hyyppä, J. (2021). Review on active and passive remote sensing techniques for road extraction. *Remote Sensing, 13*(21), 4235. https://doi.org/10.3390/rs13214235.

Kohl, H. (2019) "GLOBE Observer." Globe.gov, NASA, https://observer.globe.gov/.

Kshetri, N. (2023). Remote sensing and satellite imagery. *In Fourth revolution and the bottom four billion: Making technologies work for the poor* (pp. 103–126). University of Michigan Press. https://doi.org/10.3998/mpub.12205632.

Niche (n.d.). *Euless,* TX. Retrieved 8 September 2025, from https://www.niche.com/places-to-live/euless-tarrant-tx/#residents-content.

Singh, K. D. (2000). Role of remote sensing. *In Guidelines on national inventory of village forests* (pp. 25–28). Center for International Forestry Research. http://www.jstor.org/stable/resrep02165.11.

U.S. Census Bureau (2024). American Community Survey 5-year estimates. Retrieved from Census Reporter Profile page for Euless, TX http://censusreporter.org/profiles/16000US4824768-euless-tx/.

Waring, R. H., Way, J., Hunt, E. R., Morrissey, L., Ranson, K. J., Weishampel, J. F., Oren, R., & Franklin, S. E. (1995). Imaging radar for ecosystem studies. *BioScience*, *45*(10), 715–723. https://doi.org/10.2307/1312677.

Weishampel, J. F., Ranson, K. J., & Harding, D. J. (1996). Remote sensing of forest canopies. *Selbyana, 17*(1), 6–14. http://www.jstor.org/stable/41759918.

Best Practice

Evaluating Satellite Land Cover Accuracy in a Suburban Environment Using Citizen Science: New Hyde Park, NY

Nandini Khaneja[1,*], Russanne Low[2], and Peder Nelson[3]

[1] 12th Grade, Great Neck South High School, Lake Success, NY, USA; https://orcid.org/0009-0005-1946-7887
[2] Institute for Global Environmental Strategies; low.russanne@gmail.com; https://orcid.org/0000-0002-7912-4350
[3] Oregon State University; peder.nelson@oregonstate.edu; https://orcid.org/0000-0003-3979-9051
[*] Corresponding Author: nandiniakhaneja@gmail.com

Academic Editor: FirstName LastName
Received: 28 February 2026
Revised: 19 April 2026
Accepted: 20 April 2026
Published: 30 April 2026

Abstract: Accurate land cover classification is essential for environmental monitoring, urban planning, and climate research; however, suburban landscapes remain difficult to characterize due to heterogeneous land cover. This case study evaluates the agreement between satellite-derived land cover tools and ground-based citizen science observations in New Hyde Park, New York. Using the Adopt-a-Pixel 3 km methodology, thirty-seven primary sampling units were established within a standardized area of interest. Field observations were collected using National Aeronautics and Space Administration (NASA)'s Global Learning and Observations to Benefit the Environment (GLOBE) Observer application and supplemented with high-resolution reference classifications generated through Collect Earth Online. These datasets were compared with satellite observation, specifically from European Space Agency (ESA) WorldCover, Dynamic World, ESRI Land Cover, Landsat time-series, and Meta/WRI Global Canopy Height datasets. Results indicate frequent over-generalization of developed land cover and underrepresentation of tree canopy, with the strongest agreement observed where surface water is present. Qualitative field documentation and community accounts revealed that storm damage, aging trees, and housing management practices contributed to long-term greenery loss, helping to explain some discrepancies between ground and satellite observations. Findings demonstrate that integrating citizen science, community knowledge, and reference data will continue to improve land cover assessment in suburban regions and support more inclusive and reliable environmental monitoring.

Keywords: citizen science, land cover comparison, suburban geography, remote sensing, participatory science

1. Introduction

Satellite-derived land cover products are widely used to study environmental change, ecosystem health, and urban expansion. However, their accuracy is often constrained in suburban regions where residential development, tree canopy, and small green spaces are interwoven. Moderate-resolution imagery frequently generalizes these heterogeneous landscapes into dominant classes, particularly in areas containing a mix of developed and vegetated land cover types or where shadows are present.

Ground-based validation is therefore essential to assess and improve the reliability of these datasets. Citizen science provides a scalable mechanism for collecting such validation data by enabling public participation in environmental monitoring. National Aeronautics and Space Administration (NASA)'s Global Learning and Observations to Benefit the Environment (GLOBE) Observer program supports this effort by allowing participants to document land cover conditions using a mobile application. GLOBE is one of the world's most used citizen science platforms, and its use in increasing the availability and reliability of environmental data is used by scientists all over the world.

While citizen science expands spatial coverage, data quality is impacted by social, technical, and environmental constraints. This study presents a focused case analysis of New Hyde Park, New York, to evaluate satellite land cover accuracy in a suburban context and to examine how community characteristics and participant experience shape citizen-generated environmental data. We hypothesize that land cover may be overgeneralized and inaccurate at the granularity of satellite data accessible.

Citation: Khaneja N., Low, R., and Nelson, P. (2026). Evaluating Satellite Land Cover Accuracy in a Suburban Environment Using Citizen Science: New Hyde Park, NY. Journal of Earth Observation and Geospatial Applications, 2(1), 51–58. https://doi.org/10.65372/fnv3yf88

2. Study Area and Methods

2.1. Study Area: New Hyde Park, New York and the Surrounding Region

New Hyde Park, formerly called Hyde Park, is located in Nassau County within the New York City metropolitan region. One of the earliest settlements in the United States, with Dutch settlers arriving in the 1620s and English settlers in the 1640s, the land was first used as a racecourse and later became farmland. The arrival of the Long Island Railroad in 1837 and later trolley and bus lines transformed the area into a commuter hub, spurring waves of immigration from German, Irish, Polish, Italian, and Jewish communities (Nowakowski, n.d.). The region underwent rapid suburbanization during the mid-twentieth century, resulting in dense residential development interspersed with mature street trees, private backyards, and small municipal parks. This pattern resulted in uneven tree cover, with mature canopy concentrated along residential streets and private properties and limited vegetation in commercial and high traffic corridors.

The region has experienced environmental disturbances, including major storms such as Superstorm Sandy in 2012, which contributed to canopy loss and infrastructure damage. Ongoing redevelopment and aging tree removal have further altered land cover patterns, presenting challenges for satellite-based classification. The 3 km × 3 km area of interest (AOI) encompasses portions of New Hyde Park, North New Hyde Park, Manhasset Hills, and Garden City Park.

2.2. Data Sources

This study employed a mixed-methods approach combining citizen science observations, manually assigned classifications, remotely sensed satellite data, and qualitative field documentation to evaluate land cover patterns in New Hyde Park.

2.2.1. Citizen Science Data

Ground-based observations were collected using NASA's GLOBE Observer mobile application. At each primary sampling unit (PSU), geotagged photographs were captured in six directions (north, south, east, west, upward, and downward) to document local land cover conditions. These images provided visual context for dominant surface types, vegetation structure, and built features. Associated metadata, including geographic coordinates and timestamps, were used to align field observations with satellite datasets using ArcGIS (ESRI, 2020).

Due to residential access restrictions and positional inaccuracies in geolocation data, some observations fell outside designated PSU boundaries and were excluded from quantitative analysis. Figures 1(a-c), below, show sample images of GLOBE observations in the New Hyde Park AOI.

Figure 1. Images taken by researcher, recorded in GLOBE Observer database/visualization tool.

2.2.2. Manually Assigned Classifications

Collect Earth Online (CEO) was used to generate reference classifications. Each 100 m x100 m PSU was subdivided into a 10 x 10 grid containing 100 evenly distributed points. Land cover at each point was manually classified using high-resolution satellite imagery. This process produced over 3,700 reference observations for the AOI, serving a benchmark for evaluating sorted satellite maps. The user interface to CEO is shown in Figure 2.

Figure 2. Collect Earth Online classification user interface.

2.2.3. Satellite Data

Multiple satellite-based land cover products were analyzed to capture differences in spatial resolution, classification methodology, and temporal coverage:

- European Space Agency (ESA) WorldCover (10m, 2020/2021) (Zanaga et al., 2021)
- Dynamic World (10m) (Brown et al., 2022)
- ESRI Land Cover (2017/2024)
- Meta/ World Resources Institute(WRI) Global Canopy Height (1m)
- Landsat time-series imagery (1984–2025)

Satellite datasets were accessed through EarthMap, Google Earth Engine, and ArcGIS Online platforms. Image comparisons were conducted to align satellite classifications with PSU boundaries. To enable comparison across datasets with differing classification schemes, land cover categories were aggregated into broader functional classes, including developed surfaces, vegetation, and water. This aggregation was necessary because satellite products such as Dynamic World, ESRI, and WorldCover use differing classifications relative to each other and CEO, while Meta/WRI solely focuses on tree canopy height and presence. The analysis therefore focuses on general agreement patterns.

2.2.4. Qualitative Field Documentation and Community Accounts

In addition to quantitative datasets, qualitative documentation was collected by participant observation and Community Chronicles developed during the research process. These materials recorded resident perspectives on vegetation change, storm impacts, and household response in the long-term.

Community accounts included estimates that “20–25%” of neighborhood canopy had been lost since the 1990s due to storm damage, aging trees, and redevelopment. Longitudinal field observations based on author documentation recorded the repeated trimming and removal of mature trees at residential properties following Superstorm Sandy and subsequent severe thunderstorms, including major canopy reduction within the AOI in 2013 and 2020, as shown in Figure 3(a-c).

Figure 3. Images of a fallen tree resulting from a 2020 thunderstorm (Image credit to Nandita Khaneja).

2.3. Methods

The Adopt-a-Pixel 3 km methodology was applied following Low et al. (2021). In this approach, researchers define a standardized AOI measuring 3 km by 3 km. Each AOI is divided into a 6 by 6 grid, creating 36 coordinate points evenly spaced 500 m apart. At each point, a 100 m by 100 m square, called a PSU, is centered. The 37th square, known as the centroid, is added at the exact center of the AOI, bringing the total number of sampling units to 37.

Once applied, the Adopt a Pixel 3 km methodology clearly delineates a study area and enables methodical, repeatable observations across defined spatial units. Its structured yet accessible format makes it well-suited for both researchers and citizen scientists. In addition to the ease of comparison between in-person observed data and remotely sensed data that the methodology offers, the proximity of sampling units facilitates local participation, expanding public accessibility and participation in environmental monitoring while fostering broader engagement in Earth sciences.

To analyze the level of agreement between reference and remotely sensed data in the context of each AOI, results from each data collection method are placed side by side in a comprehensive table. The table is organized so that moving from top to bottom, each column represents all of the collected data from one specific source or data set, and moving from right to left, each row contains all of the collected data from one specific sampling unit. This table was included as part of a larger poster on the topic of the same research. The poster also included additional representations of collected data, including the full AOI mapped onto each of the satellite data sets, as well as a side-by-side series of image chips pulled from the Landsat time-series data. To demonstrate the process behind evaluating the extent to which remotely sensed data and reference data agree with one another, data is pulled from rows, or primary sampling units, where the reference data and remotely sensed data agreed, partially agreed, and completely disagreed.

3. Results

3.1. Data Agreement Patterns

Comparison tables and imagery revealed limited full agreement among datasets for most PSUs. The only PSU (1 out of 37) exhibiting consistent agreement across all data sources corresponded to a local pond, which was accurately classified as surface water. Partial agreement occurred in the majority of PSUs (33 out of 37), in residential areas containing mixed impervious surfaces and vegetation. Disagreement occurred in few PSUs (3 out of 37), most commonly along tree-lined streets and backyard spaces where satellite products frequently classified areas as fully developed.

Meta/WRI canopy height data most consistently detected tree cover. ESA WorldCover demonstrated moderate agreement with reference data, while Dynamic World and ESRI products frequently over-generalized built surfaces. For example, in Figure 4, with data excerpted from Table 1, CEO and GLOBE data in PSU #15 shows the presence of tree canopy and developed land (road). Meta/WRI and WorldCover account for this heterogeneity, while Dynamic World and ESRI classify the area as fully developed, as shown by the solid red highlight. PSUs (#14, #15, and #24) also shows the Agreement, Partial Agreement, and Disagreement examples, respectively.

Table 1. Summary of estimated data agreement patterns across all listed PSUs investigated in the New Hyde Park AOI.

Data Source	Agreement	Disagreement
Meta/WRI	27	10
WorldCover	19	18
Dynamic World	2	35
ESRI	1	36
Total	**49**	**99**

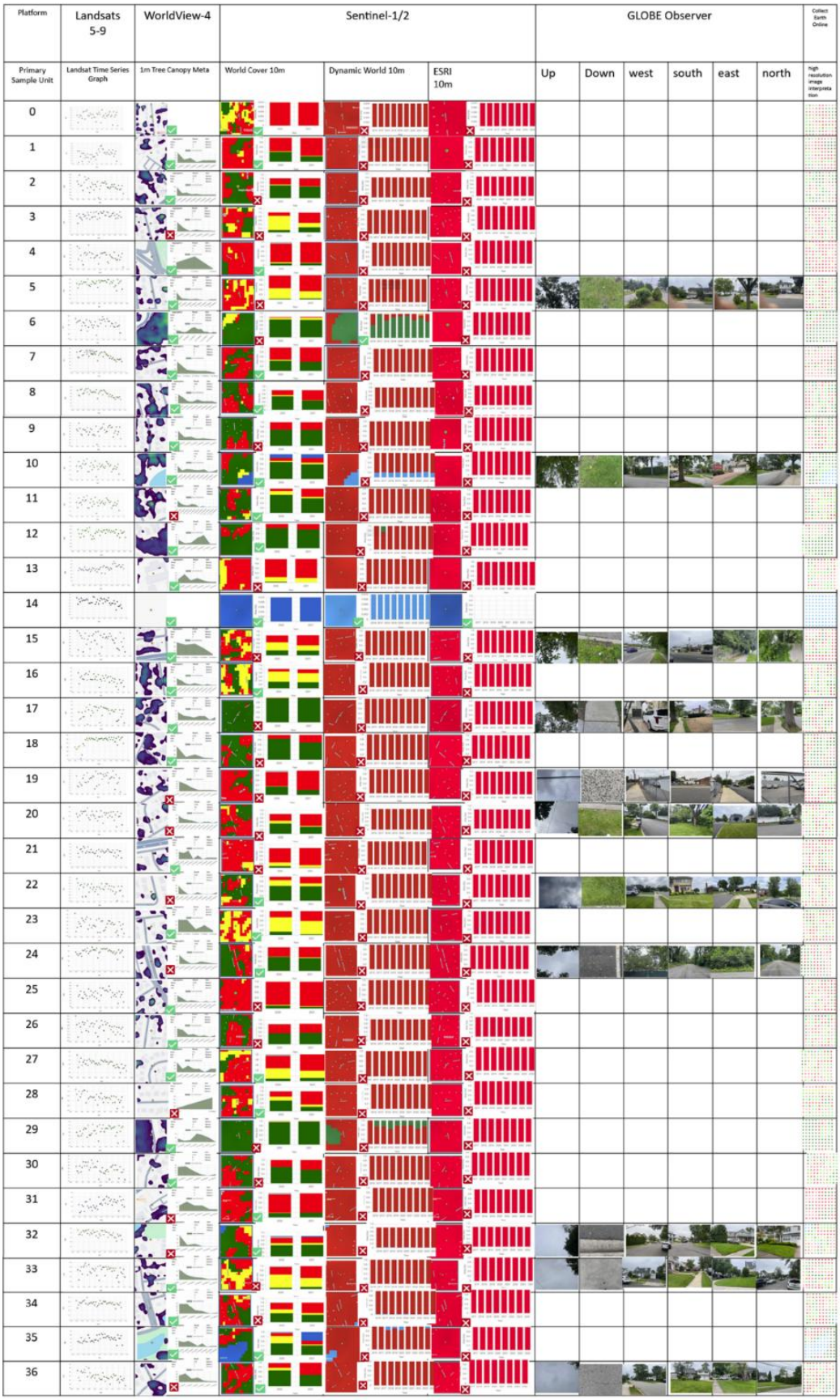

Figure 4. Adopt-a-Pixel comparison table.

Confusion matrices (Table 2) illustrate classification agreement patterns for WorldCover, Dynamic World, and ESRI, showing that vegetated areas are frequently misclassified as developed surfaces in Dynamic World and ESRI datasets. This analysis is based on the dominant land cover type in each PSU, and comparison is performed to a CEO dataset.

Table 2. Confusion matrices for the WorldCover, Dynamic World, and ESRI (Predicted) relative to CEO and GLOBE (Reference).

(a) WorldCover (Reference \ Predicted)	Developed	Vegetation	Water
Developed	12	6	0
Vegetation	5	12	0
Water	0	0	2

(b) Dynamic World (Reference \ Predicted)	Developed	Vegetation	Water
Developed	21	0	0
Vegetation	14	1	0
Water	0	0	1

(c) ESRI (Reference \ Predicted)	Developed	Vegetation	Water
Developed	21	0	0
Vegetation	15	0	0
Water	0	0	1

3.2. Effects of Data Collection Constraints

Due to GPS misalignment and access limitations in residential areas, several GLOBE observations fell outside designated PSU boundaries and were excluded from quantitative comparison. Participant concerns regarding private property and neighborhood interactions further restricted data collection in some locations. These constraints reduced the number of usable ground observations and contributed to gaps in validation coverage.

3.3. Temporal Trends

Landsat time-series analysis indicated gradual decreases in canopy cover over time, consistent with aging tree removal, storm impacts, and redevelopment. These trends aligned with local observations reported by community members and municipal records.

4. Discussion

4.1. Suburban Classification Challenges and Limitations

Results demonstrate that suburban landscapes pose persistent challenges for moderate-resolution satellite classification. Fragmented canopy, narrow vegetation corridors, and small private green spaces are systematically underrepresented in most products. Mixed pixels and spectral confusion contribute to these inaccuracies. Spectral confusion refers to the inability of satellite sensors to distinguish between land cover types with similar reflectance signatures.

Higher-resolution datasets, particularly WorldCover and Meta/WRI, performed better in capturing fine-scale features, though discrepancies remained.

A key limitation of this study is the use of aggregated land cover categories for cross-dataset comparison. Differences in classification systems across satellite products required grouping into broader functional classes, which may obscure finer distinctions between land cover types. As a result, agreement metrics should be interpreted as indicative of general classification trends rather than precise accuracy measurements. Due to differences in classification schemes, the confusion matrix reflects agreement at the aggregated category level rather than original dataset classifications.

4.2. Community Context and Citizen Sciences

Community history, land-use patterns, and participant experience played central roles in shaping both land cover structure and data collection practices in New Hyde Park. Postwar suburban development produced dense residential neighborhoods characterized by narrow vegetation corridors, mature street trees, and privately managed backyard canopy. This landscape configuration complicates satellite-based classification and limits public access for field validation.

Participant observations and community engagement revealed that private property boundaries, resident concerns, and social interactions influenced where and how GLOBE observations could be collected. These constraints resulted in uneven spatial coverage and reduced sample density in some PSUs. Rather than representing methodological weaknesses, these limitations reflect the realities of conducting environmental research in lived residential environments. Community Chronicles provided additional insight into long-term vegetation change. Resident estimates indicating approximately 25% canopy loss were consistent with Landsat-derived trends and CEO reference data. The lead author's longitudinal observations of storm-related tree trimming and removal following Hurricane Sandy further illustrated how household-level safety decisions contribute to cumulative canopy decline.

These household and community-level management practices are rarely captured in remote sensing products but represent important mechanisms driving land cover change. While satellite imagery documents net vegetation loss, qualitative data explain how extreme weather events, infrastructure vulnerability, and homeowner responses shape observed patterns.

4.3. Implications for Platform Design: Development Toward EarthLens

Findings revealed recurring technical and operational barriers that limited the scientific utility of citizen-generated data, including image compression, inconsistent metadata retention, and restricted visualization workflows.

In response, the EarthLens platform is being developed as a research-oriented extension of existing citizen science frameworks. EarthLens integrates low-altitude drone imagery, high-resolution ground photography, and satellite data within a unified analytical environment. The system incorporates visible and near-infrared cameras, compact spectrometers, and precision geotagging hardware to preserve spatial and spectral fidelity.

EarthLens supports automated land cover classification through machine-learning models trained on validated reference datasets. Native visualization tools enable multi-scale comparison between drone, satellite, and ground-based data. By grounding system design in empirical findings and participant feedback, EarthLens represents a research-informed approach to improving citizen science infrastructure.

5. Conclusions

This case study demonstrates that structured citizen science observations, when combined with the Adopt-a-Pixel methodology, provide valuable validation for satellite land cover products in suburban environments. In New Hyde Park, satellite datasets frequently over-generalize developed land cover and underestimate fragmented tree canopy. Community history, land-use patterns, and participant access constraints significantly influenced data quality and interpretation. These contextual factors are essential for understanding discrepancies between ground and satellite observations.

Limitations identified in the GLOBE Observer platform highlight the need for improved tools that support high-resolution, analysis-ready citizen-generated data. The development of EarthLens illustrates how mixed-methods research can inform the design of next-generation observation platforms grounded in community experience and empirical validation.

Funding: The authors would like to acknowledge the support of the 2025 Earth System Explorers (ESE) Team, NASA Science Mentors, and ESE peer mentors. NASA STEM Enhancement in the Earth Sciences (SEES) Virtual High School Internship program. The NASA Earth Science Education Collaborative leads Earth Explorers through an award to the Institute for Global Environmental Strategies, Arlington, VA (NASA Award NNX6AE28A). The SEES High School Summer Intern Program is led by the Texas Space Grant Consortium at the University of Texas at Austin (NASA Award NNX16AB89A0).

Data Availability Statement: Data are available in Zenodo (doi:10.5281/zenodo.18702869). Maps throughout this study were created using ArcGIS® software by Esri. ArcGIS® and ArcMap™ are the intellectual property of Esri and are used herein under license. Copyright © Esri. All rights reserved. For more information about Esri® software, please visit https://www.esri.com. All GLOBE images were sourced from the GLOBE Date Visualization System, but generated by the researchers. This dataset is produced for the Dynamic World Project by Google in partnership with National Geographic Society and the World Resources Institute.

Acknowledgment: The authors thank Dr. Cassie Soeffing, Mr. Andrew Clark, and Dr. Brianna Lind for their mentorship and guidance.

Conflicts of Interest: The authors declare no conflicts of interest. The funders had no role in the design of the study; in the collection, analyses, or interpretation of data; in the writing of the manuscript; or in the decision to publish the results.

References

Brown, C. F., Brumby, S. P., Guzder-Williams, B., Birch, T., Brooks Hyde, S., Mazzariello, J., Czerwinski, W., Pasquarella, V. J., Haertel, R., Ilyushchenko, S., Schwehr, K., Weisse, M., Stolle, F., Hanson, C., Guinan, O., Moore, R., & Tait, A. M. (2022). Dynamic World: Near real-time global 10 m land use land cover mapping. Scientific Data, 9, Article 251. https://doi.org/10.1038/s41597-022-01307-4

ESRI (2020). *ArcGIS Pro* (Version 2.6) [Computer software]. https://esri.com.

Low, R. D., Nelson, P. V., Soeffing, C., Clark, A., & SEES 2020 Mosquito Mappers Research Team. (2021). Adopt a pixel 3 km: A multiscale data set linking remotely sensed land cover imagery with field-based citizen science observation. *Frontiers in Climate*, *3*, Article 658063. https://doi.org/10.3389/fclim.2021.658063

Nowakowski, C. (n.d.). *The origins of New Hyde Park.* The Village of New Hyde Park. Retrieved on 31 August 2025 from https://villagenhpny.gov/the-origins-of-new-hyde-park/

Zanaga, D., Van De Kerchove, R., De Keersmaecker, W., Souverijns, N., Brockmann, C., Quast, R., Wevers, J., Grosu, A., Paccini, A., Vergnaud, S., Cartus, O., Santoro, M., Fritz, S., Georgieva, I., Lesiv, M., Carter, S., Herold, M., Li, Linlin, Tsendbazar, N.E., Ramoino, F., Arino, O., 2021. ESA WorldCover 10 m 2020 v100. https://doi.org/10.5281/zenodo.5571936

Best Practice

Comparison of Land Cover Classifications between Ground Observations and Remote Sensing Data in San Diego, California

Sophia Farber[1,*], Peder V. Nelson[2], and Russanne Low[3]

[1] 12th grade, Canyon Crest Academy, San Diego, California, United States of America
[2] Oregon State University; peder.nelson@oregonstate.edu
[3] Institute for Global Environmental Strategies; low.russanne@gmail.com
[*] Corresponding Author: sophiamc.farber@yahoo.com; +1-858-205-0946.

Academic Editor: Jeong Chang Seong

Received: 28 February 2026
Revised: 3 April 2026; 8 April 2026
Accepted: 20 April 2026
Published: 30 April 2026

Abstract: Land cover and its changes are intertwined with human and natural activities. Accurate land cover data is invaluable for land use decisions as well as understanding local and global land cover change. This study explored the local land cover trends of an area of interest in San Diego, California, with the goal of evaluating consistency between ground observations, manual land cover classifications, and land cover maps from remote sensing sources. Ground observations were taken using the Global Learning and Observations to Benefit the Environment (GLOBE) Observer application. Remote sensing sources were accessed through Earth Map, and included the World Cover, Dynamic World, ESRI, and Meta/WRI Global Canopy Height maps of land cover and tree canopy based on satellite imagery. While there was general agreement between ground observations and remote sensing sources over the area as a whole, small inconsistencies were found at nearly all sampling points, and blatant differences were found at three of thirty-seven sampling points between the chosen remote sensing sources as well as between ground observations and remote sensing maps. These inconsistencies were most obvious with the Dynamic World and ESRI datasets, which tended to overgeneralize urban land cover compared to the World Cover dataset. The discrepancies between sources describing the land cover of the same area show the need for caution when examining remote sensing sources and the challenges of remote sensing data, which are increased with differing classification measures.

Keywords: land cover, GLOBE Observer, remote sensing, urbanization, impervious surface

1. Introduction

Remote sensing data are an amazing tool for researchers, leaders, and citizens alike. These data, ranging from satellite images seen on Google Maps to precise measurements of atmospheric conditions, have made studying the Earth from a distance, and thus at a global scale, possible (Gorelick et al., 2017). Land cover studies particularly benefit from remote sensing data because from the satellite view, huge swaths of land can be observed and compared. Regions that may be difficult to reach can be classified with remote sensing data and give scientists a better idea of the land cover in those areas. Satellite imagery is also helpful for land cover classification in that the enormous amounts of data and "zoomed-out" view can help scientists to compare the amounts of different types of land cover more easily than with ground estimates. However, ground observations are critical to validating these remote sensing data.

Satellite images, such as those from the Landsat missions and the images discussed in this study, are taken from a bird's eye perspective, and although there are many remote sensing datasets that create topographical maps and take into account elevation, these images do not. Therefore, while a tree canopy may be clear in a satellite image, its height above the ground is not clear. Additionally, there may be different land cover underneath the tree canopy that is not visible to the satellite. Cloud coverage can also be a barrier to obtaining images of land cover in certain areas. Thus, ground observations, especially those from citizen scientists, can help to validate the land cover observed by satellite images (Low et al., 2021).

The Global Learning and Observations to Benefit the Environment (GLOBE) Observer application is a citizen science application that allows citizens to take and upload photos of the land cover in their area, and

Citation: Farber, S., Nelson, P.V. & Low, R. (2026). Comparison of Land Cover Classifications Between Ground Observations and Remote Sensing Data in San Diego, California. Journal of Earth Observation and Geospatial Applications, 2(1), 59–68. https://doi.org/10.65372/hgazje62

upload them to the GLOBE Visualization System, where they can be accessed openly (NASA, 2025). The benefit of a citizen science approach to ground observation collection is that citizen scientists are located globally, and can provide more data, faster, from many locations (Nelson et al., 2024).

The purpose of this study is to qualitatively explore the accuracy of ground observations compared to remote sensing data for the selected area of interest (AOI), located in San Diego, California. First, ground observations were made using the GLOBE Observer application to show the feasibility of citizen science contributions to land cover research (Nelson et al., 2024). Then, manual classifications of land cover were made using the Collect Earth Online (CEO) platform (Saah et al., 2019) at the same locations in order to provide a verified dataset of the land cover. Finally, land cover classifications from several remote sensing sources were compared with the CEO data and ground observations to reveal consistencies and discrepancies between the data. To provide context for the area of interest, historical land cover data were collected from the Annual National Land Cover Database (Jin et al., 2023; USGS, 2024).

Providing an example of the repeatable process of comparison of ground observations and remote sensing data, this study supports further improvement of land cover classifications based on remote sensing data. The discrepancies found between remote sensing data and manual classifications also demonstrate the need for extra consideration of remote sensing data when it is used for land use decisions because of the differences between remote sensing datasets, classification approaches, and land cover examination strategies over the same area.

2. Study Area and Methods

2.1. Study Area

The study area consisted of a 3 km × 3 km AOI in San Diego, California (Figure 1). The City of San Diego is located in the Southwest corner of the continental United States, framed by the Pacific Ocean to the west and deserts and mountains to the east. Topographic features are diverse, ranging from coastal bluffs, estuaries, and lagoons, to mountains, mesas, and canyons. Similar to much of Southern California, the most common natural disasters are earthquakes and wildfires, however San Diego's location on the coast also puts the city at risk of tsunamis. The coastal desert climate keeps temperatures consistent in the low twenties Celsius, along with consistently little rainfall (U.S. Federal Government, 2025). San Diego regularly sees a marine layer—a layer of cloud or fog that forms over the ocean and coast due to water that is colder than the air above it—in the mornings, especially in early summer (NOAA, 2023).

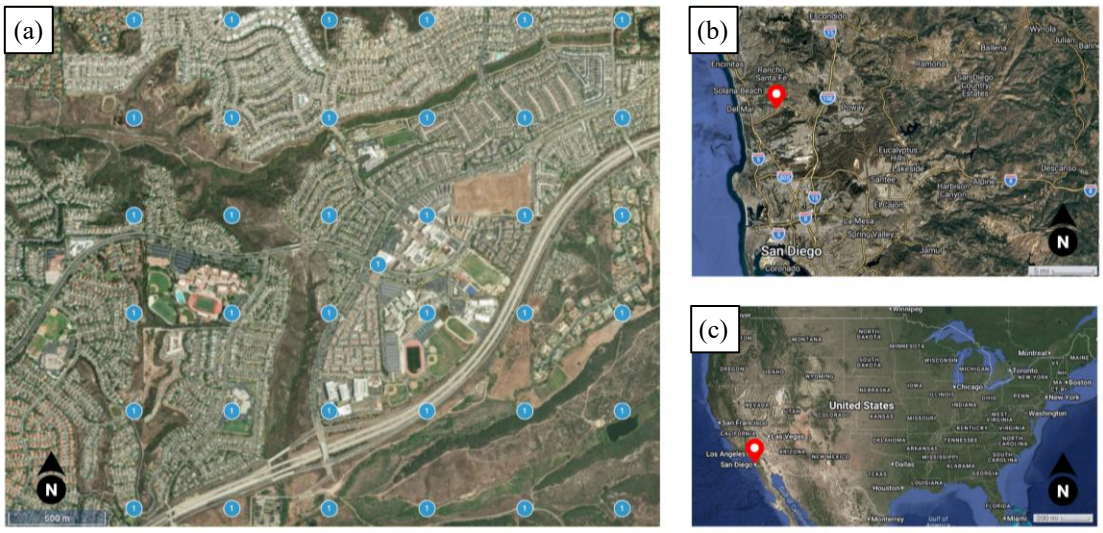

Figure 1. (a) Study area as viewed on the Collect Earth Online platform. Blue pins show the locations of each of the 37 data sites in the AOI, with the number 1 inside each point indicating one data site at the point. (b) Location of study area in California, as viewed with Google Maps. (c) Location of study area in the United States, as viewed with Google Maps.

San Diego is known globally for features ranging from the San Diego Zoo to significant military installations, including Naval and Marine Corps bases. San Diego is also a hotspot for innovative industries including biotechnology, software, and Smart City technology. The center of the study area is located around 35 miles north of the San Ysidro Border Crossing with Mexico. With 1.4 million people, the City of San Diego is the second most populous city in California, and eighth most populous in the United States. San Diego is also an incredibly multicultural city.

The AOI was centered around the Pacific Highlands Ranch community, with the California State Route 56 highway running diagonally through it in the southwest to northeast direction. Deer Canyon in the southeast corner and Gonzales Canyon in the northwest corner place the suburban area in between two natural spaces. The center portion of the AOI has rapidly urbanized within the last three decades, with construction of a majority of suburban housing developments, several apartment and condo complexes, schools, and a central shopping center appearing within the last twenty years. This rapid human development makes the AOI of use in evaluating inconsistencies between remote sensing and ground-based observations over a period of rapid change in land cover. The majority of data collection sites within the AOI consisted of built-up land, with the canyons preserving wild space.

2.2. Data

The AOI was a 3 km × 3 km area, following the Adopt a Pixel 3 km method (Low et al., 2021). The data collected consist of images at 37 points, as will be further discussed in Section 2.3: Methods, within the AOI and images of the entire AOI over a longer time period. Ground observations consisted of photos taken with the GLOBE Observer application at each of the 37 points selected within the AOI. Limitations of the ground observations came in the form of inaccessibility of exact observation sites due to private property lines and obstructive vegetation. Remote sensing sources were accessed from the Earth Map website, with the following land cover and forestry layers used: Meta/WRI Global Canopy Height (Tolan et al., 2024), World Cover 10 m (Zanaga et al., 2021), Dynamic World (Brown et al., 2022), and ESRI 2017/2024 (Karra et al., 2021). The Meta/WRI Global Canopy Height maps global tree canopy height using data from Worldview-4. World Cover 10 m is a global land cover map created with Sentinel-1 and Sentinel-2 imagery at a spatial resolution of 10 m. Dynamic World and ESRI 2017/2024 have 10 m spatial resolution and are land classification datasets based on Sentinel-2 imagery. Additionally, manual land cover classifications were made through the CEO platform (Saah et al., 2019) for the 37 data sites in the AOI. CEO classifications were made with the Mapbox Satellite base imagery, which combines several remote sensing sources to create a global layer at 1−2m spatial resolution, with higher resolution available in select locations (Saah et al., 2019; Mapbox, n.d.).

To analyze land cover change over time, two sets of image chips were compared over a 40 year period to evaluate the entire AOI area. First, annual satellite images at 30 m spatial resolution from the Landsat missions were collected through the Google Earth Engine Landsat time series (LTS) Explorer (Braaten, n.d.). These image chips cover the entire 3 km × 3 km area and utilize SWIR1/NIR/GREEN for the RGB Visualization, which assigns the red channel to Shortwave Infrared 1, green channel to Near Infrared, and blue channel to Green visible light, creating a vibrant false color composite to highlight changes in vegetation health and greater contrast between land cover elements. Second, fractional impervious surface images from the Multi-Resolution Land Characteristics (MRLC) Consortium Annual National Land Cover Database (Jin et al., 2023; MRLC Consortium, n.d.) were used. The fractional impervious surface images use a 30 m resolution based on Landsat data (USGS, 2024), thus making the LTS and MRLC data consistent in spatial resolution for comparison.

2.3. Methods

37 points within the AOI were generated in a 6 × 6 grid pattern with an additional center point, called the centroid. Each of the 36 non-centroid points is spaced 500 meters from its adjacent points, and is placed in the center of a 10000 m² (100 m × 100 m) area. The points were numbered starting with 1 in the bottom left corner, and increasing up each column of the grid, with increasing columns from left to right (Figure 2). The centroid was considered to be point 0. The coordinates for each point were stored in a CSV file, while a GeoJSON file was used to store the boundaries of the AOI, the boundaries of the 10000 m² boxes around each point, and the coordinates of each point.

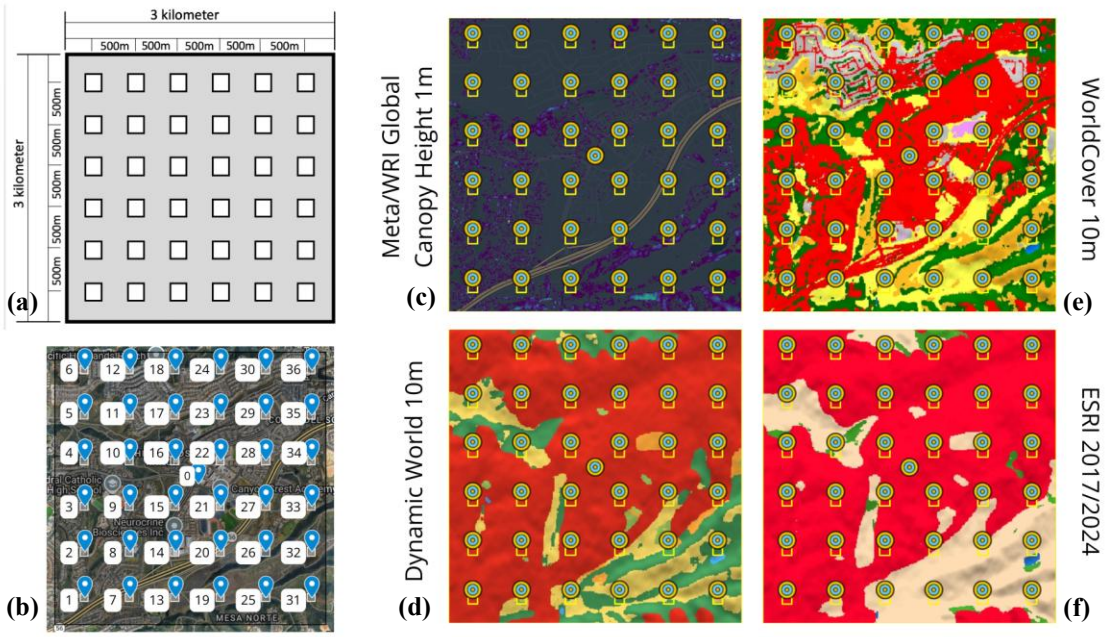

Figure 2. (a) Adopt a Pixel 3 km framework used to create an AOI (Source: Peder Nelson). (b) Numbered sampling points in AOI grid. (c–f) AOI as viewed on Earth Map with land cover and tree canopy layers; (c) Meta/WRI Global Canopy Height 1 m. (d) Dynamic World 10 m. (e) World Cover 10 m. (f) ESRI 2017/2024. All show land cover classifications that are different in some areas.

Of the 37 points, ground observations using the GLOBE Observer application were captured within the 10000 m² area at 34 points. Data were collected for the inaccessible points (33, 34, 36) slightly outside of the designated area and thus are not representative of the land cover at the point but are similar. Each ground observation included six photos: one in each of the cardinal directions, one down toward the ground, and one up towards the sky. These photos were uploaded to the GLOBE Visualization System.

At each of the 37 points, eight image chips from the Earth Map website were collected. These eight images included: one image of the 10000 m² area surrounding the point of each of the four Earth Map layers (Meta/WRI Global Canopy Height, World Cover 10 m, Dynamic World, and ESRI 2017/2024), one graph of the area distribution of tree canopy heights within the 10000 m² area from the Meta/WRI Global Canopy Height dataset, one graph of the historical distribution of land cover categories from 2020 to 2021 of the World Cover 10 m dataset, one graph of the historical distribution of land cover categories from 2016 to 2024 of the Dynamic World 10 m dataset, and one graph of the historical distribution of land cover categories from 2017 to 2023 of the ESRI 2017/2024 dataset. The image chips of the 10000 m² area surrounding each point, from each of the Earth Map layers, were chosen to use the most recent data available from each respective layer. The most recent Meta/WRI Global Canopy Height data is from 2020, the most recent World Cover 10 m layer is from 2021, and the most recent Dynamic World 10 m and ESRI 2017/2024 layers are from 2024.

Additionally, a graph generated by the LTS of the Normalized Burn Ratio (NBR) from 1984 to 2025 was included for each point. Normalized Burn Ratio values provide insight into the vegetation characteristics of an area, as lower NBR values indicate less vegetation and recent burns, while higher NBR values indicate healthy and thicker vegetation.

At each of the 37 points, manual land cover classifications were made with CEO. Each point was divided into 100 subpoints, with each subpoint classified into one of the following thirteen categories: Trees_CanopyCover, Shadow, Bush/Scrub, Unknown, Grass, Bare Ground, Cultivated Vegetation, Building, Water > Lake/Ponded/Container, Water > Rivers/Stream, Water > Irrigation Ditch, Impervious Surface, Wetlands. An image of the 100 color-coded classifications, in a 10 × 10 grid overlaid onto the 10000 m² area, was then compared to the land cover classification maps from Earth Map. These manual classifications provided an additional land cover layer to compare with the ground observations and land cover maps from Earth Map.

Finally, as stated earlier, annual satellite images of the 3 km × 3 km area were used to compare land cover over a longer period of time. Evaluating change over time in land cover was desired in order to reveal the overall trends that may have led to inconsistencies between ground observations and the remote-sensing-based land cover classification layers from Earth Map. These images revealed the rapid urbanization of the entire AOI over the twenty years between 2004 and 2024. A total of 42 images from the LTS collection correspond to the years 1984 to 2025, and 40 fractional impervious surface images from the MRLC database correspond to the years 1985 to 2024.

To quantify the overall built-up area for the entire 3km by 3km AOI, a geospatial analysis was performed in QGIS. For the MRLC fractional impervious surface data, the Zonal Statistics tool was used to calculate the mean pixel value across the AOI, which represents the total percentage of impervious surface cover. For the land cover classification layers (World Cover 10 m, Dynamic World 10 m, and ESRI), the area of the "Built-up" or "Built Area" classification was calculated as a percentage of the total 3 km × 3 km area. These calculations were performed using the 2024 layers for ESRI and Dynamic World, and the 2021 layer for World Cover. The area value for built-up classification values for each remote sensing source was found using the Change Matrix values from the Earth Map Analytics tool for the 3 km × 3 km boundary. For the CEO classifications, at each of the 37 data sites, the number of "Impervious Surface" and "Building" classifications were counted out of the 100 classifications made at the site. The total number of "Impervious Surface" and "Building" classifications were then summed. The total percentage of impervious surface cover for the AOI using CEO data was then calculated by dividing the aforementioned sum by the total number of land cover classifications made using CEO, which was 3700 classifications (100 classifications per data site).

2.4. Thematic Consistency Challenges and Qualitative Approach

Due to the lack of consistent land cover classification categories between the remote sensing sources, as well as the visual nature of the data, a contingency table for this study was not possible. A prime example of the similar but inconsistent descriptions of land cover elements is the categories provided by the Earth Map land cover layers. World Cover 10 m uses "grassland" and "shrubland" labels, while ESRI uses "rangeland" and "crops," and Dynamic World uses "grass" and "shrub & scrub." The majority of data collected for this study comes in the form of images, with the different land cover layers, satellite images, and manual photo sources providing varying numbers of pixels for the same area. Therefore, a complete statistical analysis was deemed unfeasible and the accuracy assessment is mainly qualitative rather than quantitative.

3. Results

3.1. Land Cover Change over Time and Fractional Impervious Surface in the AOI

Land cover change over time in the AOI was analyzed via comparison of the LTS images from 1984 to 2025, and the MRLC fractional impervious surface images from 1985 to 2024. These sets of images were highly consistent with each other (Figure 3). Starting in the 1980s, the coloration of the AOI was pink and red according to the LTS images, showing dirt and land without any buildings. This pink color is exaggerated by the RGB Visualization. A thin line of impervious surface crossed the center of the AOI as shown in the MRLC images. These shapes and colors remained consistent, with minimal growth of impervious surface, until 2003. 2003 shows a larger increase in impervious surface, and the following year, 2004, a substantial increase in impervious surface and transformation of the area is seen in the LTS image. Before 2003, it can be inferred that less than a quarter of the area was impervious surface, while in 2004, it can be inferred that only about a quarter of the area was not impervious surface. In the 21 years since this disruption, fractional impervious surface continued to increase slowly, with the final image in 2024 showing only the southeast corner of the AOI and a small portion of the northwest corner of the AOI not covered by impervious surface. These areas correspond to Deer and Gonzales Canyon as mentioned in Section 2.1. The LTS images show after the year 2004 a drastic change from the dominant red color before the disruption to a mix of dark green, purple, brown, and white, showing the colors of the urbanization of the area, with the building of a suburban neighborhood with schools, houses, roads, and a shopping center.

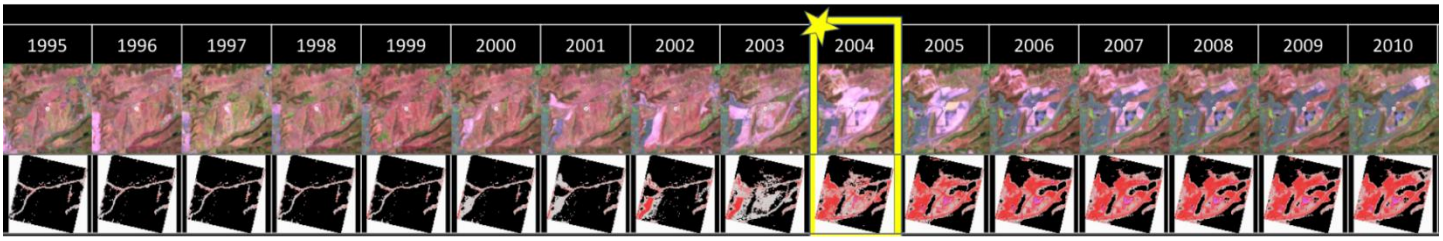

Figure 3. Comparison of annual LTS and MRLC fractional impervious surface images of the AOI from 1995 to 2010, showing the year 2004, when land cover rapidly changed. The top row shows LTS images, and the bottom row shows MRLC fractional impervious surface images.

These visual observations are confirmed by quantitative analysis of the MRLC images. From 1985 to 2001, the percentage of fractional impervious surface in the AOI remained under two percent. In 2002, this figure jumped to 4.58%, in 2003 the percentage increased to 6.22%, and in 2004, a significant increase resulting in 17.12% impervious surface. This number steadily rose to 38.82% fractional impervious surface in 2024 (see complete annual data in Zenodo repository).

The land cover layers from Earth Map, while differing in labeling schemes (as will be further explained in the Discussion section), consistently included a label for built-up areas, which we made to correspond to impervious surface as the other land cover category labels would not be considered impervious surface. To represent the most recent extent of urbanization in the AOI, built-up area percentages were calculated using the latest available data layers from each source: 2024 for ESRI and Dynamic World 10 m, and 2021 for World Cover 10 m. The manual classifications from CEO can also be used to estimate the total impervious surface in the AOI, as the manual classifications from each of the 37 points would be expected to be representative of the AOI as a whole. The total impervious surface was considered to include both the "Impervious Surface" and "Building" labels from CEO. These results, along with the MRLC 2024 fractional impervious surface value, are shown in Table 1.

While the MRLC, CEO, and World Cover 10 m data returned similar percentages of fractional impervious surface, Dynamic World 10 m and ESRI were about 30 percentage points higher. Although Dynamic World 10 m and ESRI are close to each other, within 2 percentage points, their values are far from the other three sources.

Table 1. Fractional Impervious Surface in 3 km × 3 km AOI according to remote sensing sources. The "Land Cover Category" refers to the label for impervious surface that each remote sensing source uses.

Dataset	Land Cover Label	Percent Fractional Impervious Surface
World Cover 10 m	Built-up	41.08%
Dynamic World 10 m	Built Area	69.53%
ESRI 10 m	Built Area	71.11%
MRLC	Fractional Impervious Surface	38.82%
CEO	Impervious Surface; Building	37.43%

3.2. Comparison of Land Cover Classifications at Sampling Points

At 34 of the 37 sampling points, remote sensing datasets predominantly matched GLOBE Observer ground observations and manual classifications from CEO. This "predominant" matching is assessed through visual confirmation due to the aforementioned unfeasible contingency table (for the complete table of all 37 sampling points and their associated remote sensing image chips, ground observations, and CEO manual classifications, see the poster in the Zenodo repository). Although at no data site there was 100% agreement between CEO classifications and a remote sensing land cover dataset, there were several sites with near perfect matches (Figure 4). The only 100% agreement between a remote sensing source and CEO classifications was the absence of trees shown in both CEO classifications and the Meta/WRI Tree Canopy layer, such as at points 7, and 27 (see Figure 4, indicated by green checkmarks in the Tree Canopy column). Vegetation and built-up areas were accounted for in the same or recognizably similar proportions in the remote sensing data when compared to the CEO data. However, at three points, 18, 27, and 33, remote sensing sources conflicted with each other as well as with field observations or CEO data, as indicated by the red "x" mark symbols in Figure 4.

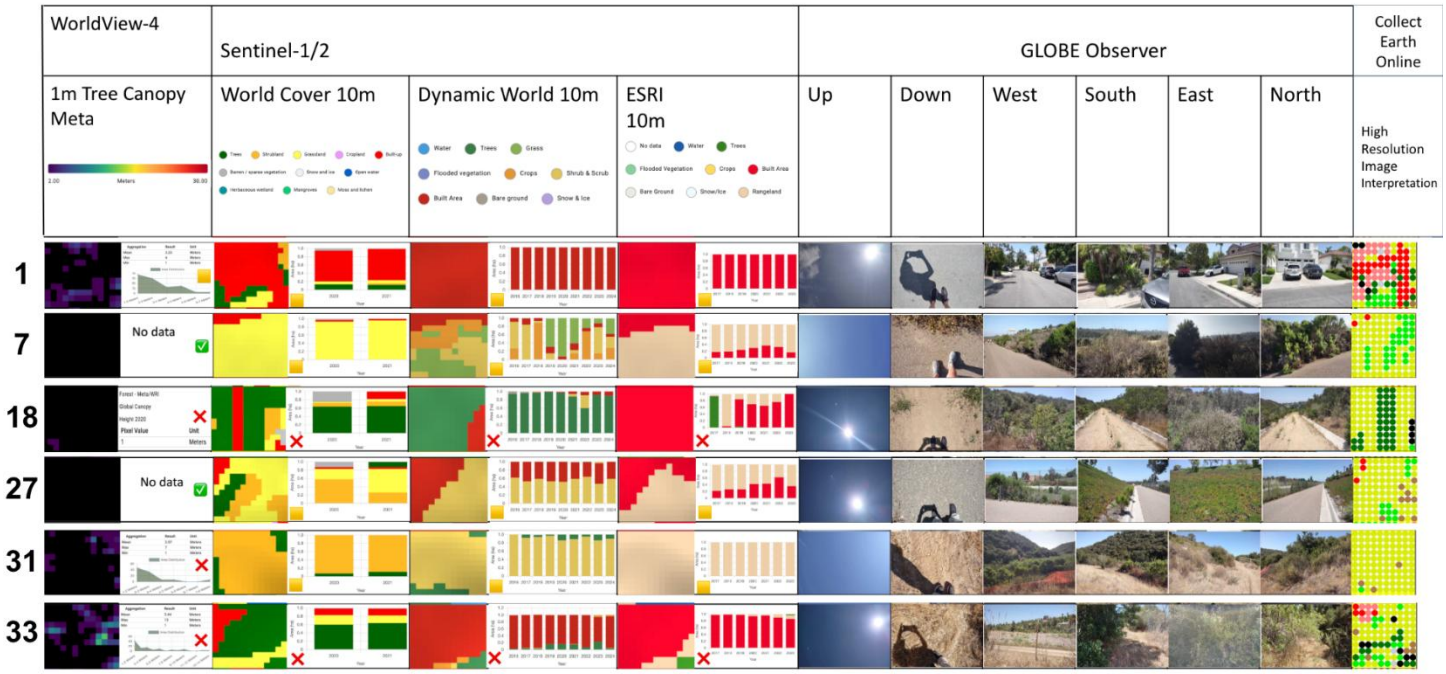

Figure 4. A sample of several data sites within the AOI where the many remote sensing sources, ground observations, and CEO manual classifications are compared. The sampling point number is on the far left. The source of the remote sensing data is listed in the top row, with the name of the dataset and key to its color code. Generally the color code of the land cover classifications is consistent with broad categories, with all 3 land cover maps and CEO classifications using red for impervious surface, dark green for trees, and yellow/orange/tan for an interpretation of grass/shrub/scrub/bush/rangeland/cropland. The data sources in the table listed from left to right are as follows: Meta/WRI Global Canopy Height 1 m image chip, Meta/WRI Global Canopy Height area distribution graph, World Cover 10 m image chip, World Cover 10 m historical distribution of land cover categories from 2020 to 2021, Dynamic World 10 m image chip, Dynamic World 10 m historical distribution of land cover categories from 2016 to 2024, ESRI 10 m image chip, ESRI 10 m historical distribution of land cover categories from 2017 to 2023, GLOBE Observer ground observations, CEO manual land cover classification grid. Sampling points 1, 7, and 31 show consistency between sources, while sampling points 18, 27, and 33 show inconsistent land cover classifications between remote sensing sources and with the ground observations and CEO classifications.

At point 18, ground observations showed a dirt trail surrounded by tall brush and small trees. Vegetation was thick and abundant around the trail. When the ground observations and CEO manual classifications did not match any of the remote sensing sources, this point highlighted a serious discrepancy among the sources of data. The Meta/WRI Global Canopy Height data gave a value of zero canopy height in the entire 10000 m² area, clearly contradicted by the trees in the photos. The World Cover 10 m data was closer to matching the ground observations, but categorized the dirt trail as impervious surface. Meanwhile, the Dynamic World 10 m data categorized nearly the entire area as tree cover, with a small corner of impervious surface, entirely missing the trail in the middle, and adding impervious surface where there was none. Finally, the ESRI data showed the entire area as built area, inconsistent with both the other remote sensing sources as well as the ground observations.

At point 27, the ground observation data was not taken directly at the center of the 10000 m² area due to the exact sampling point being located in the middle of the freeway. The ground observations included concrete road and grass and scrub along the side of the road, however due to the off-center location of the ground observation site, CEO classifications were weighed more heavily when comparing land cover with the remote sensing sources. The tree canopy data showed no canopy cover at all, which was consistent with the CEO classifications and ground observations. However, the World Cover 10 m data showed a mix of impervious surface, tree canopy, grassland, and shrubland, in a diagonal pattern that did not match the consistency of the scrub from the CEO classifications. Dynamic World 10 m data showed half of the area to be impervious surface and half shrub and scrub, but compared to the CEO classification that was majority

scrub, this increased impervious surface percentage was also inconsistent. ESRI was similar to Dynamic World 10 m in this area as well, with about half of the area classified as impervious surface and half as rangeland, but in a different pattern than Dynamic World 10 m.

At point 33, the ground observations were taken slightly outside of the 10000 m² area due to obstructive vegetation. However, the observations were representative of the land cover in the area as confirmed visually. Ground observations and CEO classifications showed dense shrub and brush coverage, with small trees. Tree canopy data showed some canopy height but not in any consistent pattern with CEO classifications. World Cover 10 m data was more consistent with the CEO classifications, but included a large corner of impervious surface that was not present in the ground observations or CEO classifications. Dynamic World 10 m data represented nearly the entire area as built up, as did ESRI, both inconsistent with the CEO classifications and ground observations.

25 of the 37 points contained at least partially built-up areas, which were mainly categorized as completely built-up by remote sensing sources despite some human-placed vegetation.

4. Discussion

Overall, land cover data from remote sensing sources were accurate when compared to field observations and manually-categorized CEO data. The Dynamic World 10 m and ESRI 10 m datasets were less detailed than the World Cover 10 m dataset when comparing the land cover classifications between the sources. This comparison is notable due to the identical spatial resolution of the data for Dynamic World, ESRI, and World Cover. While it would be expected that the finer resolution 1 m Tree Canopy data would result in more detail compared to these land cover classification layers, the differences between land cover classification layers of the same spatial resolution were surprising. World Cover 10 m tended to better capture the land cover in detail, such as capturing the trees in a residential area. This led to generalized categorization in built-up areas where Dynamic World and ESRI categorized the entire area as built-up, but in many cases vegetation, tree cover, or other features were clearly present from field observations and shown in World Cover 10 m, and sometimes in the 1 m Tree Canopy data as well. This overgeneralization of built-up areas is evident with Dynamic World 10 m and ESRI when the comparison of the overall percentage of fractional impervious surface for the AOI was calculated. The approximately 30 percentage points of overestimated impervious surface for these two datasets show how the small but numerous overestimates of built-up land led to drastic differences in fractional impervious surface for the 3 km × 3 km area, compared to the authoritative results of the MRLC data. In these cases of overestimation, remote sensing data was correct for parts of, but not the entire, 10000 m² area. As seen from the LTS images starting in 1984, and the MRLC Fractional Impervious Surface images starting in 1985, the AOI has gone from completely undeveloped to almost completely built-up, with shrub-covered canyons remaining the only unchanged areas over forty years. This rapid development has been captured by remote sensing at the majority of the points examined, with the exceptions of the points that are in disagreement. Disagreement points have the opposite issue, where remote sensing data categorizes the area as built-up, however, the area is covered in natural vegetation.

Limitations of this study arise in several forms. First, the time difference between the remote sensing data and the ground observations may be a cause of some inconsistencies. Ground observations were made in the summer of 2025, while remote sensing land cover maps relied on satellite imagery from as early as 2020. In order to consider a range of remote sensing land cover classification layers, the sources were not chosen based on their availability of data from the most recent year, 2024. Given the rapid urbanization of the area, a time span of five years could greatly change the land cover in this area and lead to misleading results. However, as shown in Section 3.1, despite the data from World Cover 10 m relying on imagery from 2021 compared to the more recent Dynamic World 10 m and ESRI data from 2024, World Cover 10 m had a more accurate percentage of impervious surface for the AOI as a whole when all three land cover maps were compared against the MRLC data and CEO observations. Another concern may be the season in which ground observations and CEO classifications were made. The San Diego climate, however, lessens the seasonal difference in vegetation because the climate is moderate and does not vary extremely throughout the year. Vegetation is fairly consistent throughout the year, so while some moderate differences in vegetation due to seasonal changes may be a factor in the differences in land cover observed between remote sensing sources and ground observations, in the specific case of this San Diego AOI, seasonal changes are not as pressing a concern. Finally, interpretation of land cover classification labels is a consideration that must be made. CEO classifications were made with thirteen different labels to choose from, while remote sensing sources had fewer possible labels. For instance, World Cover 10 m has eleven different land cover labels, Dynamic World 10 m has nine labels, and ESRI has nine labels. While many of these labels overlap, most

consistently with "built up" and "trees," the differences in labeling of land cover elements is also something to take into consideration. The question of whether a tree that was planted along a sidewalk and road may be considered to be tree coverage, cultivated vegetation, or considered to be part of the built-up area due to its small size and surrounding impervious surface provides an example of how land cover labels can sometimes be up to interpretation. Given that the remote sensing maps were generated using artificial intelligence or machine learning techniques (Karra et al., 2021; Brown et al., 2022; Tolan et al., 2024), these interpretations are bound to differ between the remote sensing sources and the manual CEO classifications.

5. Conclusions

In relation to the goal of investigating the degree of similarity between field observations and remote sensing data in the AOI, the data show a majority of matches in predominantly built-up areas and predominantly natural areas. About 90% of the 37 points investigated showed agreement between remote sensing data and field observations, based on qualitative visual matches of 34 out of 37 sampling points. As seen with the fractional impervious surface percentages, Dynamic World 10 m and ESRI greatly overestimated built-up areas compared to the authoritative MRLC and CEO data. Consistent with the qualitative findings, the World Cover 10 m land cover layer provides a more detailed and sensitive land cover classification; World Cover 10 m presented a fractional impervious surface percentage within 4 percentage points of the MRLC and CEO data. This estimate of impervious surface was far closer to the MRLC and CEO data than the nearly 30-percentage-point gap from either Dynamic World 10 m or ESRI data. However, the consistency between the CEO and MRLC fractional impervious surface percentages shows that the Adopt a Pixel 3 km strategy provides an accurate assessment of the land cover of a 3 km × 3 km AOI using the 37 points and manual land cover classifications inside 10000 m² boundaries of these points. Remote sensing data can provide a wealth of information, but different sources, as seen in the research, provide differing levels of detail and suitability for specific research objectives. Three of the field observation locations were not within the desired 10000 m² area, and many others were not centered at the desired point, which explains discrepancies between field observations and CEO classifications, both of which are considered reference data. These location differences were caused by limitations such as private property lines and safety in areas of dense vegetation. The photos collected support a successful investigation of land cover categorization similarities and prompt further research on differences among land cover datasets for the AOI over time.

Funding: This research was funded through the NASA STEM Enhancement in the Earth Sciences (SEES) Virtual High School Internship program. The NASA Earth Science Education Collaborative leads Earth Explorers through an award to the Institute for Global Environmental Strategies, Arlington, VA (NASA Award NNX6AE28A). The SEES High School Summer Intern Program is led by the Texas Space Grant Consortium at the University of Texas at Austin (NASA Award NNX16AB89A0).

Data Availability Statement: The annual fractional impervious surface calculations (1985–2024), associated geospatial data, and complete table of sampling point comparisons for this study are available in the Zenodo repository at https://doi.org/10.5281/zenodo.19395850.

Acknowledgment: The authors would like to acknowledge the support of the 2025 Earth System Explorers (ESE) Team, NASA Science Mentors, and ESE peer mentors. NASA STEM Enhancement in the Earth Sciences (SEES) Virtual High School Internship program.

Conflicts of Interest: The authors declare no conflicts of interest. The funders had no role in the design of the study; in the collection, analyses, or interpretation of data; in the writing of the manuscript; or in the decision to publish the results.

References

Braaten, J. (n.d.). *Landsat timeseries explorer* [Web application]. Retrieved July 30, 2025, from https://jstnbraaten.users.earthengine.app/view/landsat-timeseries-explorer#run=false;lon=-122.91966;lat=44.24135;from=06-10;to=09-20;index=NBR;rgb=SWIR1%2FNIR%2FGREEN;chipwidth=4

Brown, C. F., Brumby, S. P., Guzder-Williams, B., Birch, T., Hyde, S. B., Mazzariello, J., Czerwinski, W., Pasquarella, V. J., Haertel, R., Ilyushchenko, S., Schwehr, K., Weisse, M., Stolle, F., Hanson, C., Guinan, O., Moore, R., & Tait, A. M. (2022). Dynamic World, near real-time global 10 m land use land cover mapping. *Scientific Data, 9*, 251. https://doi.org/10.1038/s41597-022-01307-4

Gorelick, N., Hancher, M., Dixon, M., Ilyushchenko, S., Thau, D., & Moore, R. (2017). Google Earth Engine: Planetary-scale geospatial analysis for everyone. *Remote Sensing of Environment, 202*, 18–27. https://doi.org/10.1016/j.rse.2017.06.031

Jin, S., Dewitz, J., Danielson, P., Granneman, B., Costello, C., Smith, K., & Zhu, Z. (2023). National Land Cover Database 2019: A new strategy for creating clean leaf-on and leaf-off Landsat composite images. *Journal of Remote Sensing, 3*, 22. https://doi.org/10.34133/remotesensing.0022

Karra, K., Kontgis, C., Statman-Weil, Z., Mazzariello, J. C., Mathis, M., & Brumby, S. P. (2021). Global land use/land cover with Sentinel-2 and deep learning. In *2021 IEEE International Geoscience and Remote Sensing Symposium (IGARSS)* (pp. 4704–4707). IEEE. https://doi.org/10.1109/IGARSS47720.2021.9553499

Low, R. D., Nelson, P. V., Soeffing, C., Clark, A., & SEES 2020 Mosquito Mappers Research Team. (2021). Adopt a pixel 3 km: A multiscale data set linking remotely sensed land cover imagery with field-based citizen science observation. *Frontiers in Climate, 3*, 658063. https://doi.org/10.3389/fclim.2021.658063

Mapbox. (n.d.). *Mapbox Satellite* [Technical documentation]. Retrieved April 1, 2026, from https://docs.mapbox.com/data/tilesets/reference/mapbox-satellite/#overview

Multi-Resolution Land Characteristics Consortium. (n.d.). *Annual National Land Cover Database (NLCD) fractional impervious surface*. Retrieved July 30, 2025, from https://www.mrlc.gov/

National Aeronautics and Space Administration (NASA). (2025). Global Learning and Observations to Benefit the Environment (GLOBE) Data User Guide, 2025, version 3.0, https://www.globe.gov.

National Oceanic and Atmospheric Administration (NOAA). (2023, May 2). The marine layer. https://www.noaa.gov/jetstream/ocean/marine-layer

Nelson, P. V., Low, R., Kohl, H., Overoye, D., Yang, D., Huang, X., Chellappan, S., Azam, F. B., Carney, R. M., Falk, M., Garriga, J., Schelkin, L., Boger, R., & Schwerin, T. (2024). GLOBE Observer: A case study in advancing Earth system knowledge with AI-powered citizen science. *Citizen Science: Theory and Practice, 9*(1), 33. https://doi.org/10.5334/cstp.747

Saah, D., Johnson, G., Ashmall, B., Tondapu, G., Tenneson, K., Patterson, M., Poortinga, A., Markert, K., Nguyen, H. Q., Aung, K. S., Schlichting, L., Matin, M., Uddin, K., Aryal, R. R., Dilger, J., Ellenburg, W. L., Flores-Anderson, A. I., Wiell, D., Lindquist, E., Goldstein, J., Clinton, N., & Chishtie, F. (2019). Collect Earth: An online tool for systematic reference data collection in land cover and use applications. *Environmental Modelling & Software*, *118*, 166–171. https://doi.org/10.1016/j.envsoft.2019.05.004

Tolan, J., Yang, H.-I., Nosarzewski, B., Couairon, G., Vo, H. V., Brandt, J., Spore, J., Majumdar, S., Haziza, D., Vamaraju, J., Moutakanni, T., Bojanowski, P., Johns, T., White, B., Tiecke, T., & Couprie, C. (2024). Very high resolution canopy height maps from RGB imagery using self-supervised vision transformer and convolutional decoder trained on aerial lidar. *Remote Sensing of Environment, 300*, 113888. https://doi.org/10.1016/j.rse.2023.113888

U.S. Federal Government. (2025). *U.S. Climate Resilience Toolkit climate explorer*. https://crt-climate-explorer.nemac.org/

U.S. Geological Survey. (2024). *Annual NLCD Collection 1 science products* (Version 1.1) [Data set]. U.S. Geological Survey. https://doi.org/10.5066/P94UXNTS

Zanaga, D., Van De Kerchove, R., De Keersmaecker, W., Souverijns, N., Brockmann, C., Quast, R., Wevers, J., Grosu, A., Paccini, A., Vergnaud, S., Cartus, O., Santoro, M., Fritz, S., Georgieva, I., Lesiv, M., Carter, S., Herold, M., Li, L., Tsendbazar, N. E., ... Arino, O. (2021). *ESA WorldCover 10 m 2020 v100* [Data set]. Zenodo. https://doi.org/10.5281/zenodo.5571936

Best Practice

Evaluating Satellite Land Cover Classification Accuracy Using Participatory Remote Sensing

Aren Finelt[1,*], Russanne Low[2], and Peder Nelson[2]

[1] 12th Grade, Saint John's School, San Juan, Puerto Rico, USA; https://orcid.org/0009-0004-7841-5086
[2] Institute for Global Environmental Strategies; low.russanne@gmail.com; https://orcid.org/0000-0002-7912-4350
[3] Oregon State University; peder.nelson@oregonstate.edu; https://orcid.org/0000-0003-3979-9051
[*] Corresponding Author: finelt.aren@gmail.com

Abstract: Satellite remote sensing has become a foundational tool for monitoring land cover change and urban development. However, classification accuracy remains limited in complex urban environments where vegetation, built infrastructure, and water coexist within small spatial scales. This study evaluated the accuracy of multiple satellite land cover datasets within a 3 km × 3 km area of interest in Hato Rey, Puerto Rico, using the National Aeronautics and Space Administration (NASA) Adopt-a-Pixel participatory remote sensing framework. Ground observations were collected at 23 sampling locations using the Global Learning and Observations to Benefit the Environment (GLOBE) Observer application and compared with land cover classifications derived from European Space Agency (ESA) WorldCover, Dynamic World, ESRI Land Cover, Meta Tree Canopy, and Landsat imagery. Results showed that several satellite datasets frequently overgeneralized land cover as entirely urban, failing to detect localized vegetation and water features observed on the ground. Dynamic World and ESRI Land Cover achieved higher overall accuracy (91.3%) due to consistent classification of urban areas, while Meta Tree Canopy and ESA WorldCover demonstrated improved detection of vegetation in heterogeneous environments, despite slightly lower overall accuracy (87.0%). Landsat time series analysis revealed mixed vegetation trends over time, reflecting both urban expansion and persistent vegetation. These findings demonstrate the importance of integrating participatory ground observations with satellite data to improve land cover classification accuracy and enhance environmental monitoring in rapidly developing urban environments.

Keywords: remote sensing, land cover, urban environment, Puerto Rico, participatory science

Academic Editor: FirstName LastName
Received: 1 March 2026
Revised: 25 April 2026
Accepted: 27 April 2026
Published: 30 April 2026

Citation: Finelt, A., Low, R., and Nelson, P. (2026). Evaluating Satellite Land Cover Classification Accuracy Using Participatory Remote Sensing. Journal of Earth Observation and Geospatial Applications, 2(1), 69–77. https://doi.org/10.65372/3w1fbk03

1. Introduction

Remote sensing provides one of the most powerful tools available for understanding Earth's surface. Satellites continuously collect data that allow scientists to monitor environmental change across spatial scales ranging from individual cities to the entire planet. These observations have become essential for studying urban development, vegetation change, and environmental processes that affect both ecosystems and human populations (Gorelick et al., 2017). Land cover classification derived from satellite imagery plays a critical role in this effort. These classifications allow researchers to quantify the extent of built infrastructure, vegetation, water, and other land cover types. Such information is used to evaluate changes in urban development and the environmental effect of said developments. However, despite advances in satellite technology, classification accuracy remains limited, particularly in heterogeneous urban environments where multiple land cover types exist within small areas (Brown et al., 2022). Satellite classification relies on spectral reflectance, which measures how surfaces reflect electromagnetic radiation; while this method is highly effective for identifying large, uniform land cover types such as forests or open water, it becomes less reliable when applied to mixed landscapes. In urban environments, individual satellite pixels often contain a combination of buildings, vegetation, and pavement, creating classification uncertainty and can result in

misrepresentation of actual land cover (Karra et al., 2021). Recent global land cover products such as European Space Agency (ESA) WorldCover, Dynamic World, and ESRI Land Cover have improved spatial resolution and classification methods, achieving overall accuracies of approximately 70–85% depending on land cover type and region (ESA, 2021; Brown et al., 2022). However, classification accuracy remains highly variable in dense urban environments, where shadows, vegetation canopy, and complex infrastructure interfere with classification algorithms. Participatory remote sensing offers an effective method for addressing these limitations. The National Aeronautics and Space Administration (NASA) Adopt-a-Pixel framework combines satellite observations with ground-based citizen science data to evaluate land cover classification accuracy (Low et al., 2021). Using the Global Learning and Observations to Benefit the Environment (GLOBE) Observer mobile application (GLOBE Observer, 2023), participants collect ground photographs that provide direct evidence of land cover conditions. These observations allow researchers to compare satellite classification with real-world conditions and identify classification errors. This approach provides critical validation data that cannot be obtained through satellite observation alone. Ground observations capture fine-scale land cover variability that is often invisible to satellite sensors. By integrating satellite and ground data, participatory remote sensing improves classification accuracy and enhances understanding of land cover patterns. Hato Rey, Puerto Rico, provides an ideal study area for evaluating satellite classification accuracy. Located in San Juan, Hato Rey is the island's primary financial district and has experienced significant urban development. Despite extensive construction, vegetation remains present throughout the area, creating a heterogeneous land cover environment that challenges satellite classification. The objective of this study was to evaluate the accuracy of satellite land cover classification in Hato Rey using participatory remote sensing methods. It was hypothesized that satellite datasets would frequently overgeneralize land cover classification, particularly by misclassifying heterogeneous urban environments as entirely built-up.

2. Study Area and Methods

2.1. Study Area

The study area (Figure 1) encompasses the district of Hato Rey within the municipality of San Juan, Puerto Rico. Hato Rey is located in the north-central portion of the San Juan metropolitan region and serves as the island's primary financial and commercial center. Often referred to as the "Wall Street of the Caribbean," the district contains a dense concentration of high-rise office buildings, residential complexes, transportation infrastructure, and commercial areas. In addition to heavily developed urban land, the landscape also includes smaller parks, roadside vegetation, and water features associated with the Río Piedras river and engineered drainage systems. This combination of built infrastructure and fragmented vegetation creates a heterogeneous land cover environment, making it a suitable location for evaluating the accuracy of satellite-based land cover classification in a dense urban setting.

Figure 1. (a) Study area as viewed on the Collect Earth Online platform. (b) Location of study area in Puerto Rico. (c) Location of study area in the United States.

2.2. Data

The primary data for this study consisted of ground-based observations and satellite-derived land cover datasets. Ground observations were collected using the GLOBE Observer Land Cover mobile application at 23 accessible points within a 3 km × 3 km Adopt-a-Pixel area of interest containing 37 total sampling locations arranged in a grid pattern. The remaining sampling points were inaccessible due primarily to their location within private property, reflecting the highly developed nature of the study area. Observations were conducted over several weeks, and each accessible sampling location was documented using the standard GLOBE Observer protocol, which includes photographs taken in six directions: north, south, east, west, up, and down. These ground observations provided a reference dataset for evaluating satellite land cover classification accuracy. Figure 2 shows the location of the study area within Puerto Rico and the Adopt-a-Pixel sampling grid overlay.

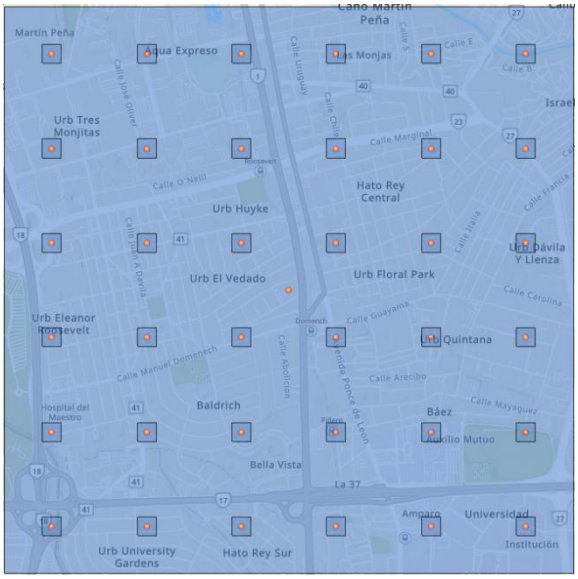

Figure 2. Location of the study area in Hato Rey, Puerto Rico, with the Adopt-a-Pixel 3 km × 3 km sampling grid overlay, Courtesy of ArcGIS.

Ground observations were collected at 23 accessible sampling locations. Satellite datasets provided spatially continuous land cover information for the study area and included the Meta 1 m Tree Canopy dataset (Tolan et al., 2023), ESA WorldCover (10 m resolution), Dynamic World (10 m resolution), and ESRI 10 m Land Cover datasets. These datasets were accessed and analyzed using the EarthMap platform, which allows visualization and comparison of multiple satellite-derived land cover products. Additional data were obtained from Landsat satellite imagery (USGS, 2020) spanning from 1984 to 2025 to evaluate long-term vegetation and land cover trends. Collect Earth Online (Saah et al., 2019) was also used to manually classify land cover based on high-resolution aerial imagery. All data, including satellite classification, ground observations, and manual classification results, were exported in CSV and GeoJSON formats to allow integration across platforms and facilitate comparison between datasets.

2.3. Methods

Land cover classification within the area of interest was evaluated through comparison of satellite-derived datasets, manual image interpretation, and ground observations. Satellite land cover products, including ESA WorldCover, Dynamic World, ESRI Land Cover, and Meta Tree Canopy, were examined using the EarthMap platform. Each dataset was visually analyzed across the area of interest and at individual sampling locations to identify differences in classification, particularly between built and vegetated land cover. Manual classification was conducted using Collect Earth Online to provide an additional reference for comparison. High-resolution imagery was used to visually assess land cover within each primary sample unit, allowing satellite classifications to be evaluated against observed land cover patterns.

Ground observations collected through the GLOBE Observer application were used to validate satellite classification at selected sampling points. Each sampling location was assigned a dominant land cover class (Urban or Vegetation) based on ground photographs taken in six directions. Satellite-derived classifications were then compared directly with these ground-based labels to determine agreement.

A confusion matrix was constructed for each dataset to quantify classification performance. Overall accuracy, producer's accuracy, and user's accuracy were calculated following standard remote sensing accuracy assessment methods. Agreement was defined as a match between the dominant ground-observed land cover and the satellite classification for the corresponding location. In cases where both built and vegetated features were present, classification was based on the dominant observed land cover.

Inaccessible sampling points were excluded from quantitative analysis, resulting in a total of 23 evaluated locations. Differences in spatial resolution between datasets (e.g., 1 m Meta Tree Canopy vs. 10 m land cover products) were considered when interpreting classification discrepancies, particularly in areas with fragmented vegetation.

Landsat imagery was also examined to assess recent land cover stability within the study area. Satellite images from multiple years were visually compared to identify any major changes in land cover. This combined qualitative and quantitative approach allowed differences between satellite datasets and actual land cover conditions to be systematically identified and evaluated.

3. Results

3.1. Comparison Between Dynamic World and ESRI Land Cover

Land cover classification derived from the Dynamic World and ESRI datasets showed strong agreement at Point 31, where both datasets classified the area as built environment. As shown in Figure 3, both classification products identified the entire primary sample unit as developed land, with no vegetation detected. This result is consistent with the highly urbanized nature of Hato Rey, where large areas consist of buildings, roads, and impervious surfaces.

The agreement between these two independent datasets suggests that both classification methods are effective at identifying heavily developed urban areas. However, the uniform classification also indicates a lack of sensitivity to more detailed land cover features such as individual trees or fragmented vegetation, which may be present but not detected at the spatial resolution of the datasets. Table 1 shows that both datasets classified all 23 points as Urban, yielding a producer's accuracy of 0% for vegetation. Overall accuracy = 91.3%, inflated by the dominance of urban cover in the study area.

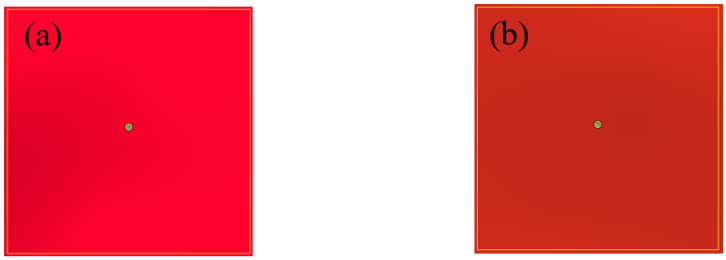

Figure 3. Comparison of Dynamic World (a) and ESRI (b) land cover classification at Point 31. Both datasets classify the area as built environment, demonstrating agreement in highly urbanized areas.

Table 1. Confusion matrix for Dynamic World and ESRI vs. GLOBE Observer (n = 23).

GLOBE \ Satellite	Urban	Vegetation	Row Total
Urban	21	0	21
Vegetation	2	0	2
Column Total	23	0	23

3.2. Comparison Between ESA WorldCover and Meta Tree Canopy

Comparison between the ESA WorldCover and Meta Tree Canopy datasets revealed both agreement and disagreement depending on location. At Point 20, both datasets indicated the presence of vegetation. As shown in Figure 4, the Meta Tree Canopy dataset detected tree canopy in areas where ESA WorldCover also identified vegetation. This agreement suggests that both datasets accurately captured vegetation at this location.

In contrast, disagreement was observed at Point 10. While the Meta Tree Canopy dataset detected tree canopy, ESA WorldCover classified the same area as built environment. This discrepancy suggests that ESA WorldCover may underrepresent vegetation in dense urban environments where tree canopy exists alongside built infrastructure. The higher spatial resolution of the Meta Tree Canopy dataset allows it to detect smaller vegetation features that may not be captured in lower-resolution land cover products.

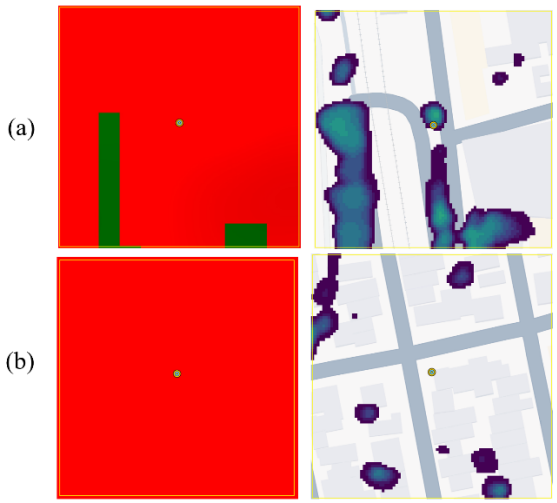

Figure 4. Comparison between ESA WorldCover (Left) and Meta Tree Canopy datasets (Right). (a) Agreement at Point 20 shows both datasets detecting vegetation, while (b) disagreement at Point 10 demonstrates ESA WorldCover failing to identify tree canopy detected by the Meta dataset.

Table 2. Confusion matrix for WorldCover and Tree Canopy Meta vs. GLOBE Observer (n = 23). Both datasets produced identical classification results. Overall accuracy = 87.0%. The 3 Urban points classified as Vegetation likely reflect sub-pixel green cover present in ground imagery.

GLOBE \ WorldCover	Urban	Vegetation	Row Total
Urban	18	3	21
Vegetation	0	2	2
Column Total	18	5	23

3.3. Comparison Between Satellite Classification and Ground Observations

Comparison between satellite classification and ground observations revealed varying levels of agreement depending on location. At Point 5, ground photographs showed a fully developed urban roadway with no visible vegetation, and both ESA WorldCover and ESRI datasets correctly classified the area as built environment (Figure 5). This result demonstrates that satellite classification can accurately represent land cover in fully urbanized areas.

At Point 11, partial agreement was observed. Ground photographs showed a developed area with nearby vegetation, and while both satellite datasets classified the majority of the area as built environment, ESA WorldCover identified a small portion of vegetation. This suggests that satellite datasets can partially detect

vegetation in mixed environments but may underestimate its extent.

In contrast, disagreement was observed at the third ground observation point, where ground photographs showed visible vegetation, but satellite datasets classified the area as entirely built environment. This misclassification demonstrates a limitation of satellite land cover datasets in detecting small or fragmented vegetation in dense urban areas. These findings highlight the importance of ground observations in validating satellite classification accuracy.

Table 3 shows the accuracy by data source. The overall accuracy is misleading here. Dynamic World and ESRI score higher (91.3%) purely by defaulting every point to Urban. Tree Canopy Meta and WorldCover score lower (87.0%) but are the only datasets that detected any vegetation at all.

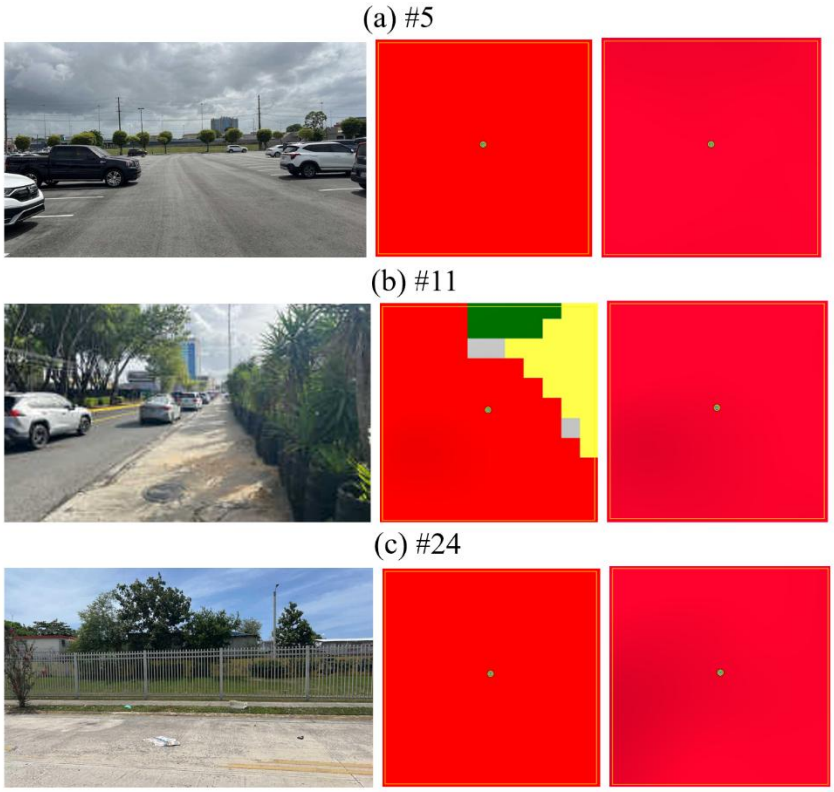

Figure 5. Comparison between ground observations and satellite classification at #5 (a), #11 (b), and #24 (c) observation points. Satellite datasets show varying levels of agreement with actual land cover conditions.

Table 3. Comparison of four satellite land cover datasets against GLOBE Observer ground truth (n = 23). Datasets ranked by ability to detect sub-pixel vegetation in a predominantly urban landscape.

Dataset	Overall Accuracy	Agreement (n=23)	Urban Detection	Vegetation Detection	Green Pocket Sensitivity	Rank
Tree Canopy Meta	87.0%	20 / 23	Strong	Strong	Best	1st
WorldCover (ESA)	87.0%	20 / 23	Strong	Moderate	2nd best	2nd
Dynamic World	91.3%	21 / 23	Strong	None	None	3rd
ESRI	91.3%	21 / 23	Strong	None	None	3rd

3.4 Landsat Time-Series Comparison

Comparison of Landsat imagery between 2020 and 2025 revealed minimal visible change in land cover within the study area. As shown in Figure 6, the overall spatial distribution of built infrastructure and vegetation remained largely consistent between the five years. This stability suggests that the study area has

already undergone significant urban development and that land cover patterns have remained relatively stable in recent years. Minor variations in vegetation may be present, but no major changes in land cover were observed.

4. Discussion

The results show that satellite land cover classification accuracy in Hato Rey varied depending on land cover type and dataset resolution. Dynamic World and ESRI Land Cover showed strong agreement in fully

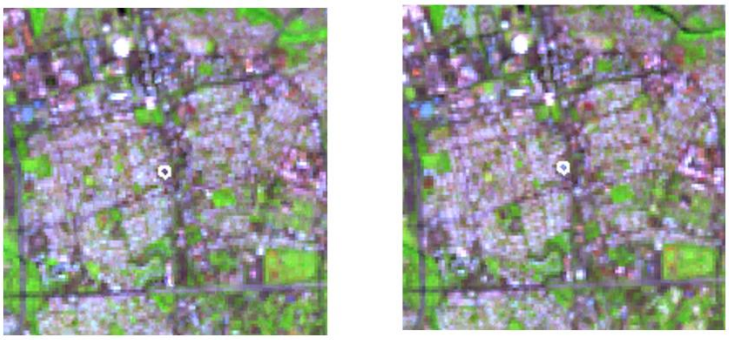

(a) 2020 (b) 2025

Figure 6. Landsat imagery comparison between 2020 and 2025 showing stable land cover patterns within the study area.

developed areas, correctly classifying locations dominated by buildings and impervious surfaces. This indicates that satellite classification performs reliably where land cover is uniform and clearly defined. However, both ESA WorldCover and Meta Tree Canopy revealed differences in vegetation detection. The Meta dataset identified tree canopy in locations classified as built environment by WorldCover, indicating that lower-resolution land cover products may underestimate vegetation in dense urban environments. This is likely due to mixed pixels, where vegetation and built surfaces occur within the same satellite pixel. Comparison with ground observations confirmed this limitation. Satellite datasets accurately classified fully developed areas but failed to detect vegetation at some mixed land cover locations. This demonstrates that classification accuracy decreases where vegetation is fragmented or located near infrastructure. Landsat imagery showed minimal recent land cover change, suggesting that classification differences between datasets were primarily due to methodological differences rather than actual environmental change. Overall, the Meta Tree Canopy dataset provided the most accurate representation of vegetation, while Dynamic World and ESRI Land Cover were most consistent in identifying built areas. These results highlight the importance of combining satellite datasets with ground observations to improve interpretation of urban land cover. In Table 4, the producer's accuracy of 0% for Vegetation in Dynamic World and ESRI indicates complete failure to detect green cover despite its presence in ground-level imagery. Tree Canopy Meta and WorldCover both achieved 100% producer's accuracy for Vegetation, though user's accuracy (40.0%) reflects over-prediction of vegetated cover at urban-dominated points.

Table 4. Producer's and user's accuracy by class and dataset.

Dataset	Class	Correct	Actual	Predicted	Producer's Accuracy	User's Accuracy
Tree Canopy Meta	Urban	18	21	18	85.7%	100.0%
	Vegetation	2	2	5	100.0%	40.0%
WorldCover (ESA)	Urban	18	21	18	85.7%	100.0%
	Vegetation	2	2	5	100.0%	40.0%
Dynamic World	Urban	21	21	23	100.0%	91.3%
	Vegetation	0	2	0	0.0%	N/A
ESRI	Urban	21	21	23	100.0%	91.3%
	Vegetation	0	2	0	0.0%	N/A

5. Conclusions

This study evaluated the accuracy of satellite-derived land cover classification within Hato Rey, Puerto Rico, through comparison of ESA WorldCover, Dynamic World, ESRI Land Cover, and Meta Tree Canopy datasets with ground observations collected using the GLOBE Observer application. The results showed that Dynamic World and ESRI Land Cover consistently and accurately classified fully developed urban areas but were less effective at identifying vegetation in mixed land cover environments. The Meta Tree Canopy dataset detected vegetation that was not represented in the ESA WorldCover dataset, demonstrating the importance of higher spatial resolution for identifying tree canopy in dense urban settings.

Comparison with ground observations confirmed that vegetation was present in some locations classified as built environment by satellite land cover datasets, indicating limitations in the ability of moderate-resolution classification products to detect fragmented urban vegetation. Analysis of Landsat imagery showed minimal land cover change in the study area in recent years, suggesting that observed differences between datasets were primarily the result of classification limitations rather than actual environmental change.

These findings demonstrate that while satellite land cover datasets such as Dynamic World, ESRI Land Cover, and ESA WorldCover provide reliable identification of large-scale urban development, higher-resolution datasets such as Meta Tree Canopy and ground-based observations are necessary to accurately characterize vegetation in complex urban environments. Integrating satellite datasets with participatory ground observations improves the accuracy and interpretation of urban land cover classification.

Funding: This research was funded by NASA CSR SEES.

Data Availability Statement: Data are available at https://zenodo.org/records/19747877

Acknowledgment: The authors would like to acknowledge the support of the 2025 Earth System Explorers (ESE) Team, NASA. Science Mentors, and ESE peer mentors. NASA STEM Enhancement in the Earth Sciences (SEES) Virtual High School Internship program. The NASA Earth Science Education Collaborative leads Earth Explorers through an award to the Institute for Global Environmental Strategies, Arlington, VA (NASA Award NNX6AE28A). The SEES High School Summer Intern Program is led by the Texas Space Grant Consortium at the University of Texas at Austin (NASA Award NNX16AB89A0).

Conflicts of Interest: The authors declare no conflicts of interest. The funders had no role in the design of the study; in the collection, analyses, or interpretation of data; in the writing of the manuscript; or in the decision to publish the results.

References

Brown, C. F., Brumby, S. P., Guzder-Williams, B., Birch, T., Hyde, S. B., Mazzariello, J., Czerwinski, W., Pasquarella, V. J., Haertel, R., Ilyushchenko, S., Schwehr, K., & Weisse, M. (2022). Dynamic World, near real-time global 10 m land use land cover mapping. *Scientific Data*, *9*(1), 251. https://doi.org/10.1038/s41597-022-01307-4

European Space Agency (ESA). (2021). *ESA WorldCover 10 m 2020 v100 product user manual.* https://worldcover2020.esa.int/

GLOBE Observer. (2023). *GLOBE Observer land cover protocol.* https://observer.globe.gov/

Gorelick, N., Hancher, M., Dixon, M., Ilyushchenko, S., Thau, D., & Moore, R. (2017). Google Earth Engine: Planetary-scale geospatial analysis for everyone. *Remote Sensing of Environment*, *202*, 18–27. https://doi.org/10.1016/j.rse.2017.06.031

Karra, K., Kontgis, C., Statman-Weil, Z., Mazzariello, J. C., Mathis, M., & Brumby, S. P. (2021). Global land use / land cover mapping with Sentinel-2 and deep learning. *IEEE International Geoscience and Remote Sensing Symposium (IGARSS)*, 4704–4707. https://doi.org/10.1109/IGARSS47720.2021.9553499

Low, R. D., Nelson, P. V., Soeffing, C., Clark, A., & SEES 2020 Mosquito Mappers Research Team. (2021). Adopt a pixel 3 km: A multiscale data set linking remotely sensed land cover imagery with field based citizen science observation. *Frontiers in Climate*, *3*, Article 658063. https://doi.org/10.3389/fclim.2021.658063

National Oceanic and Atmospheric Administration (NOAA). (2023). *Climate data for Puerto Rico*. https://www.noaa.gov/

Saah, D., Johnson, G., Ashmall, W., Tondapu, G., Tenneson, K., Patterson, M., & Poortinga, A. (2019). Collect Earth Online: A web-based tool for land cover and land use reference data collection. *Remote Sensing*, *11*(21), 2535. https://doi.org/10.3390/rs11212535

Tolan, J., Yang, H. I., Nosarzewski, B., Couairon, G., Vo, H. V., Brandt, J., Spore, J., Majumdar, S., Haziza, D., & Vamaraju, J. (2023). Global tree canopy height map from high-resolution satellite imagery. *Science*, *380*(6655), 1245–1249. https://doi.org/10.1126/science.ade7957

U.S. Environmental Protection Agency (US EPA). (2022). *Climate change indicators: Puerto Rico.* https://www.epa.gov/

U.S. Geological Survey (USGS). (2020). *Landsat 8 data users handbook*. https://www.usgs.gov/

Research Article

Predictive Modeling of Flash Floods: Investigating Hydrology and Land Cover Dynamics through Remote Sensing Data

Saad Ali[1,*]

[1] 12th Grade, Tyler Legacy High School, Tyler, Texas, USA
[*] Corresponding Author: saad.aali@outlook.com; +1-903-283-7476

Academic Editor: Jeong Chang Seong
Received: 1 March 2026
Revised: 18 April 2026
Accepted: 27 April 2026
Published: 30 April 2026

Abstract: Accounting for more than 75% of Federal Disaster Declarations, floods in the United States of America have increased both in intensity and frequency, outpacing the development of reliable predictive models and warning systems. This issue has only been exacerbated by a lack of large-scale public participation and access to predictive models. This paper focuses on classifying risk factors and building a prototype flood-prediction tool to clearly communicate results within a defined Area of Interest (AOI). The investigative strategy involves gathering and analyzing several geospatial indicators, which could result in high-risk flood conditions, such as relevant soil properties, elevation/slope, Curve Number (CN) values, and land cover types within an AOI. To ensure dataset reliability and scientific validity, the considered geological and atmospheric variables were sourced from a range of open-source databases such as Earth Map, GLOBE Citizen Science, FEMA, and Collect Earth Online. The second portion of this study concentrates on developing a classification-based prototype machine learning model that outputs flood risk in a given area into five levels. This model facilitates citizen science efforts through an interactive Colab project and subsequent GitHub repository, which allows for user input. Findings were that Land cover and slope/elevation are key factors in determining runoff potential, while soil properties do not contribute to Curve Number differences in the AOI due to a lack of detailed data. The S.H.I.E.L.D. model can easily be ported into a cross-platform application, further integrating citizen science observations based on the findings of this paper.

Keywords: remote sensing, hydrological modeling, citizen science, machine learning

1. Introduction

Accounting for more than 75% of Federal Disaster Declarations, floods in the United States of America have increased both in intensity and frequency (Patel, 2025), Recent floods that have devastated regions in Texas and New Jersey illustrate a growing crisis of climate-driven disasters and subsequent gaps in preparedness throughout the United States. In Central Texas alone, The July 2025 flooding of the Guadalupe River led to more than 130 deaths. Many residents did not receive timely warnings due to lack of funding for flood alert systems (NYT, 2025). These disasters also result in massive structural damage costs, with flooding in the United States causing between $179.8 and $496.0 billion in damages annually (Joint Economic Committee Democratic Staff, 2024). To analyze contributions to flood risk in the area of interest (AOI), Curve Number (CN) measures, land cover, hydrological soil groups (HSG), and slope/elevation readings were combined to determine a correlation between the significance of each potential and runoff as described by average CN readings. Flint, Texas, (or the greater Tyler area), is experiencing rapid urbanization driven by increased housing development. Despite this growing urban area, it has not experienced significant flooding events in the past. This highlights an opportunity for proactive flood-risk management and planning. The findings from this section are used in the development of a classification-based prototype machine learning model that outputs flood risk in a given area into five levels.

Citation: Ali, S. (2026). Predictive Modeling of Flash Floods: Investigating Hydrology and Land Cover Dynamics Through Remote Sensing Data. Journal of Earth Observation and Geospatial Applications, 2(1), 78-89. https://doi.org/10.65372/wnj9nc66

2. Study Area and Methods

2.1. Study Area

The Study Area is a 3 km² section of the greater Tyler–Flint region of East Texas, characterized by humid subtropical climate with warm and humid summers averaging highs around 93°F and capping at 100°F on some days. Winters average 48°F, with highs reaching the mid-50s and lows rarely going below 32°F. Rainfall is almost evenly spread throughout the year, totaling around 46 inches annually, mostly falling in late spring and early fall (NOAA, no date). Although floods due to heavy rain are not uncommon, the area's infrastructure handles challenges well. The Climate Explorer Tool in Figure 1 (NOAA, no date) highlights the study area's humid subtropical climate, with even rainfall distribution and peaks in the late spring and early fall. Dark gray bars represent averages for each year from 1950-2013. The horizontal line from which the bars extend up or down is the average from 1961-1990. According to the Toolkit, the light gray band shows the range of values modeled (hindcast) for 1950–2005; the blue band shows projections for 2006–2100 based on a future in which humans stop increasing global emissions of heat-trapping gases by 2040 and then dramatically reduce them through 2100; the darker blue line shows the weighted mean of projections for lower emissions; the red band shows projections for 2006–2100 based on a future in which global emissions of heat-trapping gases continue increasing through 2100; and, the red line shows the weighted mean of all projections for higher emissions.

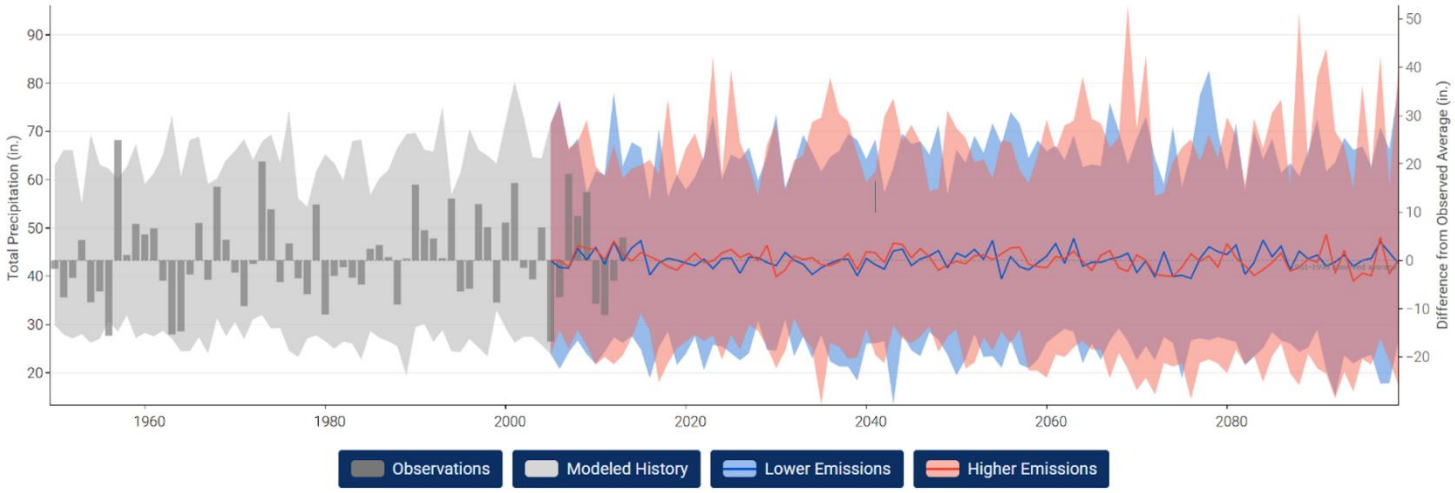

Figure 1. Total annual precipitation from the Climate Explorer

Tyler, Texas (Figure 2) is experiencing rapid urbanization driven by efforts to develop entertainment centers, housing complexes, and government buildings spurred by partnerships between county and city governments and private real estate companies, according to the Genecov Group (https://genecov.com/). Despite this growing urban area, Tyler has not experienced significant flooding events in the past. This underscores an opportunity for proactive flood-risk management and planning. The findings from this section are used to develop a classification-based prototype machine learning model that outputs flood risk in a given area into five levels. This model facilitates citizen science efforts through an interactive interface where users can input personal vector data through CSV uploads.

To allow personal input, an area of interest (AOI) of 3 km^2 was created that serves as the basis for data values. This AOI is made up of 36 sampling points spaced 500 meters apart, with an additional center point totaling 37 specific coordinates, as shown in Figure 2. Each point is defined by a 100 m bounding box centered at the individual coordinate (Low et al., 2021; Nelson, 2024). To ensure scientific validity and high data density, each 100 m box was further divided into 100 sub-points, resulting in a total of 3,700 generated data points across the AOI. The GLOBE Observer application was used at these locations to record multi-directional ground image observations (North, East, South, West, Up, and Down) to validate the accuracy of satellite map layers.

2.2. Data and Methodology

Initially, the GLOBE Observer application was used to record ground image observations within each AOI point's bounding box. Up, Down, North, East, South, and West directions were recorded at each sampling point location for later assessment of map layer accuracy. The 2020 Meta Tree Canopy, 2020-2021 World Cover, 2024 Dynamic World, and 2024 ESRI map layer datasets were then pulled from Earth Map to evaluate differences in land cover classification across map types. These layers also highlighted the change in land cover/landuse over time. In addition, Collect Earth Online was used to further classify each 100 m bounding box. Each point was then divided into 100 sub-points; totaling 3,700 generated points. These were systematically assigned to various land cover categories like: Trees-CanopyCover, Bush/Scrub, Grass, Cultivated Vegetation, Water-lake, Water-rivers/stream, Water-irrigation ditch, Shadow, Unknown, Bare Ground, Building, Wetland, and Impervious Surface. This process ensured that land cover characteristics for the AOI were explicitly stated within an individual case study.

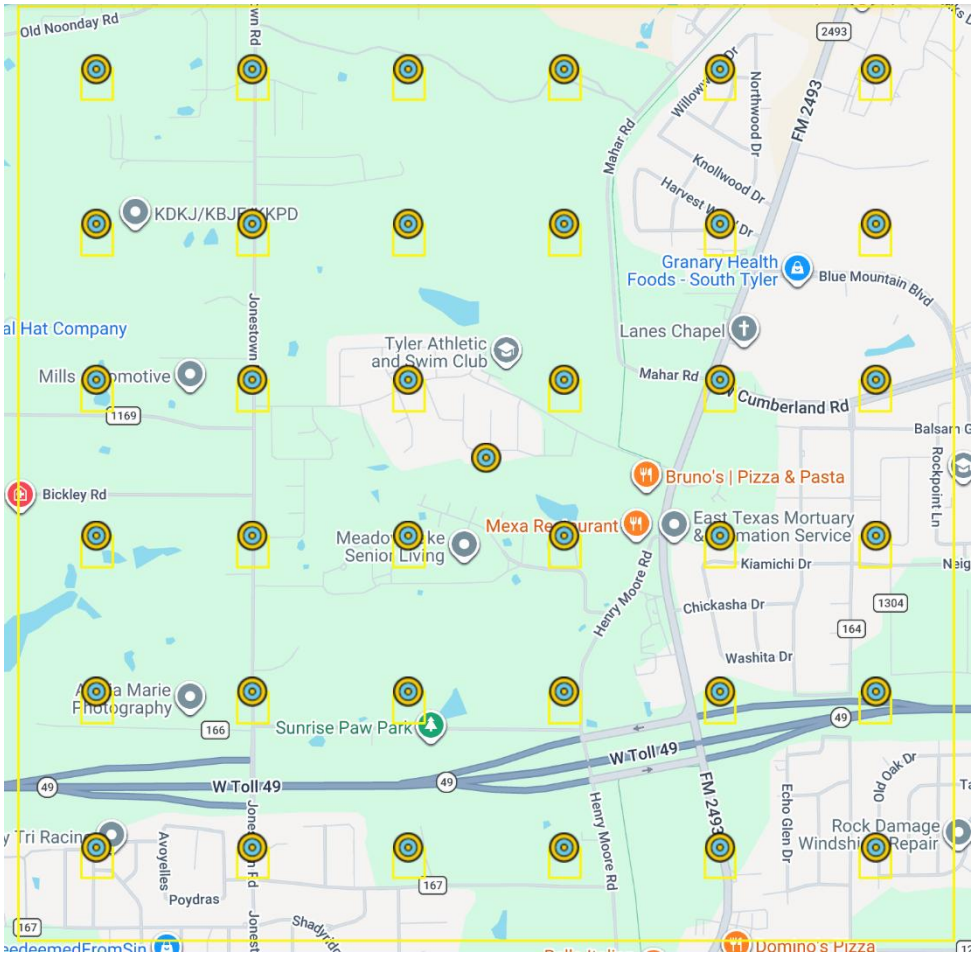

Figure 2. Study area and 37 sampling points, Tyler, Texas.

2.2.1. Curve Number

The Curve number (CN) is a hydrology parameter used to predict runoff/infiltration from excess rainfall. Originally developed by the USDA Soil Conservation Service (now the Natural Resources Conservation), the method was initially intended for use in small agricultural watersheds but has since evolved into a global standard for runoff prediction. It compiles Hydrological Soil Group (HSG) derived from 2020 SRIC SoilGrids, 2019 CCI Land Cover 300 m, and slope generated from USGS SRTM–30 m into a single index to estimate surface runoff in response to rainfall, with values ranging from ~30 (indicating highly permeable soils with low runoff potential) to ~100 (indicating impermeable surfaces with high runoff potential). This

varies with antecedent moisture conditions (AMC) classified as dry, average, and wet. Dry CN values have low soil moisture and runoff potential, and wet CN values have soaked or otherwise impermeable soils that produce the most runoff. The rationale of the CN method lies in its ability to consolidate complex variables into a single predictive value. This method also accounts for antecedent moisture conditions, adjusting risk index based on whether the soil is dry (low runoff potential) or wet (soaked/impermeable, producing maximum runoff).

2.2.2. Data Preprocessing and Preparation

Before importing map layers into the S.H.I.E.L.D. FloodScope tool, available at the following URL: https://github.com/onesixaali/FloodScope, data was very minimally processed to avoid anomalies and complications while modeling.

(1) Feature/Attribute Refinement: Removal of duplicate and overlapping features, deletion of irrelevant fields, and standardization of naming.
(2) Layer Reclassification: Land cover and soil type layers reclassification into analysis-ready categories based on the classification scheme adopted for this project.
(3) File Backup: Backup of all files to save progress and prevent data loss.

CN values were then compared with land cover classifications, hydrological soil groups, and slope/elevation to observe correlations between the degree and significance of each runoff potential on flood risk. Zones at high risk for flooding were described by taking multiple factors into account. Areas with CN > 75 were then classified as showing high runoff potential (U.S. Army Corps of Engineers, Hydrologic Engineering Center, 2025; USDA, 2021), indicative of impervious or less permeable land cover/soil conditions. These thresholds were then combined with slope, elevation, and land cover data into a table (Appendix 1). In the table, the 37 sampling points were characterized by curve number values, land cover classifications, hydrological soil groups, slope percentages, and elevation values. The land cover types were aggregated from the original Dynamic World layer into four categories to allow for simplified analysis: Built-up, Tree, Grass, and Bare Ground. HSG classes: **A**, **B**, & **C** show soil permeability levels, while slope and elevation data help visualize certain topographic dynamics. This approach uses up-to-date criteria selection based on best-practice regional flood planning, providing an explicit, and therefore repeatable framework for identifying areas in increased danger (Texas Water Development Board, 2025).

CN values across the 3 km^2 region ranged from 33 to 95, with a mean CN of 74.7. This reflects varying land cover and soil conditions. The mean value of 74.7 suggests impervious surfaces and less infiltratable soils, which is typical of areas with mixed land use, urban aspects, and varying soil properties *(USDA, 2021)*. This was further verified using previous GLOBE Observer photos, which confirmed varying landscape that depicted urbanization mixed with grassland/forested regions.

Figure 3 shows the CN values categorized by land cover types. It shows how only Built-up areas have CN averages of around 67.9, while only Grassland + Forested points have average CN values of 73.69 showing that impervious surfaces drive ~5-8% higher runoff potential. In addition, values for Tree, Tree + Built-up, Grass + Built-up, Bare Ground, and Built-up + Tree are also included. Figure 4 shows the aggregated land cover types, revealing that 59.4% of categorized points were in a region of Built-up land, while roughly 40.6% were in only grassland or forested regions, reflecting urbanization which correlates to the mean AOI CN of 74.7 and thus elevated flood vulnerability. Figure 5 describes the distribution of hydrological soil groups.

Urban/impervious areas raise CN, highlighting urbanization as a flood risk driver (USDA, 2021). Urban and impervious surfaces (62.1% of the area; 23/37 points) showed a mean CN of 75.33, compared to forested/grassland only regions (37.8% of the area; 14/37 points) with a mean CN of 75.82.

Hydrological soil groups **A**, **B**, and **C** were used to classify areas, with **A** having typically sandier soils with the highest infiltration rates, and **C** typically having the slowest infiltration rates due to higher clay content (from Earth Map). Hydrological group **C** soils, making up 64.9% of the area (614 hectares), averaged a CN of 76.71, showing low potential for permeability and therefore increased potential for runoff. On the other side, HSG **A** soils proved to also show soil with low potential for permeability, comprising 16.2% of the area (109 hectares), and averaging a CN of 76.19. Hydrological group **B** soils were counted as the remainder with 18.9%. The dominance of HSG **C** soils (65% of the area) suggests a higher potential for runoff and localized flooding during heavy rainfall events, because water doesn't infiltrate as easily into clay-rich soils, it tends to flow over the surface, according to Earth Map. The coarse nature of HWSD/IPCC soil

map datasets does not allow for this detailed level of analysis. This is likely the reason for overall similar CN values for hydrologically different soil groups.

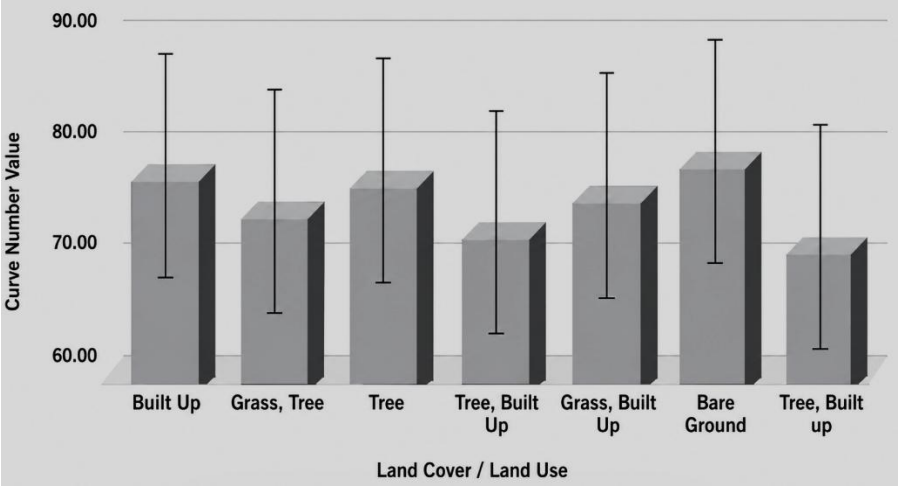

Figure 3. CN values vs. land cover types.

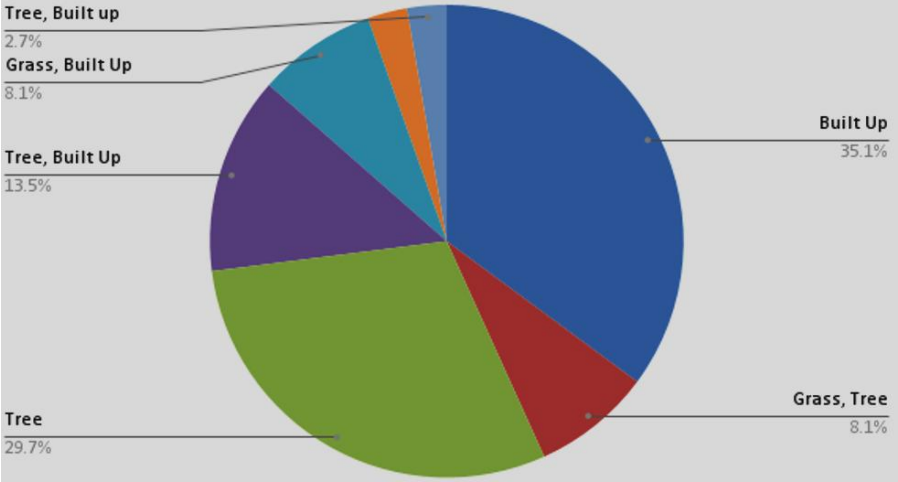

Figure 4. Aggregated land cover types.

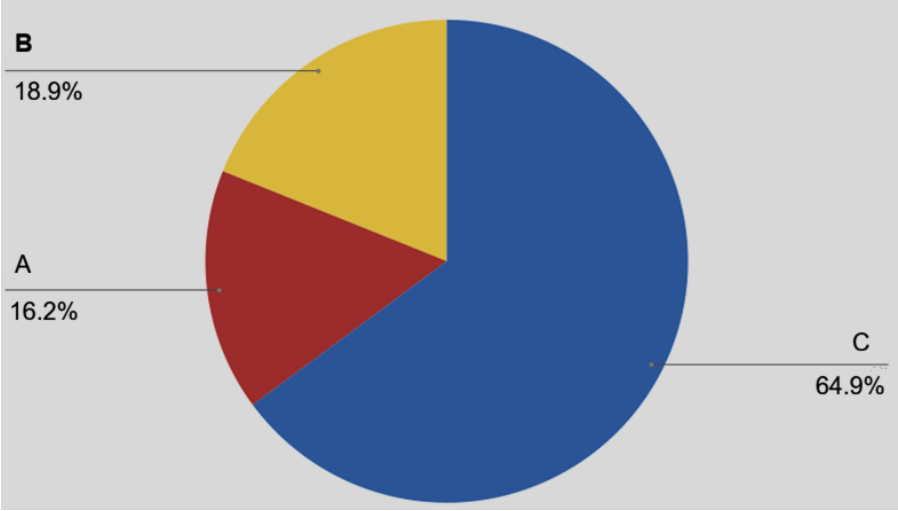

Figure 5. Distribution of hydrological soil groups.

Elevation in the area varies from 140 meters (lowest point) to 195 meters (highest point). This indicates a moderately unchanging landscape rather than steep mountains or deep valleys. After analyzing the slope, it was revealed that gentle slopes (3–9% gradient) cover about 61% of the area, while 18% of the area has little or no slope (0–3%). In addition, moderate (9–15%) and steep (15–30%) slopes account for 17% and 3%, respectively, with excessively steep terrain (>60%) only translating to 2%. The mean slope of 3.53% suggests an overall gentle terrain that facilitates runoff accumulation flow.

2.2.3. FloodScope

The S.H.I.E.L.D. FloodScope tool, developed by the author, employs a hybrid approach by comparing CN values, land cover classifications, hydrological soil groups, and slope/elevation to observe correlations between the degree and significance of each runoff potential on flood risk. The 37 sampling units within the 3 km² AOI each hold feature vectors of Curve Number, aggregated land cover class (Built-up, Tree, Grass, Bare Ground), hydrological soil group (**A**–**C**), slope, and elevation, which can be generated into a defined, five-level flood risk label derived from a multi-criteria threshold: CN > 75 (USDA, 2021), gentle slopes 0–9%, low relative elevation, impervious land cover, and HSG C. This directly enables the use of tree-based machine learning methods such as random forests and gradient boosted decision trees such as Extreme Gradient Boosting (XGBoost) to learn interactions among the factors classified in this study in controlling runoff potential. For this workflow, the AOI table (Appendix 1) was transformed into a training set where each row represents a 100 m pixel and each column a normalized predictor (CN, slope, elevation, land cover and HSG). XGBoost was then trained to approximate a rule-based classifier. Figure 6 depicts the FloodScope Model Framework, describing the process from data collection and translation into the CSV template to output of graphic and quantitative features.

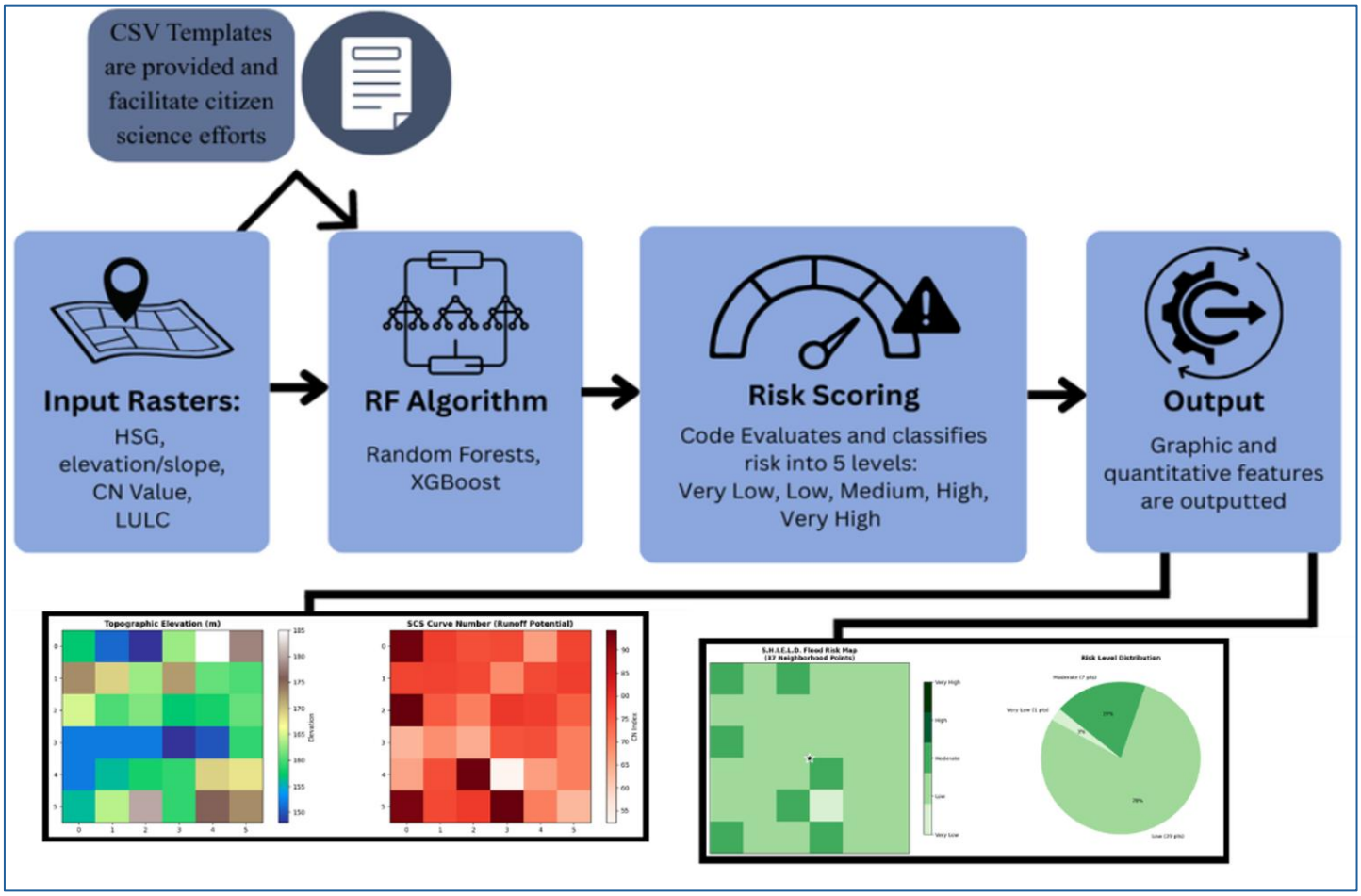

Figure 6. FloodScope model framework.

The core of the FloodScope tool implements the physical SCS Runoff Equation. The tool calculates the depth of runoff (Q) inches based on a design storm event. This ensures the model outputs are grounded in fluid dynamics rather than arbitrary weights. (U.S. Army Corps of Engineers, Hydrologic Engineering Center, 2025; USDA, 2021). The relationship is defined by the following equations:

$$S = \frac{1000}{CN} - 10 \tag{1}$$

$$Q = \frac{(P - 0.2S)^2}{P + 0.8S} \tag{2}$$

Where P represents the precipitation depth (standardized to 5.0 inches for high-intensity storm modeling in this study) and S representing the maximum amount of water, the soil can retain before it is completely saturated. A high Curve Number leads to a low S, meaning the soil reaches capacity almost immediately.

The equations were implemented as the following code block, where Ia (i.e., initial abstraction) accounts for water that is lost at the start of a storm due to surface storage, interception by vegetation, and initial infiltration. In addition, by setting the rainfall_depth to 5.0 inches (i.e., representing a 10-year or 50-year extreme storm for East Texas), the actual physical depth of water that will contribute to flooding is calculated.

```
def calculate_runoff_depth(cn, rainfall_depth=5.0):

    if cn <= 0: return 0
    S = (1000 / cn) - 10
    Ia = 0.2 * S
    return ((rainfall_depth - Ia)**2) / (rainfall_depth - Ia + S) if rainfall_depth > Ia else 0)
```

To ensure the model is applicable across diverse terrains, a local relief calculation was introduced, as shown in the following code block. Instead of using absolute elevation, which varies globally, the model identifies accumulation zones by calculating the height of a pixel relative to the minimum elevation within the AOI. By subtracting the minimum elevation in the study area, points where water naturally pools because they are lower than the surrounding 100 m pixels, or sinks are identified. This allows the model to identify hydrological sinks regardless of whether the study area is at sea level or in a high-altitude basin. This in turn corresponds to the Dynamic World Built Area classification. It applies a mathematical penalty for impervious surfaces like asphalt or concrete, which prevent natural drainage, and sophisticates the model through weighing of land cover and topography alongside soil properties.

```
def refined_flood_risk(row, df):

    q = calculate_runoff_depth(row['cn'])
    local_relief = row['elev'] - df['elev'].min()
    risk_score = 0

    if q > 3.5: risk_score += 4    # Physical Runoff Depth
    elif q > 2.5: risk_score += 3
    elif q > 1.5: risk_score += 2

    if local_relief < 3 and row['slope'] < 3: risk_score += 2 # Accumulation Zone
    if row['lulc'] == 6: risk_score += 2 # Built-up Area (Standardized ID)

    return min(4, max(0, risk_score // 2))
```

As shown in the following code block, the XGBoost algorithm was chosen because it excels at handling non-linear geospatial relationships. For example, a high slope might be safe in a forest but extremely dangerous in an urban Built Area. XGBoost is an algorithm that builds decision trees by being fed raw data from (Appendix 1) and final risk scores. Because XGBoost builds non-linear decision trees, it naturally

mimics the if-then mechanics of fluid dynamics and topography. When XGBoost predictions match the FloodScope model's labels (achieving high accuracy), it verifies that the manual mathematical rules are statistically sound and free of logical contradictions. If the model's physical rules were flawed or random, the artificial intelligence (AI) would fail to find a pattern and the accuracy would be low. By having the AI predict risk levels without any mathematical formulas or logical rules, it calculates a convergence rate. If the AI matches the physical model, it proves that the S.H.I.E.L.D logic is mathematically consistent and ready for deployment as a regional predictive tool.

```
xgb_model = xgb.XGBClassifier(use_label_encoder=False, eval_metric='mlogloss', random_state=42)
    xgb_model.fit(X, y)
    df['ml_pred'] = xgb_model.predict(X)
```

The trap of mimicking in machine learning is called overfitting. To prove the FloodScope model is learning physics and not just memorizing the 37 coordinates and their attached risk factor vectors, the code uses stratified k-fold cross-validation which splits 37 points into five different groups (folds). It completely hides one group from the AI. The AI is then forced to train on the remaining unhidden points and asked to predict risk for the hidden fold of points. This process is repeated five times, with a different group and number of points hidden each time, and the final values are averaged.

Because the AI can accurately predict flood risk of points it was never trained on, it mathematically proves the algorithm has successfully reverse-engineered the underlying hydrological rules and can now apply those rules to entirely new, unseen environments.

3. Results

The elevation chart (Figure 7a) renders points into a terrain color map to emphasize relative highs and lows. Elevation ranges from 150 m to 185 m, emphasizing low-lying accumulation zones. When viewed alongside the risk map (Figure 7b), it shows that higher risk classes tend to cluster in relatively lower or gently sloping parts of the AOI. The CN chart (Figure 7b) similarly reshapes 36 CN values into a separate image using a red scale palette, with higher CN values in darker tones. It depicts a 55 to 95 CN value range, with values >75 having a darker shade. This map visually encodes the association between high CN, urban/impervious land cover, and elevated flood risk (USDA, 2021). Together, the elevation and CN plots create a spatial topographic context for the risk grid and subsequent AI/ML models that treat these variables as key predictors. Figure 8 shows flood risks at individual cells and the distribution of flood risk levels.

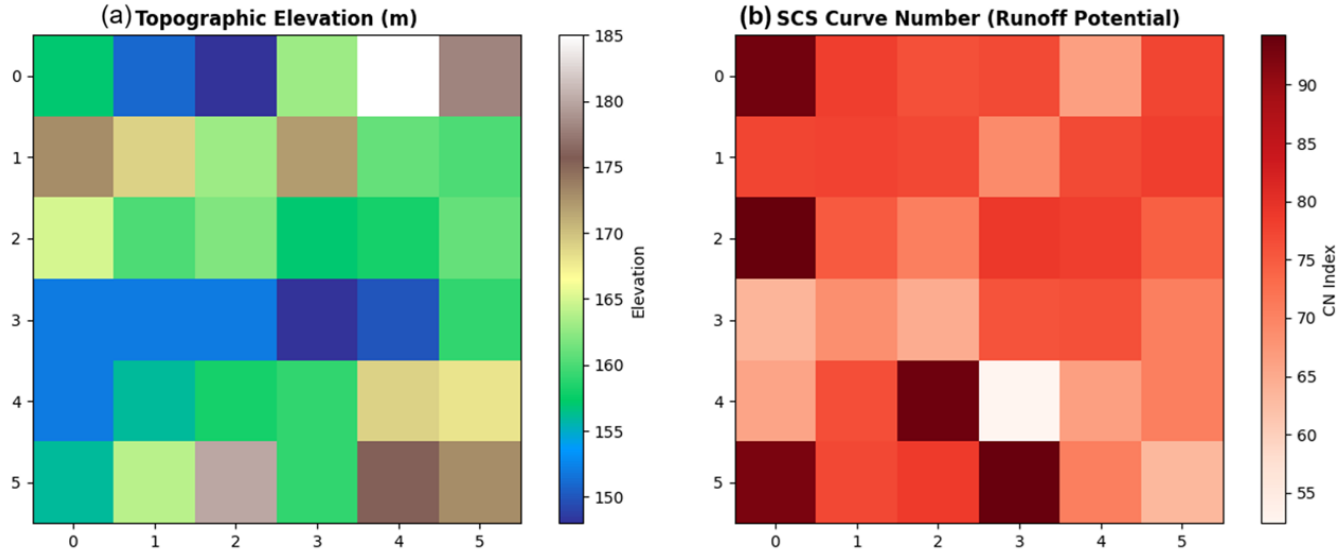

Figure 7. Terrain-ramped elevation (a) vs. curve number heat map (b).

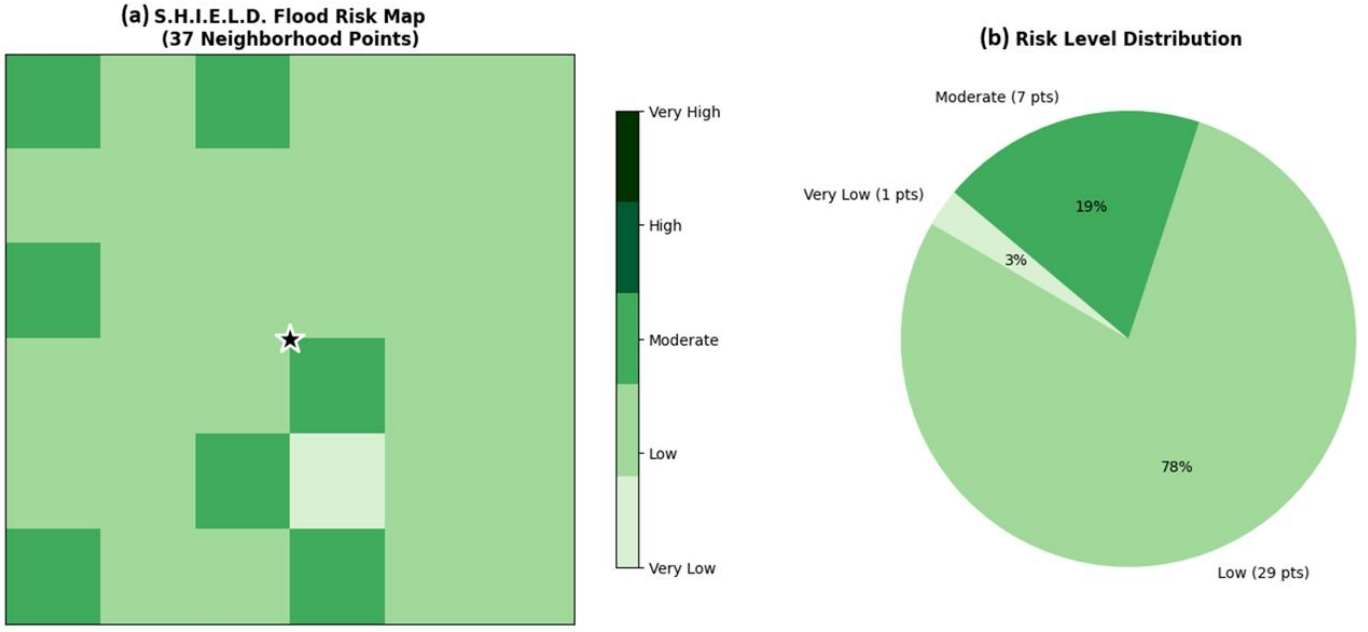

Figure 8. Flood risks at individual cells (a) and the distribution of flood risk levels (b).

Under a standardized 5.0-inch extreme precipitation event, the FloodScope model demonstrates high sensitivity to CN fluctuations. For instance, in urbanized pixels characterized by a CN of 95, the potential retention is constrained to 0.53 inches, yielding a significant runoff depth of 4.42 inches. Conversely, in forested regions with a CN of 60, the retention capacity expands to 6.67 inches, mitigating surface runoff to negligible levels. The model prioritizes these physical values over simple heuristics by assigning a maximum risk weight (+4) to any coordinate where Q exceeds 3.5 inches, establishing runoff depth as the primary driver of flood vulnerability within the Tyler-Flint study area.

Beyond volumetric runoff, the model incorporates topographic variability to identify hydrological sinks that facilitate water accumulation. Coordinates characterized by a local relief of less than 3 meters and a surface slope of less than 3% are classified as high-risk accumulation zones. This topographic weighting (+2) accounts for gravitational migration of runoff from high-elevation pervious zones to low-lying impervious depressions. The spatial results indicate that these sinks often align with the transition zones between natural landscapes and anthropogenic developments, creating localized hotspots of vulnerability that coarse-resolution regional models frequently overlook.

The integration of 10 m resolution Sentinel-2 data through the Dynamic World classification standard allows the model to assess the impact of land use/land cover (LULC) on flood propagation. Specifically, the presence of Class 6 (Built Area) serves as a proxy for impervious surfaces which change the natural hydrological cycle by eliminating infiltration pathways. The model applies a deliberate penalty (+2) to these built environments to account for overland flow and the lack of subsurface drainage capacity. The resulting risk map reveals a clear geospatial diversity: while the central study coordinate (shown by the star marker) exhibits moderate stability, it is adjacent to high-risk urbanization, highlighting the risk of flash-flood isolation even in areas that do not directly experience peak runoff.

The statistical output of the model reveals a significant concentration of moderate-risk across approximately 33% of the AOI. This distribution suggests that the study area possesses a baseline level of vulnerability that is manageable under standard conditions but highly sensitive to localized shifts in precipitation intensity. Notably, roughly 11% of the sampled coordinates are categorized as Very High risk. These points represent a critical intersection of high CN values (>90), low local relief (<3 m), and impervious LULC. From an urban planning perspective, these data provide a quantitative basis for targeted intervention.

To validate the reliability of the predictive engine, the research utilized Extreme Gradient Boosting (XGBoost) to assess the convergence between machine learning predictions and physical hydrological logic. The validation maps demonstrate a near-total equivalence between the physical model and the AI-predicted outputs. This convergence is statistically significant because it confirms that the XGBoost algorithm successfully identified the non-linear associations between the five input parameters without being explicitly programmed with the SCS-CN equations. By utilizing stratified k-fold cross-validation, the model achieved

a high accuracy rate, proving that it has internalized the underlying laws of hydrology, such as the inverse relationship between slope and accumulation, rather than mimicking the training dataset. This establishes the S.H.I.E.L.D framework as a thorough and reproducible system capable of generalizing flood risk in unseen geospatial environments.

4. Discussion and Conclusions

Several limitations were identified in this research. First, the model utilizes 2024 Dynamic World and Sentinel-2 data, which provides a snapshot of land cover. However, flash floods are highly dynamic events. A limitation of this research is that it does not account for seasonal vegetation changes that significantly affect infiltration and runoff rates in the Tyler-Flint region. Second, there is a notable resolution gap between the 10 m resolution of Sentinel-2 LULC and the 250 m resolution of Global Curve Number and HWSD 2.0 soil data. This data integration between coarse Global Curve Number and HWSD 2.0 Soil Data vs. Fine Sentinel-2 LULC data can introduce spatial averaging errors, where a single soil classification is incorrectly assumed for a diverse 100 m bounding box. Third, currently, the model classifies potential risk based on physical geography (CN, slope, and elevation). It does not yet integrate real-time rainfall intensity (mm/hour) or duration data. A high-risk zone in the model identifies susceptibility, but the actual flood event depends on storm-specific variables not currently present in the dataset. Fourth, the XGBoost model achieved 100% accuracy reproducing FloodScope's rule-based outputs across three randomized trials, showing strong alignment in data patterns. However, this likely indicates generalization due to the limited 37 sampling points and coarse-resolution input data (CN, HSG, and LULC). Last, as a citizen science tool, FloodScope depends on the accuracy of user-uploaded CSV data. The tool currently lacks an automated data cleaning or quality control layer to filter out erroneous user entries (e.g., impossible elevation values or incorrect soil codes), which could lead to misleading risk outputs.

Despite the limitations, this research is significant in many aspects. A primary contribution of this research is the democratization of geospatial analytics through the transition from proprietary, high-cost software to open-access, reproducible frameworks. Historically, precise hydrological modeling has been gatekept by the requirement for expensive GIS licenses and specialized computational hardware. The S.H.I.E.L.D. FloodScope architecture leverages Google Colab, GitHub, and Earth Map, removing these economic barriers. The model fosters a transparent, participatory approach to disaster management that enhances public trust and data accuracy simultaneously. The S.H.I.E.L.D prototype demonstrates that high-fidelity risk analysis can be performed without the need for expensive, proprietary GIS software or computationally prohibitive hydrodynamic simulations. For municipal planners in rapidly urbanizing areas like the Tyler-Flint area, this tool provides a quantitative basis for optimizing resource allocation and the development of green infrastructure. By focusing on current land cover dynamics (via 10 m Sentinel-2 data) and physical runoff potential rather than solely on historical flood insurance rate maps (FIRMs), the tool accounts for the variability of the modern climate. This allows for the identification of risk in rapidly urbanizing corridors where past records may show no flood history, yet current imperviousness and topographic depressions create a high-probability hazard.

Data Availability Statement: Data are available at https://zenodo.org/communities/nasaglobe/records?q=&l=list&p=1&s=10&sort=newest.

Acknowledgment: The author thanks Dr. Russane Low, Peder Nelson, Dr. Cassie Soeffing, Mr. Andrew Clark, and Dr. Brianna Lind for their guidance.

Conflicts of Interest: The authors declare no conflicts of interest. The funders had no role in the design of the study; in the collection, analyses, or interpretation of data; in the writing of the manuscript; or in the decision to publish the results.

References

Joint Economic Committee Democratic Staff. (2024, June). *Climate exacerbated flooding costs the U.S. between $179.8 and $496.0 billion each year* [Report]. U.S. Senate. Retrieved April 17, 2026, from https://www.jec.senate.gov/public/_cache/files/4a8c4aab-669e-4249-a181-499c0791a9ab/jec-report-on-economic-cost-of-flooding.pdf

Low, R. D., Nelson, P. V., Soeffing, C., Clark, A., & SEES Mosquito Mappers Research Team. (2021). Adopt a Pixel 3 km: A multiscale data set linking remotely sensed land cover imagery with field-based citizen science observation. *Frontiers in Climate, 3*, 658063. https://doi.org/10.3389/fclim.2021.658063

National Oceanic and Atmospheric Administration. (n.d.). *The U.S. Climate Resilience Toolkit: Climate Explorer*. Retrieved April 17, 2026, from https://crt-climate-explorer.nemac.org/climate_graphs/?county=Smith%2BCounty&city=Tyler%2C+TX&fips=48423&lat=32.3512601&lon=-95.30106239999999&id=pcpn&area-id=48423&zoom=7&mode=daily_vs_climate

Nelson, P. (2024). *Adopt-a-Pixel Research Framework*. Global Learning and Observations to Benefit the Environment. https://storymaps.arcgis.com/stories/3c02bd1d895348e4b2ffc6ddfd5eeca2 (Last accessed: April 25, 2026)

Patel, S. (2025, March 25). Major disaster in the US declared every four days in 2024, IIED analysis shows. *International Institute for Environment and Development*. Retrieved April 17, 2026, from https://www.iied.org/major-disaster-us-declared-every-four-days-2024-iied-analysis-shows

Texas Water Development Board. (2025, February). *Technical guidelines for regional flood planning (2028 RFP).* Retrieved April 17, 2026, from https://www.twdb.texas.gov/flood/planning/planningdocu/2028/doc/Exhibit_C_TechnicalGuidelines_2028RFP_Feb2025.pdf

The New York Times. (2025, July 30). *The lives lost to the Texas floods.* Retrieved April 17, 2026, from https://www.nytimes.com/interactive/2025/07/09/us/texas-floods-victims.html

U.S. Army Corps of Engineers, Hydrologic Engineering Center. (2025). *HEC-RAS River Analysis System.* Retrieved April 17, 2026, from https://www.hec.usace.army.mil/confluence/rasdocs/ras1dtechref/latest/overview-of-optional-capabilities/modeling-precipitation-and-infiltration/curve-number

U.S. Department of Agriculture, Natural Resources Conservation Service. (2021). *Chapter 2: Estimating runoff volume and peak discharge.* Retrieved April 17, 2026, from https://directives.nrcs.usda.gov/sites/default/files2/1712930818/31754.pdf

Appendix 1. Sampling Points

(Note: HSG classes A, B, & C indicate soil permeability levels.)

Point #	Curve Number (CN)Value	Land Cover	Hydrological Soil Group (HSG)	% Slope	Elevation (m)
0	79.00	Built-up	C	3.00	155
1	93.25	Built-up	A	2.44	157
2	78.11	Grass, Tree	C	5.83	151
3	76.14	Tree	C	1.66	148
4	76.82	Tree, Built-up	C	2.69	163
5	66.33	Tree	B	3.91	185
6	77.29	Grass, Tree	C	3.45	178
7	77.29	Built-up	A	6.83	173
8	77.67	Grass, Built-up	C	2.82	169
9	77.00	Grass, Built-up	C	3.67	163
10	69.00	Tree, Built-up	B	6.89	172
11	76.78	Tree	C	2.75	161
12	78.14	Bare Ground	C	4.75	160
13	94.25	Tree	B	4.13	165
14	75.00	Tree	C	3.33	160
15	70.50	Tree, Built-up	B	3.65	162
16	79.00	Built-up	C	4.16	157
17	78.11	Tree	C	3.98	158
18	74.43	Tree	C	1.56	161
19	63.67	Built-up	B	2.39	152
20	68.56	Built-up	C	2.58	152
21	64.71	Built-up	A	2.85	152
22	75.80	Tree	C	2.82	148
23	76.11	Tree	C	4.47	150
24	70.43	Grass, Built-up	C	3.20	159
25	65.67	Grass, Tree	B	3.05	152
26	76.33	Tree, Built-up	C	1.93	156
27	93.50	Built-up	C	3.17	158
28	52.40	Built-up	A	2.99	159
29	66.33	Tree, Built-up	B	2.20	169
30	70.43	Tree, Built-up	C	3.11	168
31	92.50	Built-up	A	2.64	156
32	77.00	Tree	A	2.66	164
33	78.71	Built-up	C	5.39	180
34	94.00	Built-up	C	3.21	159
35	70.44	Tree	C	3.58	176
36	63.29	Built-up	C	2.67	173

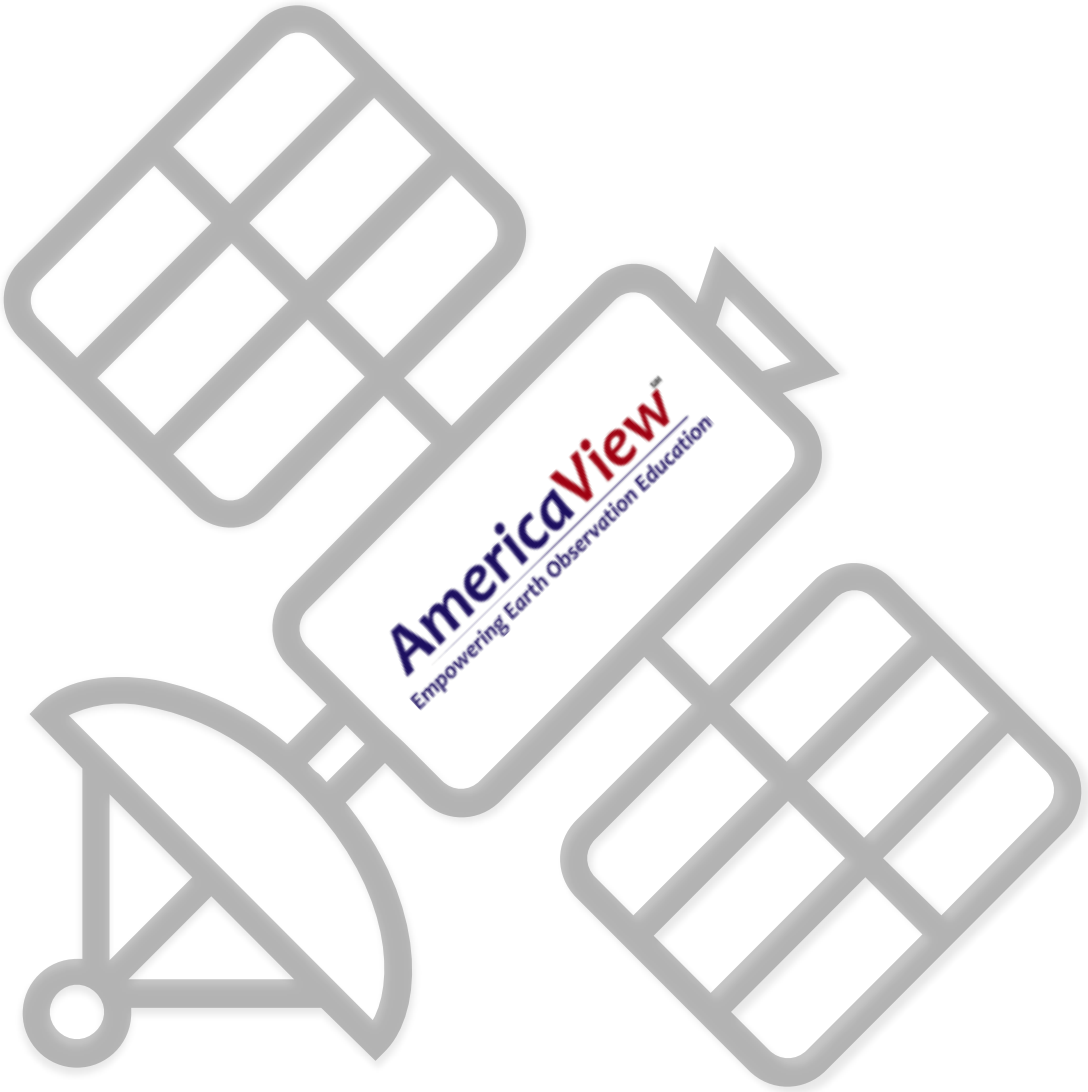

ISSN (online): 3070-3867

A Publication of AmericaView
https://AmericaView.org

Front Page Image:
Adopt-a-Pixel sampling locations symbolized with land-cover types. Credits: Alyssa Tyndale. Image courtesy of Esri and the USDA Farm Service Agency.

JEOGA Journal Home